Energy Harvesting through Electromechanical Transducers

Mentor: Kevin Farinholt

Abstract

Energy is an essential component in every aspect of human life. Within the scientific and engineering communities energy serves a critical role in our ability to observe, measure, analyze and control various systems in our physical world. Recent advances in low-power wireless sensors, electronics and microelectromechanical systems have fostered an increasing need for highly developed mobile power systems. The standard approach for powering such mobile or remotely-based systems is the use of conventional batteries for energy storage. While this approach is suitable for many applications, there are limitations due to finite lifespan and the need to recharge or replace spent battery cartridges. One alternative to the exclusive use of batteries is energy harvesting, a process which would serve to extend the operational lifetime and overall robustness of mobile power systems. In this manner the energy harvester would extract ambient or unwanted energy from a system's surroundings; storing this energy in batteries, capacitors, or directly using it to power necessary hardware.

Project Outline

The overall objective of this research project will be to compare the energy harvesting capabilities of two electromechanical transducers: the piezoelectric polymer Polyvinylidene Fluoride (PVDF) and the ionically conductive ionic polymer transducer (IPT). We will discuss the fundamental mechanisms behind each material's transduction properties and how they give rise to the respective polymer's intrinsic ability to convert energy between electrical and mechanical domains. The first material to be examined will be the piezoelectric polymer PVDF. This material will serve as the introductory phase of the project due to the wealth of information available in present literature [1-4]. The second material under consideration will be the ionically conductive polymer Nafion™ which is commonly used in the ionic polymer transducer (also known as the ionic polymer-metal composite - IPMC).

During the first weeks of this project our primary focus will be on the PVDF transducer, gaining an understanding of its electromechanical properties and how the piezoelectric constitutive models can be used to predict available power. These models will be coupled with physical models of the material to simulate internal strain within the material, which will then be used to model the energy generation for a dynamic mechanical load. Once a fundamental theoretical understanding of the PVDF transducer has been obtained, students will move into the lab where a series of tests will be conducted to (1.) characterize the physical and electromechanical coupling properties of the transducer and (2.) evaluate the energy harvesting abilities of a sample PVDF transducer. Tests will focus on the axial loading of the PVDF membrane, as shown in the experimental setup of Figure 1.

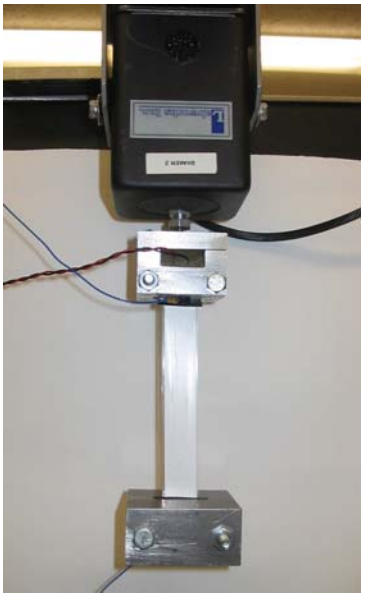

Figure 1: Experimental test fixture for axial loading of PVDF transducers.

The results of these tests will then be brought back into the analytical process to provide validation for the modeling approach.

As the students become comfortable with the modeling process for PVDF membranes, we will shift our focus toward the more compliant ionically conductive polymer. We will discuss the current modeling approaches discussed in literature, focusing the majority of our attention on the constitutive models of Newbury and Leo [5-6] which compare nicely to the commonly accepted models for piezoelectric materials. We will conduct a series of experimental studies to characterize the electromechanical properties of the ionic polymer transducer, incorporating these values into the modeling approach to predict the expected power levels from these materials under higher strains (1-5%). Following the theoretical development and material characterization, students will perform a series of experiments designed to quantify the energy harvesting abilities of the ionically conductive polymer. If time permits, we will investigate different circuit designs for storing the generated energy in super-capacitors and/or electrochemical batteries. Once the testing has been completed, students will begin compiling the accumulated data, tabulating the benefits and disadvantages of the piezoelectric and ionically conductive polymers for a vibration-based energy harvester.

Project Schedule

This project will focus on developing a comprehensive understanding of how ionically conductive materials can be used in harvesting electricity from ambient vibrations. This work will be conducted over an eight week period. The expected work is outlined in the following timeline.

Week 1:	Safety training and project introduction
Week 2:	Analytical study of piezoelectric polymer
Week 3:	Study the physical response of PVDF under axial loading
Week 4:	Shift modeling approach to ionic polymer transducers (IPTs)
Week 5:	Characterize electromechanical properties of IPT
Week 6:	Design and test harvesting circuitry for IPTs
Week 7:	Finish testing and begin preparing results
Week 8:	Present project findings

References/ Suggested Reading

1. Park, G., Farrar, C.R., Todd, M.D., Hodgkiss, W., Rosing, T., 2007, "Energy Harvesting for Structural Health Monitoring Sensor Networks," www.lanl.gov/projects/ei/pdf_files/**LA-14314-MS**.pdf
2. Sodano, H., Inman, D., Park, G., 2005, "Comparison of Piezoelectric Energy Harvesting Devices for Recharging Batteries." *JIMSS*, vol. 16, pp. 799-807.
3. Sodano, H., Park, G., Inman D.J., 2004, " A Review of Power Harvesting Using Piezoelectric Materials," Shock and Vibration Digest, vol. 36, no. 3, pp. 197-206.
4. Sodano, H., Granstrom, J., Feenstra, J., Farinholt, K., 2007, "Harvesting of Electrical Energy from a Backpack using Piezoelectric Shoulder Straps," *Proceedings of SPIE*, no. 6525-01.
5. Newbury, K., Leo, D. 2003 "Linear Electromechanical Model of Ionic Polymer transducers – Part I: Model Development," *JIMSS*, vol. 14, pp.333-342.
6. Newbury, K., Leo, D. 2003 "Linear Electromechanical Model of Ionic Polymer transducers – Part II: Experimental Validation," *JIMSS*, vol. 14, pp.343-357.

Equipment Requirements

PVDF and ionic polymer transducers will be needed for experimental studies. Basic breadboard components will be needed to assemble energy harvesting circuitry. An electromagnetic shaker will be needed to oscillate samples, and a suitable mass will be needed to provide loading. Tests will rely on a laser vibrometer or accelerometer to measure input motion and a standard Fourier analyzer to capture data.

Software Requirements

Standard mathematical software (MATLAB or Mathematica) will be required for simulations.

Comparison of Piezoelectric Energy Harvesting Devices for Recharging Batteries

HENRY A. SODANO,[1,*] DANIEL J. INMAN[2] AND GYUHAE PARK[3]

[1]*Department of Mechanical Engineering - Energy Mechanics, Michigan Technological University, Houghton, MI 49931, USA*

[2]*Center for Intelligent Material Systems and Structures, Virginia Polytechnic Institute and State University Blacksburg, VA 24061, USA*

[3]*Engineering Sciences and Applications, Weapons Response Group, Los Alamos National Laboratory Los Alamos, NM 87545, USA*

ABSTRACT: Piezoelectric materials can be used as a means of transforming ambient vibrations into electrical energy that can then be stored and used to power other devices. With the recent surge of microscale devices, piezoelectric power generation can provide a convenient alternative to traditional power sources used to operate certain types of sensors/actuators, telemetry, and MEMS devices. However, the energy produced by these materials is in many cases far too small to directly power an electrical device. Therefore, much of the research into power harvesting has focused on methods of accumulating the energy until a sufficient amount is present, allowing the intended electronics to be powered. In a recent study by Sodano et al. (2004a) the ability to take the energy generated through the vibration of a piezoelectric material was shown to be capable of recharging a discharged nickel metal hydride battery. In the present study, three types of piezoelectric devices are investigated and experimentally tested to determine each of their abilities to transform ambient vibration into electrical energy and their capability to recharge a discharged battery. The three types of piezoelectric devices tested are the commonly used monolithic piezoceramic material lead–zirconate–titanate (PZT), the bimorph Quick Pack (QP) actuator, and the macro-fiber composite (MFC). The experimental results estimate the efficiency of the three devices tested and identify the feasibility of their use in practical applications. Different capacity batteries are recharged using each device, to determine the charge time and maximum capacity battery that can be charged. The results presented in this article provide a means of choosing the piezoelectric device to be used and estimate the amount of time required to recharge a specific capacity battery.

Key Words: power harvesting, energy scavenging, piezoelectric, macro-fiber composite, MFC, self-powered.

INTRODUCTION

THE increasing demand for completely self-powered electronics has caused an increase of research into power harvesting devices over the past decade. With the advances being made in wireless technology and low power electronics, sensors are being developed that can be placed almost anywhere. However, because these sensors are wireless, they require their own power supply which in most cases is the conventional electrochemical battery. Once these finite power supplies are extinguished of their power, the sensor must be obtained and the battery replaced. The task of replacing the battery is tedious and can become very expensive when the sensor is placed in a remote location. These issues can be potentially alleviated through the use of power harvesting devices. The goal of a power harvesting device is to capture the normally lost energy surrounding a system and convert it into usable energy for the electrical device to consume. By utilizing these untapped energy sources, electronics that do not depend on finite power supplies, such as the battery, can be developed. One source of typically lost energy is the ambient vibrations present around most machines and biological systems. This source of energy is ideal for the use of piezoelectric materials, which have the ability to convert mechanical strain energy into electrical energy and vice versa.

The concept of utilizing piezoelectric material for energy generation has been studied by many researchers over the past few decades. One early study into power harvesting by Hausler and Stein (1984) investigated the ability to generate energy from the expansion and contraction of the rib cage during breathing. A prototype of the power harvesting system was constructed

*Author to whom correspondence should be addressed.
E-mail: hsodano@vt.edu

1045-389X/05/10 000799–9 $10.00/0 DOI: 10.1177/1045389X05056681

using polyvinylidene fluoride (PVDF) film and was implemented *in vivo* on a mongrel dog. The prototype was demonstrated to produce a peak voltage of 18 V, which corresponded to a power of about 17 μW. Another investigation into the ability to use piezoelectric materials for power harvesting from the motion of humans and animals, was performed by Ramsey and Clark (2001), who studied the ability to power an *in vivo* microelectromechanical system (MEMS) application. The research used a thin square plate driven by blood pressure to provide power and was shown to be capable of powering the electronics if they were used intermittently. Another form of excitation commonly used is the ambient vibration of mechanical structures. Umeda et al. (1996) quantified the amount of energy that could be produced when a steel ball impacted a piezoelectric plate. The authors used an equivalent circuit model to predict the energy while modifying numerous parameters in the system to find the best combination. It was determined that a significant amount of energy was returned to the steel ball in the form of kinetic energy as it bounced of the plate, making the system ineffective. Sodano et al. (2004b) formulated a model of a power harvesting system that consisted of a cantilever beam with piezoelectric patches attached. The model was developed such that any combination of boundary conditions and location of piezoelectric material could be accommodated, but was verified on a cantilever beam experiencing a base excitation from the clamped condition. The model was found to accurately estimate the energy generated and was also used to demonstrate the damping effect of power harvesting.

With the research into power harvesting devices growing, it was determined that the amount of energy generated by piezoelectric materials was not sufficient to power most electronic devices. Thus, for power harvesting technology to make its way into the commercial market, methods of accumulating and storing the harvested energy until a sufficient amount can be recovered to power the portable electronics, are the key to a successful power harvesting system (Sodano et al., 2004c). One of the first researchers to realize the need for power storage circuitry was Starner (1996), who speculated the use of piezoelectric materials for harvesting numerous sources of energy around the body, including limb and finger motion. Additionally, the idea of using a capacitor and rechargeable battery for power harvesting was discussed with some advantages and disadvantages of each listed. This concept was taken a step farther by Umeda et al. (1997), who followed their earlier study up with an investigation into the use of a capacitor with piezoelectric materials. They theoretically and experimentally tested the circuit in various configurations to determine the optimal design. Shortly after the publication of this work, a power harvesting patent was issued to Kimura (1998) for a means of storing the rectified energy from a piezoelectric device in a capacitor. However, a circuit containing only a single capacitor is not sufficient to provide power to other electronic devices without additional circuitry. Therefore, Kymissis et al. (1998) developed a piezoelectric system that would harvest the energy lost during walking and used it to power a radio transmitter. Their circuit also used a capacitor as the storage medium, but the additional components allowed it to charge to a desired level before discharging. Once the capacitor had discharged to a pre-specified level, an electronic switch would be triggered to stop the flow of energy, thus allowing the capacitor to recharge. It was found that the two piezoelectric devices used produced sufficient energy to power a transmitter that could send a 12-bit radio frequency identification (RFID) code every 3–6 steps. The proof that power harvesting could supply sufficient energy to power a transmitter opened up many doors for research into wireless sensors. In a later study, Elvin et al. (2003) developed a self-powered damage detection unit that used PVDF for energy generation and a capacitor to store the energy. The circuit was capable of transmitting a signal that held information on the integrity of the structure.

Much of the research into power harvesting has dealt with optimizing the power harvesting configuration or developing circuitry to store the energy. However, some researchers have looked into the ability to use circuitry for extracting more energy from the piezoelectric material. One such study was performed by Kasyap et al. (2002), who developed a circuit whose impedance could be modified to match that of the piezoelectric device. This circuit was based on the principle that the maximum energy transfer from the piezoelectric to the load occurs when the impedance of the two is matched. The authors provide a description of the fly back converter circuit and the equations needed to set the circuit impedance to the desired value. Ottman et al. (2002) studied the use of an adaptive step down DC–DC converter to maximize the power output from a piezoelectric device. It was found that at very high levels of excitation, the power output could be increased by as much as 400%. However, this study did have a drawback, the additional electronic components required to optimize the power output dissipated energy. This additional circuitry needed an open circuit voltage >10 V for an increase in the generated power. To overcome this problem, Hofmann et al. (2002) modified the circuit by removing the adaptive circuitry and used a fixed switching frequency. However, the improvements made to the circuit now required more than 25 V open circuit for increased power to be supplied to the load. Furthermore, the level of excitation necessary to produce >25 V open circuit is far greater than that present in any typical vibrating machinery, making the circuitry unrealistic.

Sodano et al. (2004c) concluded the use of the capacitor as a fundamental problem with the research that had been performed in power storage methods. Because of the poor energy storage characteristics of the capacitor, it could only be used to send out short pulses of energy, which severely limited the number of applications for power harvesting. Therefore, Sodano et al. (2004c) investigated the ability to use the energy from the piezoelectric material to recharge a discharged battery. Their study showed that a watch battery could be recharged from a completely discharged state, in less than 1 h by vibrations consistent in amplitude with those found on a typical vibrating machine. Furthermore, the authors compared this new concept to the more traditional method of storing the energy in a capacitor and found that the use of a battery provided more flexibility in the electronics to be powered, due to the capacitor's quick discharge time. In the present study, the efficiency of three different piezoelectric devices is studied and the energy from the excitation of a piezoelectric patch is used to recharge various capacity nickel metal hydride batteries. The three actuators are the traditionally used lead–zirconate–titanate (PZT) material, the Quick Pack (QP) actuator, and the macro-fiber composite (MFC) that was recently developed at the NASA Langley Research Center.

The MFC actuator is constructed using piezofibers surrounded in an epoxy matrix and covered with a Kapton shell (Wilkie et al., 2000, 2002). The construction of this actuator allows it to be extremely flexible, as well as robust to damage and environmental conditions. These are two desirable properties for power harvesting applications. Additionally, the MFC uses an interdigitated electrode pattern that capitalizes on the higher d_{33} piezoelectric coupling coefficient, which means the device is more efficient in converting energy between the mechanical and electrical domains. For these reasons, the MFC could be an ideal candidate for use as a power harvesting device; however the MFC's ability to be used for power harvesting has yet to be identified. The QP actuator is a bimorph piezoelectric device that uses monolithic piezoceramic material embedded in an epoxy matrix. The use of monolithic material causes the device to be far less flexible than the MFC but the epoxy shell does make it more robust than raw monolithic material. Lastly, the traditionally used monolithic piezoceramic material PZT is tested. The PZT material is effective but extremely brittle and susceptible to accidental breakage, making it the least robust of the three piezoelectric devices tested. In the following sections, the efficiency of each device is first identified to allow the work to be scaled to other sized actuators and piezoelectric materials. Next, the study provides the time required by each piezoelectric device to charge batteries ranging from 40 to 1000 mAh, followed by a discussion of each actuator's performance.

EXPERIMENTAL SETUP

Each of the three actuators was mounted with cantilever boundary conditions, thus allowing the excitation to be applied using base motion of the clamped edge. Due to the brittle nature of the PZT material and the extreme flexibility of the MFC, these two devices were bonded to a 0.0025 in. aluminum plate. The plate was very thin and added little stiffness but allowed the MFC to support its own weight and provided the PZT with added durability. The PZT material was PSI-5H4E piezoceramic from Piezo Systems Inc. and had dimensions as shown in Figure 1. The dimensions of the MFC are shown in Figure 2. The QP actuator do not require bonding to an aluminum plate because it is not too stiff like the PZT or too flexible like the MFC. The dimensions of the QP actuator are shown in Figure 3. While the QP actuator may appear to be much smaller than the other two piezoelectric devices, it is a bimorph actuator and contains four individual piezoelectric patches that make it roughly the same size as the other two.

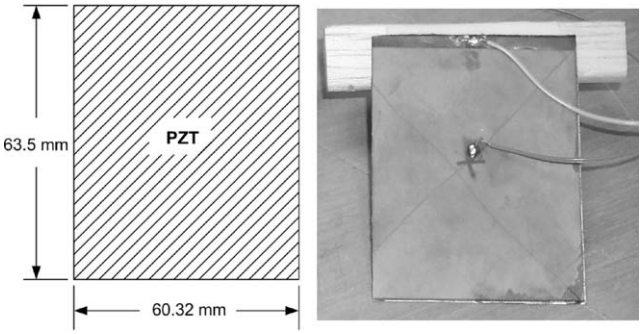

Figure 1. *Size and layout of the PZT plate.*

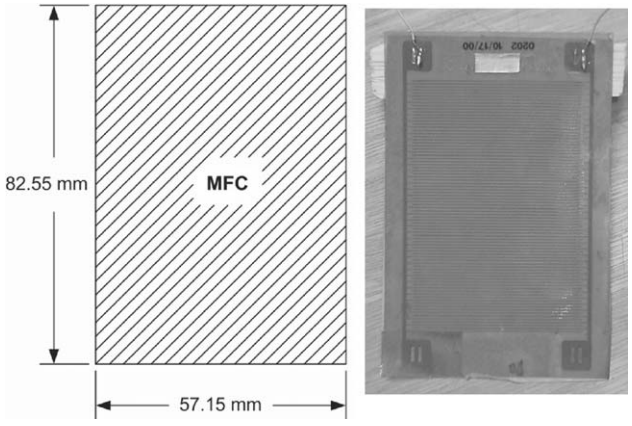

Figure 2. *Size and layout of the MFC plate.*

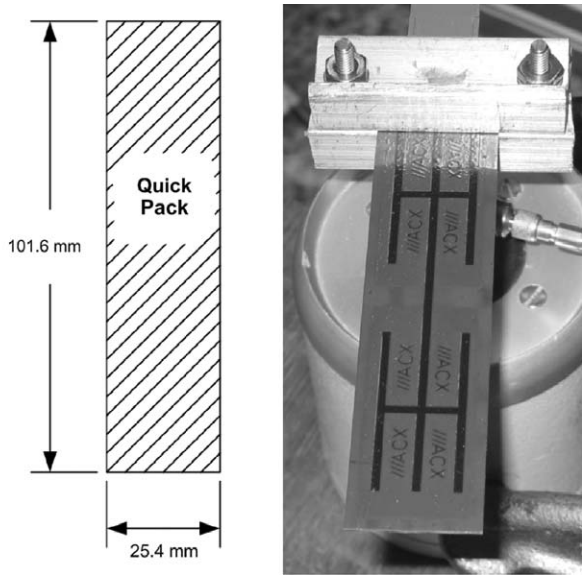

Figure 3. *Size and layout of the Quick Pack actuator.*

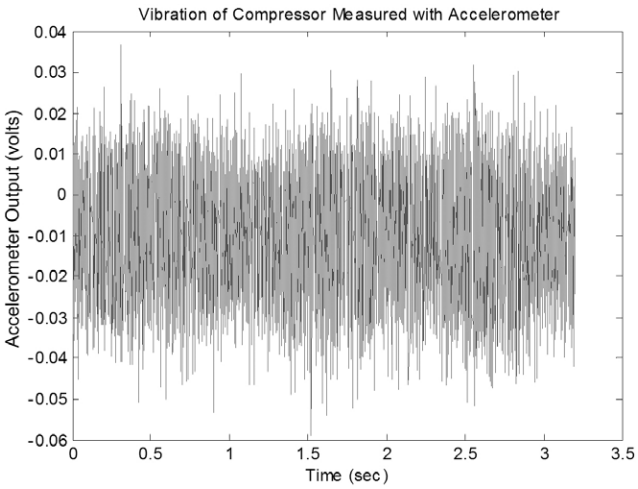

Figure 4. *Vibration of an automobile compressor measured by an accelerometer.*

One of the goals of this research is to identify the time required to charge various capacity batteries when subjected to a realistic ambient vibration source. Thus, the vibration of a typical machine was measured. Then a signal similar in frequency content and amplitude was used to excite the three piezoelectric devices. Examples of a few mechanical systems that experience ambient vibration are ships, bridges, railroad cars, and aircraft. However, for the tests performed in this study, the engine compartment of an automobile was chosen because the system was readily available. To measure the vibration signature of the automobile, a PCB accelerometer, model 352C22, was randomly placed on the air compressor of a car. The term 'random location' is used because no effort was made in optimizing the placement of the accelerometer to produce the maximum magnitude of vibration, nor is the compressor

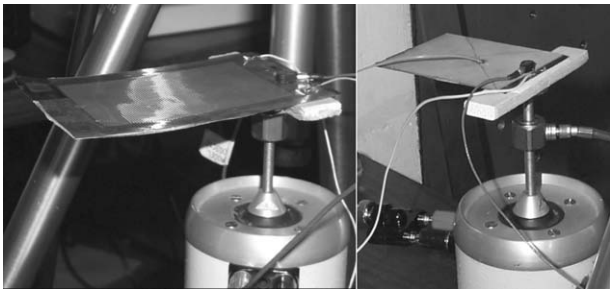

Figure 5. *Experimental setup with the MFC plate and PZT plate in a cantilever configuration.*

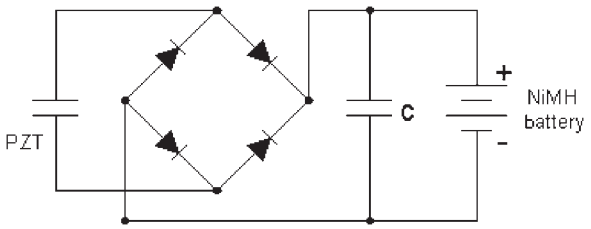

Figure 6. *Schematic of the battery charging circuit.*

the optimal location in the engine compartment for obtaining vibration energy. The engine was run at various speeds and the response was measured. The signal measured from the compressor had the appearance of random vibration from 0 to 1000 Hz, a typical response is shown in Figure 4. Using the measured data, a function generator was used to excite a LDS V203 shaker with the same PCB accelerometer attached to it. The excitation was then adjusted until the function generator supplied a signal of similar amplitude and frequency content as identified from the compressor.

The excitation of the piezoelectric devices was accomplished by mounting the clamped end of each to the shaker, thus exciting the system using base motion as shown in Figure 5. Using this setup, the displacement of the clamped boundary condition was measured with a Polytec laser vibrometer and a PCB force transducer (model 208) was used to measure the applied force. These two pieces of information allowed the power into the system to be determined, while the power output from the system was found by measuring the voltage drop across a load resistor that was matched to the impedance of each particular piezoelectric at its first resonant frequency. With the resistance and voltage drop known, the power output can be determined using Ohm's law.

For the battery charging experiments, nickel metal hydride batteries were chosen because they have a high charge density and, unlike lithium ion batteries, they do not require any type of charge controller or voltage regulator to be incorporated into the circuitry. The circuit constructed to charge the battery consisted of a full wave rectifier, capacitor, and the battery intended to be charged, as shown in Figure 6. The voltage

produced by the PZT was first full wave rectified and then accumulated in a large capacitor, typically >1000 μF, followed by the battery intended to be charged, which was placed in parallel with the capacitor. The simplicity of this circuit allows it to be constructed very compactly and without additional components that would result in increased power dissipation.

EFFICIENCY OF EACH PIEZOELECTRIC DEVICE

The first goal of this work was to compare the effectiveness of the MFC, QP, and PZT for use as power harvesting devices. This was done by determining the efficiency of each device used in the experiments. With the data obtained from the laser vibrometer, force transducer, and voltage output from the piezoelectric, the following was numerically calculated to determine the average efficiency:

$$\eta = \frac{P_{\text{out}}}{P_{\text{in}}} \times 100\% = \frac{1}{m}\sum_{n=2}^{m} \frac{(V_n + V_{n-1})^2/R}{[(F_n + F_{n-1}) \cdot (d_n - d_{n-1})]/(t_n - t_{n-1})} \times 100\%$$

where η is the efficiency, V is the voltage drop across load resistance R, F is the force applied to the base of the plate, d is the displacement of the plate, t is the time increment between data points, n is the data point index, and m is the total number of data points measured. The efficiency of each piezoelectric device was calculated when excited at the first resonant frequency (50 Hz for the PZT, 108 Hz for the MFC, and 32 Hz for the QP), with a chirp from 0 to 500 Hz and with a random signal from 0 to 500 Hz. As mentioned before, the automobile compressor vibrated randomly; therefore the efficiency corresponding to random vibration most likely represents the piezoelectric device being subjected to ambient vibration. The resulting efficiencies are shown in Table 1. It must be noted that the efficiencies do not represent that of the actuator itself, because the experimental configuration and other factors may vary. However, these efficiencies do provide a comparison between the three actuators tested. For each signal, three measurements were made to show consistency. The efficiency of the PZT plate is fairly consistent when excited using all three signals and is higher than the other two devices. The PZT's efficiency is slightly low at resonance because the resonance frequency used was that of the largest voltage output, not the frequency with the best force-in and voltage-out characteristics. Additionally, it can be seen that the QP performs poorly at resonance; this is thought to be due to the construction of the device with four separate piezoelectric patches, which causes there to be an area with no piezoelectric material in the middle of the beam. This results in an area of decreased stiffness causing much of the stain to be concentrated to this area. However, all of the efficiencies are fairly low because the excitation method used does not transfer all of the applied energy to the piezoelectric device.

Table 1. Efficiency of the PZT, MFC, and QP with three different inputs.

Signal	PZT efficiency (%)	MFC efficiency (%)	QP efficiency (%)
Resonant	4.54	1.7871	0.4662
	4.51	1.7211	0.6094
	4.2312	1.7377	0.946
Chirp 0–500 Hz	3.102	0.2927	1.6505
	3.0725	0.3033	1.2611
	3.0293	0.3368	1.492
Random 0–500 Hz	6.57	1.2103	3.097
	6.954	1.3013	2.9664
	6.8562	1.4663	3.1551

From Table 1, it can be seen that the MFC performed poorly for all of the excitation signals used. Through these tests, it was found that the MFC performed inadequately as a power harvesting medium. The electrical output from the MFC contained a very large voltage component but an extremely low current. It may be thought that the power would still be the same even if the voltage was large and the current was low, but for the case of the MFC the power generated is over a factor of ten smaller as can be seen in Figure 7, which shows the current output of each device at its first natural frequency. It is believed that the performance of the MFC is degraded due to increased impedance caused by the use of interdigitated electrodes. Another way to think of this situation is to consider each segment of piezoelectric fiber between the interdigitated electrodes

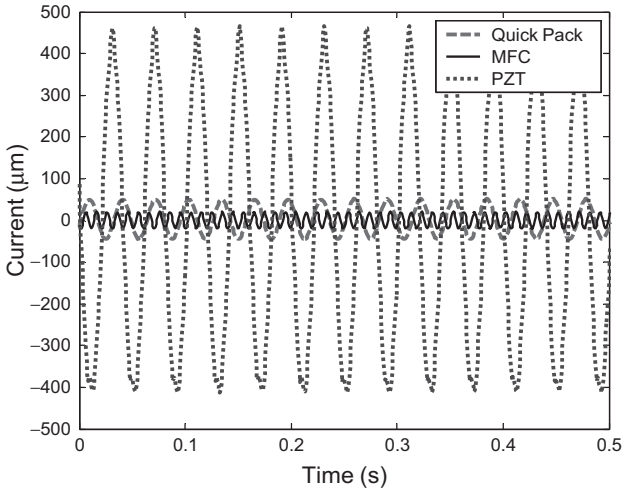

Figure 7. *Current output of each of the three piezoelectric devices at their respect fundamental frequency.*

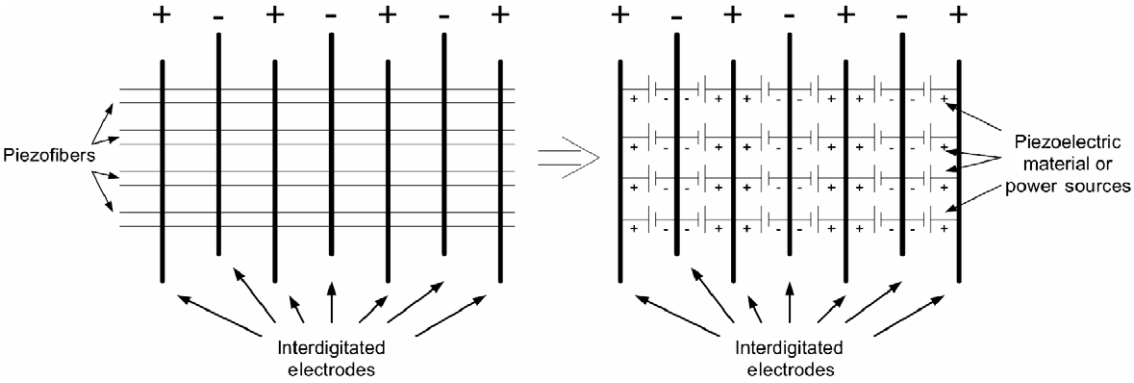

Figure 8. *Layout of a MFC patch and the equivalent circuit layout.*

as a small power supply (when used for power harvesting this is essentially what happens); this is shown by the schematic in Figure 8. Along the fiber, there are numerous sections of electrodes that cause the majority of these small power sources to be electrically connected to one another in series. When two power sources are connected in series, the voltages add but the current does not. This concept of series connections can be used to describe the reason for the low power generated by the MFC. Due to the series connection, the MFC produces a much higher voltage while the current remains far smaller than that of the PZT. The low current also causes much of the power generated to be dissipated by electronic devices, such as diodes, resulting in a lower efficiency. However, because the MFC was constructed for actuation purposes, a definitive and full understanding of the electrical properties of the MFC when used for power harvesting is not completely understood yet, and is currently being investigated by the authors. Additional effects resulting from the low current generation of the MFC will be detailed in the next section.

BATTERY CHANGING RESULTS

The tests presented in this section, investigate the ability of the three piezoelectric devices to recharge batteries ranging in size from 40 up to 1000 mAh (the unit 'mAh' stands for milli-amp-hour and is a measure of the battery's capacity, a 40 mAh capacity means that the batteries will last for 1 h if subjected to a 40 mA discharge current), the charge time required is also provided to demonstrate the relative effectiveness of each device. The charge time was recorded using a dSpace real time control board over a period ranging from 1 to 50 h, depending on the size of the battery. It was determined through testing the MFC that it was unable to recharge even the lowest capacity battery tested; unless the excitation signal provided by the shaker was unrealistically large (the goal of this work is to show that piezoelectric devices can charge batteries when experiencing typical levels of ambient vibration). The MFC's inability to charge batteries can be attributed to the issue of low current generation, as discussed in the previous section. When charging a battery, the most important electrical factor of the power supply is that it should be able to provide a fairly significant amount of current. The charge time of a rechargeable battery is directly dependent on the amount of current supplied to it. Since the MFC generates such a low current and the battery requires a fairly high current (usually one-tenth the battery's capacity or higher), the MFC actuator is not compatible with rechargeable batteries. With this point in mind, the results from tests using the MFC to charge batteries will not be presented.

Working with the two piezoelectric devices left, the PZT and QP, two signals were applied to the shaker to excite each device for charging batteries; a sinusoidal signal at the first bending frequency and a random signal ranging from 0 to 500 Hz. As indicated in the experimental setup section, the magnitude of the signals applied to the shaker caused the excitation of the piezoelectric devices to closely resemble the vibration that would be experienced in the engine compartment of an automobile. During the experiments, the time required for the battery to charge past the cell voltage of 1.2 V was measured in each case. This is not a complete charge but is $\approx$90% full, and provides an easy method of comparing the time needed by the PZT and QP to charge the battery. To finish charging the battery, a charge controller is needed to detect either a temperature change inside the battery cell or a slope change in the charge cycle. The electronics required to do this would complicate the system and dissipate a significant amount of the energy generated, potentially negating the ability of the piezoelectric to recharge the battery. For this reason and the inability to detect a full charge due to the absence of a charge controller compatible with the power output from the PZT, 90% was considered a full charge. To give an idea of the amount of energy that can be stored in the batteries

being tested, a 40 mAh battery contains enough energy to power a Casio LW22H watch for 2 y (Casio Inc.), and a 750 mAh battery is equivalent to a typical AAA battery.

Using the methods outlined, each battery was charged while the voltage on the battery was measured. The resulting charge time for each battery is shown in Table 2 and plots of the typical battery charging cycles are shown in Figure 9 for the PZT and QP excited at resonance and in Figure 10 for the PZT and QP excited with a random signal. In both figures, the charging of the 300 mAh battery is shown to demonstrate how each excitation and device performs. Although the larger batteries will reach a charge level of 1.2 V, it is unknown without a charge controller how long the piezoelectric material would take to supply sufficient current for a full charge of these batteries to be achieved. From Table 2, it is apparent that both the PZT and QP are capable of recharging a discharged battery. However, it can be seen that as the capacity of the battery increases, the QP begins to become less effective than the PZT. Additionally, as mentioned before, the QP has a section along its span that does not contain piezoelectric material causing a localized area with low bending stiffness, which leads to a majority of bending energy being concentrated at this point. Therefore, at higher frequencies, such as the second mode, significant bending strain is not utilized to generate power causing the QP to function poorly at higher frequencies. This point is demonstrated by looking at the difference between the charge times of the QP when excited at resonance and randomly, for instance the charge time for a 750 mAh battery at resonant excitation is 8.5 h and is increased to 25 h with random excitation. In contrast to this issue with the QP, the PZT does not experience this issue, from the efficiency tests; the PZT was shown to perform well when excited at a range of frequencies. This is demonstrated when charging the batteries also, for example the charge time for a 750 mAh battery at resonant excitation is 7 h and is only increased by ≈20% up to 8.6 h with random excitation. In some cases, the time required for a larger battery to be charged is slightly shorter than a smaller battery, this is caused by variations from test to test. The major variation that caused the charge times to perform in this manner was due to the batteries not being monitored during discharge, thus causing the amount of residual charge left in the battery to be unknown. Because of this, some batteries had slightly more energy stored upon beginning the recharge than others; this can be seen by looking at the voltage at the beginning of the charge as shown in Figures 9 and 10.

The results presented provide a platform to build off when using piezoelectric materials to charge batteries. Using the information from Tables 1 and 2, the type of piezoelectric device for recharging batteries and the capacity that can be charged in a required time can be determined, thus allowing the ideal power harvesting

Table 2. Time required charging different sized batteries using a piezoelectric.

	Resonant charge time (h)		Random signal charge time (h)	
Battery size (mAh)	**PZT**	**Quick Pack**	**PZT**	**Quick Pack**
40	1.62	0.75	1.6	7
80	1.2	2.9	2	12.5
200	4	3	1.2	20
300	6	10.8	9.8	22
750	7	8.7	8.6	25
1000	22	>50	32	>50

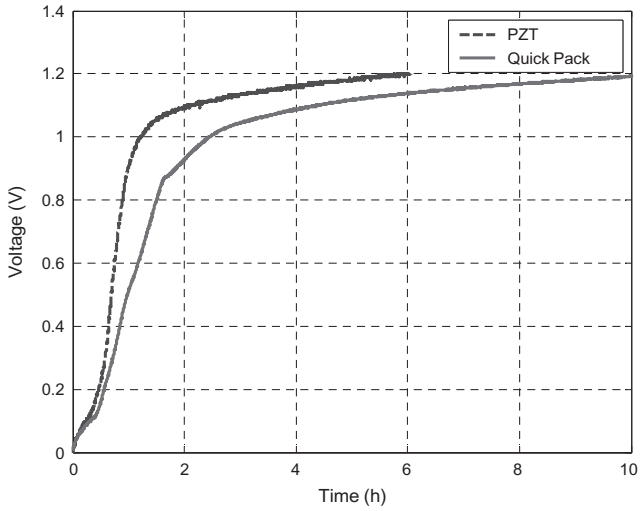

Figure 9. *Comparison of the charge history of a 300 mAh battery with resonant excitation of the PZT and Quick Pack.*

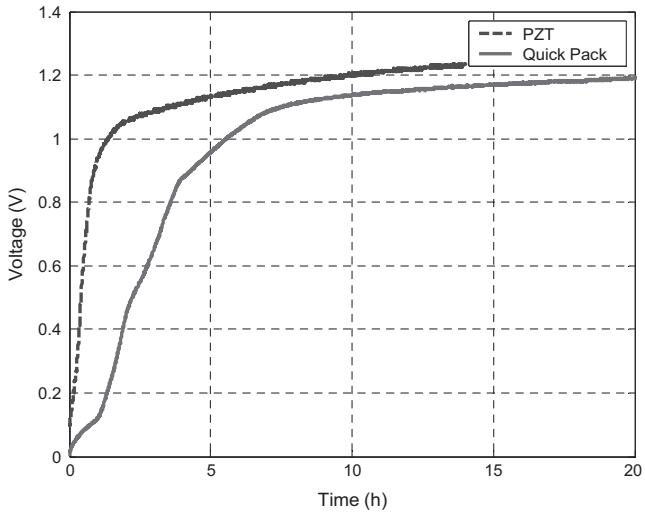

Figure 10. *Comparison of the charge history of a 300 mAh battery with random excitation of the PZT and Quick Pack.*

components to be found for a specific application. Sodano et al. (2004a) stated the result that piezoelectric materials that can be utilized for recharging batteries brings power harvesting significantly closer to the commercial market and opens up many doors for its application. The rational for this comment revolves around the severe limitations that are brought on an electrical system when energy is stored in a capacitor. The major factor that really limits the electronics is the quick charge and discharge time of the capacitor: it can only be used to provide short bursts of power. This makes the use of computational electronics or data processing impossible. Additionally, the capacitor does not have a cell voltage that it maintains at a constant voltage, but rather charges up to a high voltage; then releases a quickly changing output, making the use of a voltage regulator, which dissipates energy, a necessity. Furthermore, portable electronics that are commercially available utilize batteries, allowing power harvesting systems that use rechargeable batteries to be easily adapted to the currently available electronics. Power harvesting systems that utilize rechargeable batteries are the key to developing commercially viable self-powered electronic systems that have short duty cycles.

CONCLUSIONS

The idea of power harvesting has become increasingly popular over the past few decades. With advances in wireless technology and low power electronics, portable electronics and remote sensors are now part of our everyday lives. The key to replacing the finite power supplies used for these applications is the ability to capture the ambient energy surrounding the electronics. Piezoelectric materials form a convenient method of capturing the vibration energy that is typically lost and converting it into usable electrical energy. This material has been used in the power harvesting field for some time; however, the energy generated by these materials is far too small for directly powering most electronic systems. This problem has been found by most researchers that have investigated this field, thus showing the need for methods to accumulate the generated energy until a sufficient amount is present. Typically, the storage medium used has been the capacitor, but the capacitor is not a good candidate because it can only provide short bursts of power. Realizing this issue, Sodano et al. (2004a) showed that the rechargeable battery could be used with piezoelectric materials as an alternative to the capacitor. Using this idea, the present study has investigated the ability of three different piezoelectric devices, the PZT, MFC, and QP, to recharge various capacity nickel metal hydride batteries. First, the efficiency of each power harvesting device was tested under different excitation conditions to show the relative performance and allow the work to be compared to other studies. The results of the study found that both the QP and the monolithic piezoceramic material PZT were capable of recharging the batteries in question. However, the PZT was shown to be more effective in the random vibration environment that is usually encountered when dealing with ambient vibrations. Furthermore it was shown that the MFC was not well suited for power harvesting. Reasons for the poor performance were discussed, but the electrical characteristic of the MFC are unknown for power harvesting and are currently being investigated by the authors (Sodano et al., 2004d). The study presented provides a means for determining the ideal piezoelectric device and capacity rechargeable battery for a specific power harvesting application. Without a method of storing energy more effective than the capacitor, power harvesting will never become a viable power supply in commercial applications.

REFERENCES

Elvin, N., Elvin, A. and Choi, D.H. 2003. "A Self-Powered Damage Detection Sensor," *Journal of Strain Analysis for Engineering Design*, 38(2):115–124.

Hausler, E. and Stein, E. 1984. "Implantable Physiological Power Supply with PVDF Film," *Ferroelectrics*, 60:277–282.

Hofmann, H., Ottman, G.K. and Lesieutre, G.A. 2002. "Optimized Piezoelectric Energy Circuit Using Step-Down Converter in Discontinuous Conduction Mode," *IEEE Transactions on Power Electronics*, 18(2):696–703.

Kasyap, A., Lim, J., Johnson, D., Horowitz, S., Nishida, T., Ngo, K., Sheplak, M. and Cattafesta, L. 2002. "Energy Reclamation from a Vibrating Piezoceramic Composite Beam," In: *Proceedings of 9th International Congress on Sound and Vibration*, Orlando, FL, Paper No. 271.

Kimura, M. 1998. "Piezoelectric Generation Device," United States Patent Number 5,801,475.

Kymissis, J., Kendall, D., Paradiso, J. and Gershenfeld, N. 1998. "Parasitic Power Harvesting in Shoes," In: *Second IEEE International Conference on Wearable Computing*, August, pp. 132–336.

Ottman, G.K., Hofmann, H., Bhatt, C.A. and Lesieutre, G.A. 2002. "Adaptive Piezoelectric Energy Harvesting Circuit for Wireless, Remote Power Supply," *IEEE Transactions on Power Electronics*, 17(5):1–8.

Ramsey, M.J. and Clark, W.W. 2001. "Piezoelectric Energy Harvesting for Bio MEMS Applications," In: *Proceedings of SPIE's 8th Annual Smart Materials and Structures Conference*, Vol. 4332, Newport Beach, CA, pp. 429–438.

Starner, T. 1996. "Human-Powered Wearable Computing," *IBM Systems Journal*, 35:618–629.

Sodano, H.A., Inman, D.J. and Park, G. 2004a. "Generation and Storage of Electricity from Power Harvesting Devices," *Journal of Intelligent Material Systems and Structures*, 16(1), pp. 67–75.

Sodano, H.A., Park, G. and Inman, D.J. 2004b. "Estimation of Electric Charge Output for Piezoelectric Energy Harvesting," *Journal of Strain*, 40(2):49–58.

Sodano, H.A., Park, G. and Inman, D.J. 2004c. "A Review of Power Harvesting from Vibration using Piezoelectric Materials," *The Shock and Vibration Digest*, 36(3):197–205.

Sodano, H.A., Lloyd, J. and Inman, D.J. 2004d. "An Experimental Comparison between Several Active Composite Actuators for Power Generation," In: *Proceedings of SPIE's 11th Annual International Symposium on Smart Structures and Materials*, San Diego, CA, March 14–18, Vol. 5390, pp. 370–378.

Umeda, M., Nakamura, K. and Ueha, S. May 1996. "Analysis of Transformation of Mechanical Impact Energy to Electrical Energy Using a Piezoelectric Vibrator," *Japanese Journal of Applied Physics, Part 1*, 35(5B):3267–3273.

Umeda, M., Nakamura, K. and Ueha, S. 1997. "Energy Storage Characteristics of a Piezo-Generator Using Impact Induced Vibration," *Japanese Journal of Applied Physics, Part 1*, 35(5B):3146–3151.

Wilkie, W.K., Bryant, R.G., High, J.W., Fox, R.L., Hellbaum, R.F., Jalink, A., Little, B.D. and Mirick, P.H. 2000. "Low-Cost Piezocomposite Actuator for Structural Control Applications," In: *Proceedings of SPIE's 7th International Symposium on Smart Structures and Materials*, Newport Beach, CA, March 5–9, Vol. 3991, pp. 323–334.

Williams, B.R., Park, G., Inman, D.J. and Wilkie, W.K. 2002. "An Overview of Composite Actuators with Piezoceramic Fibers," In: *Proceedings of 20th International Modal Analysis Conference*, Los Angeles, CA, February 4–7, Vol. 4753, pp. 421–427.

A Review of Power Harvesting from Vibration using Piezoelectric Materials

Henry A. Sodano, Daniel J. Inman and Gyuhae Park

ABSTRACT—The process of acquiring the energy surrounding a system and converting it into usable electrical energy is termed power harvesting. In the last few years, there has been a surge of research in the area of power harvesting. This increase in research has been brought on by the modern advances in wireless technology and low-power electronics such as microelectromechanical systems. The advances have allowed numerous doors to open for power harvesting systems in practical real-world applications. The use of piezoelectric materials to capitalize on the ambient vibrations surrounding a system is one method that has seen a dramatic rise in use for power harvesting. Piezoelectric materials have a crystalline structure that provides them with the ability to transform mechanical strain energy into electrical charge and, vice versa, to convert an applied electrical potential into mechanical strain. This property provides these materials with the ability to absorb mechanical energy from their surroundings, usually ambient vibration, and transform it into electrical energy that can be used to power other devices. While piezoelectric materials are the major method of harvesting energy, other methods do exist; for example, one of the conventional methods is the use of electromagnetic devices. In this paper we discuss the research that has been performed in the area of power harvesting and the future goals that must be achieved for power harvesting systems to find their way into everyday use.

KEYWORDS: power harvesting, energy scavenging, energy generation, piezoelectric.

1. Introduction

With the recent advances in wireless and microelectromechanical systems (MEMS) technology, the demand for portable electronics and wireless sensors is growing rapidly. Because these devices are portable, it becomes necessary that they carry their own power supply. In most cases this power supply is the conventional battery; however, problems can occur when using batteries because of their finite lifespan. For portable electronics, replacing the battery is problematic because the electronics could die at any time and replacement of the battery can become a tedious task. In the case of wireless sensors, these devices can be placed in very remote locations such as structural sensors on a bridge or global positioning system (GPS) tracking devices on animals in the wild. When the battery is extinguished of all its power, the sensor must be retrieved and the battery replaced. Because of the remote placement of these devices, obtaining the sensor simply to replace the battery can become a very expensive task or even impossible. For instance, in civil infrastructure applications it is often desirable to embed the sensor, making battery replacement unfeasible. If ambient energy in the surrounding medium could be obtained, then it could be used to replace or charge the battery. One method is to use piezoelectric materials to obtain energy lost due to vibrations of the host structure. This captured energy could then be used to prolong the life of the power supply or in the ideal case provide endless energy for the electronic devices lifespan. For these reasons, the amount of research devoted to power harvesting has been rapidly increasing. In this paper we review and detail some of the topics in power harvesting that have been receiving the most research, including energy harvesting from mechanical vibration, biological systems, and the effects of power harvesting on the vibration of a structure.

2. Fundamentals of Power Harvesting

The piezoelectric effect exists in two domains: the first is the direct piezoelectric effect that describes the material's ability to transform mechanical strain into electrical charge; the second form is the converse effect, which is the ability to convert an applied electrical potential into mechanical strain energy. The direct piezoelectric effect is responsible for the material's ability to function as a sensor and the converse piezoelectric effect is accountable for its ability to function as an actuator. A material is deemed piezoelectric when it has this ability to transform electrical energy into mechanical strain energy, and likewise to transform mechanical strain energy into electrical charge.

Piezoelectric materials belong to a larger class of materials called ferroelectrics. One of the defining traits of a ferroelectric material is that the molecular structure is oriented such that the material exhibits a local charge separation, know as an electric dipole. Throughout the material composition the electric dipoles are orientated randomly, but when the material is heated above a certain point, the Curie temperature, and a very strong electric field is applied, the electric dipoles

Henry A. Sodano and Daniel J. Inman, Center for Intelligent Material Systems and Structures, Virginia Polytechnic Institute and State University, Blacksburg, VA 24061, USA.
Gyuhae Park, Engineering Sciences and Applications, Weapon Response Group, Los Alamos National Laboratory, Los Alamos, NM 87545, USA.

The Shock and Vibration Digest, Vol. 36, No. 3, May 2004 197–205

DOI: 10.1177/0583102404043275

reorient themselves relative to the electric field; this process is termed poling. Once the material is cooled, the dipoles maintain their orientation and the material is then said to be poled. After the poling process is completed the material will exhibit the piezoelectric effect.

The mechanical and electrical behavior of a piezoelectric material can be modeled by two linearized constitutive equations. These equations contain two mechanical and two electrical variables. The direct effect and the converse effect may be modeled by the following matrix equations (IEEE Standard on Piezoelectricity, ANSI Standard 176-1987):

$$\text{direct piezoelectric effect: } \{D\} = [e]^T\{S\} + [\alpha^S]\{E\} \quad (1)$$

$$\text{converse piezoelectric effect: } \{T\} = [c^E]\{S\} - [e]\{E\} \quad (2)$$

Here, {D} is the electric displacement vector, {T} is the stress vector, [e] is the dielectric permittivity matrix, $[c^E]$ is the matrix of elastic coefficients at constant electric field strength, {S} is the strain vector, $[\alpha^S]$ is the dielectric matrix at constant mechanical strain, and {E} is the electric field vector.

After the material has been poled, an electric field can be applied in order to induce an expansion or contraction of the material. However, the electric field can be applied along any surface of the material, each resulting in a potentially different stress and strain generation. Therefore, the piezoelectric properties must contain a sign convention to facilitate this ability to apply electric potential in three directions. For the sake of keeping this discussion simple, the piezoelectric material can be generalized for two cases. The first is the stack configuration that operates in the –33 mode and the second is the bender, which operates in the –13 mode. The sign convention assumes that the poling direction is always in the "3" direction, with this point the two modes of operation can be understood. In the –33 mode, the electric field is applied in the "3" direction and the material is strained in the poling or "3" direction; in the –31 mode, the electric field is applied in the "3" direction and the material is strained in the "1" direction or perpendicular to the poling direction. These two modes of operation are particularly important when defining the electromechanical coupling coefficient that occurs in two forms: the first is the actuation term *d*, and the second is the sensor term *g*. Thus g_{13} refers to the sensing coefficient for a bending element poled in the "3" direction and strained along "1".

A full description of the piezoelectric effect and the methods used to model the behavior of these materials is beyond the scope of this paper. However, a significant number of journal papers and conference proceedings develop accurate models and discuss the fundamentals of these materials in great detail (Crawley and de Luis, 1987; Crawley and Anderson, 1990; Hagood et al., 1990; Smits and Choi, 1991; Smits et al., 1991; Near, 1996; Inman and Cudney, 2000; Niezrecki et al., 2001) as well as numerous books published on this topic (Gandhi and Thompson, 1992; Ikeda, 1996; Banks et al., 1996; Culshaw, 1996; Clark et al., 1998; Srinivasan and McFarland, 2001; Worden et al., 2003).

In the following sections of the paper we break the various works on power harvesting into the following groups: mechanical vibration, power harvesting efficiency, power storage and circuitry, implantable and wearable power supplies, and damping induced by power harvesting. In Section 3, we discuss one paper that investigates the amount of energy available from one power harvesting device subjected to a vibration environment. In Section 4 we look at research that was performed to classify the efficiency of certain methods of power harvesting. In Section 5 we look at research into various types of power storage mediums and different circuits developed to maximize the electric power generated. A large portion of work has been performed in the field of power harvesting from biological systems and, while the papers found in section 6 may deal with various subjects, they all have a major focus on the ability to obtain energy from human or animal activity. Section 7 will detail work into quantifying the effect of power harvesting on the dynamics of a vibrating structure.

3. Mechanical Vibration

One of the most effective methods of implementing a power harvesting system is to use mechanical vibration to apply strain energy to the piezoelectric material or displace an electromagnetic coil. Power generation from mechanical vibration usually uses ambient vibration around the power harvesting device as an energy source, and then converts it into useful electrical energy, in order to power other devices. The research in the following three sections has made use of mechanical vibration in order to quantify the efficiency and amount of power capable of being generated, as well as to power various electronic systems, ranging from digital electronics to wireless transmitters.

Williams and Yates (1996) proposed a device, which generated electricity when embedded in a vibrating environment. For their evaluation, an electromagnetic transducer was chosen. A harmonic analysis of the generator was performed in order to evaluate the viability of the device and to optimize the design. It was determined from the analysis that the amount of power generated was proportional to the cube of the vibration frequency. This illustrated that the generator was likely to perform poorly at low frequencies. It was also determined that a low damping factor was required to maximize power generation, therefore the design must allow for large deflections of the mass. For a typical device the predicted power generation was 1 μW at an excitation frequency of 70 Hz, and 0.1 mW at 330 Hz (assuming a deflection of 50 μm).

4. Power Harvesting Efficiency

The two papers in this section investigate the efficiency of a piezoelectric generator. The first paper looks at the efficiency of a piezoelectric vibrating in the –31 direction and the second paper tests a stack that operates in the –33 direction. It is important to quantify the efficiency of the power harvesting medium in order to allow the device to be designed to function optimally in its intended environment.

Umeda et al. (1996) carried out an investigation concerning the fundamentals of a generator, which transformed mechanical energy to electrical energy using a piezoelectric vibrator and a steel ball. They also investigated the effect of the various characteristics of the piezoelectric vibrator. To simulate the generation mechanism, they introduced an electrical equivalent model. The fundamental modes of bending

vibration for two models were calculated: model A (the transducer with the steel ball) and model B (the transducer only). The admittance characteristics of each model were measured and they found that it was clear that the peak frequencies corresponded to the vibration modes. It was seen that the calculated waveforms of the output voltage were similar to the measured ones; therefore, the model provided an accurate simulation of the output voltage. An efficiency curve was drawn for various input mechanical energies, and they determined that as the potential energy of the ball increased the maximum efficiency decreased. A large part of the applied energy was returned to the steel ball in the form of kinetic energy causing it to bounce off the plate. It was concluded that the energy generated would be large if the steel ball did not bounce off after an impact but rather vibrated with the piezoelectric plate. This case was simulated and it was determined that a maximum efficiency of 52% could be obtained. The effects of the characteristics of the piezoelectric vibrator were investigated and it was determined that the efficiency increased if the mechanical quality factor increased, the electromechanical coupling coefficient increased and the dielectric loss decreased.

Goldfarb and Jones (1999) have analyzed the efficiency of the piezoelectric material in a stack configuration for the purpose of electric energy generation. An analytical model is presented and suggests that the fundamental problem in generating electrical power from the piezoelectric material is that it stores the majority of the energy produced and returns it to the excitation source that initially caused the charge to be generated. They state that this occurrence is particularly problematic when the piezoceramic is placed in parallel with a capacitor that is in series with the load. Therefore, it is suggested that the maximum efficiency of power generation can be achieved by minimizing the amount of energy stored inside the piezoelectric material. The efficiency of the model was determined across a spectrum of frequencies and resistive values. It was found that, at frequencies above 100 Hz, the efficiency of the stack actuator was negligible and that the highest efficiency was obtained at 5 Hz. This frequency is far lower than the first mechanical and electromechanical resonances of the stack, which occur at approximately 40 and 60 kHz, respectively. The authors state that the frequency of maximum efficiency occurs so low because of the energetic structure of the stack. In addition, it is found that the efficiency of the stack is most strongly dependent on the frequency of excitation, with the load resistance providing a lower effect on it.

5. Power Storage and Circuitry

When using piezoelectric materials as a means of gathering energy from the surroundings, in most cases it is a necessity that a means of storing the energy generated be used. Without accumulating a significant amount of energy, the power harvesting system will not be a feasible power source for most electronics. The following research has made use of circuitry to either store the energy generated by the piezoelectric material or to develop circuits that allow the energy to be removed from the piezoelectric in a more efficient way allowing more power to be generated.

Umeda et al. (1997) continued their investigation with a study into the characteristics of energy storage by a piezo-generator with a bridge rectifier and capacitor. As in their previous research, the piezo-generator consisted of a steel ball and a piezoelectric vibrator, and with the introduction of a bridge rectifier and capacitor they were able to determine the energy storage characteristics both theoretically and experimentally. To simulate the generation and storage mechanism they employed an equivalent circuit model, where the input mechanical energy was translated into an initial electrical energy. Changing the parameters of the circuit simulated the separation of the vibrator and the ball. After examining the storage characteristics for the first impact they determined that as the capacitance increased the electrical charge increased due to an increased duration of oscillation. They also determined that for each value of capacitance as the initial voltage increased the stored electric charge decreased, and the efficiency increased. When considering the overall storage characteristics for multiple impacts they determined that, for each value of capacitance, the first impact gave the largest electric charge. The overall storage characteristics were observed when the initial voltage was changed; as the initial voltage increased, the electric charge decreased for each value of capacitance, while the efficiency increased. Their prototype achieved a maximum efficiency of 35%, over three times that of a solar cell.

Elvin et al. (2001) used a polyvinylidene fluoride (PVDF) piezofilm sensor attached to a simply-supported Plexiglas beam with an aspect ratio of 0.11 to generate an electrical signal. The goal of this power harvesting experiment was to generate sufficient energy from the strain induced on the piezofilm by the bending beam to power a telemetry circuit. The energy generated from the PVDF patch was accumulated in a capacitor. A switch was added to the circuitry to allow the capacitor to charge to a predetermined value of 1.1 V, at which point the switch would open and the capacitor would discharge through the transmitter. Once the capacitor had discharged to a value of 0.8 V, the switch would close and the capacitor would be allowed to recharge and repeat the process. The operation of the power harvesting system was found to provide the required energy to power the circuitry and transmit a signal containing information regarding the strain of the beam a distance of 2 m.

Kasyap et al. (2002) developed a lumped element model (LEM) using an equivalent circuit model to describe the power generated from the forced vibration of a cantilever beam with a piezoelectric element attached. It was found that the LEM provided results consistent with those generated using a finite element model from excitation frequencies ranging from DC through the first resonance of the beam. A similar result was found during a second model validation using experimental results. The goal of the study was to use a flyback converter to increase the efficiency of the power transfer from the piezoelectric patch to a power storage medium. The use of a flyback converter allows the circuit impedance to be matched with the impedance of the piezoelectric device. It was found that when using the flyback converter a peak power efficiency of 20% was achieved.

The previous papers in this section concentrated their efforts on the use of a capacitor as the storage medium. However, in most cases the capacitor is not an efficient method of storing energy. Sodano et al. (2002) performed a study to investigate the amount of power generated through the vibration of a piezoelectric plate, as well as two methods of power

storage. The plate was excited using an electromagnetic shaker with both resonant and random excitation signals. It was found that the piezoelectric could generate a maximum power of 2 mW when excited at the resonant frequency of the clamped-free plate. In addition, the ability of the piezoelectric plate to store its power in both a capacitor circuit and a rechargeable battery was tested. This paper was the first to demonstrate that the power output of piezoelectric material was able to recharge a fully discharged battery without the use of external energy sources. It was also shown that both methods of power storage could be used; however, the use of rechargeable batteries was found to possess power storage qualities that would allow a far larger range of electronic devices to be powered than the capacitor. This is because of the capacitor's poor ability to store large amounts of power and its fast discharge rate, which caused the output of the circuit to switch on and off making a periodic power supply.

Following the work of Sodano et al. (2002), a second paper was published (Sodano et al., 2003) to further investigate the ability of piezoelectric materials to recharge batteries. This study compared the macro-fiber composite (MFC) actuator with the monolithic piezoceramic material PZT for recharging batteries. The MFC is an actuator that uses piezofibers and interdigitated electrodes to capitalize on the higher g_{33} piezoelectric coupling coefficient, allowing it to produce higher strain and force than typical monolithic PZT (Sodano et al., 2004a). This property of the actuator makes it attractive for power harvesting applications. First, the efficiency of both the MFC and PZT was determined in order to compare their ability to generate electrical energy. It was determined that the MFC was less effective for power harvesting than the PZT because of a very low current generation by the MFC. Reasons for the low current generation were proposed. Furthermore, because of the poor current output of the MFC it was found to be ineffective at charging the batteries due to their requirement for fairly significant current. However, the PZT was used to charge a variety of different capacity nickel metal hydride batteries; a typical charge cycle of one battery is shown in Figure 1. The charge time for each was supplied and the maximum capacity battery capable of efficiently being charged was determined.

Another investigation into the ability to store and use the energy generated from a power harvesting device was performed by Amirtharajah and Chandrakasan (1998). They designed and tested a chip which integrated a finite impulse response (FIR) filter, power field-effect transistors (FETs) and pulse width modulation (PWM) control circuitry, in order to demonstrate the possibility of running a digital system from the power generated by vibrations in its environment. They proposed a self-powered system consisting of a load circuit, a generator to create voltage that could vary depending on the environment, a voltage regulator to set the voltage to a desired level, and a backup power source. The implementation of a backup power source was required at circuit startup because of the need for the voltage regulator to obtain its power from a source other than the generator, whose output was too uncontrolled to be utilized. An inertial electromechanical generator and acoustic generator were proposed as the power supply and a prototype of each was built to test its ability to power the digital circuitry. It was found that the electromagnetic generator was capable of supplying 400 μW of power during a typical excitation that was intended to represent that of a human walking. The electromagnetic prototype was tested and it was shown that the portable digital system could be powered entirely from ambient environmental vibrations for a period of 23 ms. A second investigation into the use of incident sound as a form of excitation energy was also tested and it was found that it could generate power sufficient to run the system; however, the acoustic energy source was limited to very high noise environments (about 114 dB).

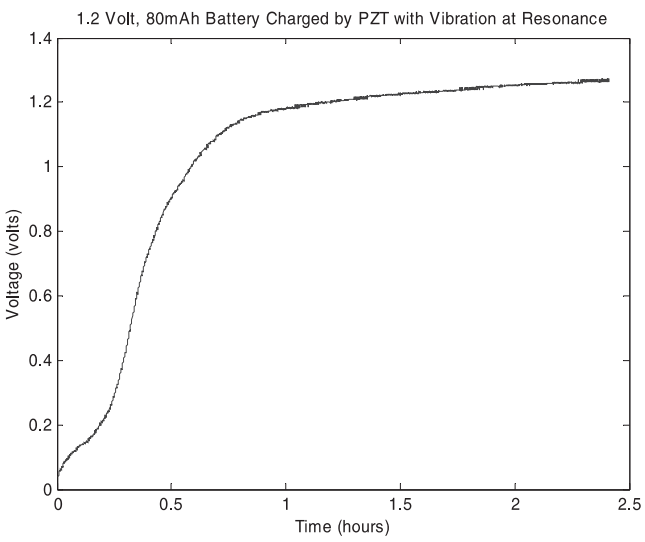

Figure 1. Typical charge cycle of a nickel metal hydride battery; in this case an 80 mAh battery was charged (Sodano et al., 2003)

Rather than developing methods of accumulating the energy developed by piezoelectric materials, Ottman et al. (2002) worked to develop a circuit that would maximize the power flow from the piezoelectric device. A DC–DC step-down converter was implemented in coordination with a wave rectifier, capacitor, and electrochemical battery. In addition to the circuitry, an adaptive control technique was developed to continuously implement optimal power transfer theory and to maximize the power flow into the battery. This active controller varied the switching frequency of the step-down converter to maximize to the power flow from the piezoelectric elements and to raise the current to levels more acceptable for maintaining the charge on batteries. The circuit and controller were built and tested on a bimorph piezoelectric cantilever plate excited at resonance. It was found that when using the circuit, over four times the energy was transferred to the battery than with direct charging alone. However, if the power harvesting medium produced less than 10 V, then power flow into the battery was reduced because of losses in the additional circuit components.

Hofmann et al. (2002) have continued the work of Ottman et al. (2002) by implementing circuitry to maximize the power flow from the piezoelectric device. This study uses a similar circuit as before, but realizes that one of the drawbacks of their previous work was that the PWM control circuitry required more power than was produced at low levels of excitation. In order to correct this problem, the authors realized that the optimal duty cycle changes very little at higher levels of energy generation when excited with a sinusoidal sig-

nal. Therefore, the control circuitry was removed and a constant duty cycle was used. Furthermore, at low levels of power generation the optimal duty cycle varies greatly, causing the PWM generation circuitry to be ineffective; thus, this circuitry is bypassed at a certain threshold and a pulse-charging circuit is used. The optimal value of the duty cycle was investigated both analytically and experimentally, resulting in a value of 2.8%. With this circuit, the power flow was increased by over a factor of 3 at a peak resonant excitation level of 70 V open circuit. Additionally, their circuitry was found to reach values as high as 70% efficiency at an optimal value of excitation.

Lesieutre et al. (2002) discuss two topics: the first is an energy harvesting circuit and the second a measure of the damping induced in a structure due to energy harvesting, which will be discussed in a section 7. The goal of the first portion of this research was to further improve upon a circuit that would maximize the energy output of the piezoelectric material through the use of a DC–DC step-down converter. The energy harvesting circuit was developed to improve on two previously constructed circuits in Ottman et al. (2002) and Hoffman et al. (2002). The first circuit used a controller to modify the PWM of a DC–DC step-down converter, which consumed a significant amount of power. Additionally, their circuit used the controller at all times, which means that when the piezoelectric produces a very small amount of energy the controller would be drawing more energy than available. To correct this problem, a second circuit was developed using a constant near-optimal duty cycle and the control circuitry was removed. However, the circuit was still inefficient when less than 25 V open circuit was generated. Therefore, to further correct this issue the pulse-charging circuitry that turned on below 25 V open circuit was done away with and only direct charging was used in this range. This circuit was found to provide a 324% increase in power when excited at a level sufficient to produce 68 V open circuit and it alleviated many of the shortcomings of the previously used circuits.

6. Implantable and Wearable Power Supplies

In an effort to incorporate computers and digital systems into our everyday lives, research has been carried out to investigate the possibility and practicality of imbedding them into our clothing, or inside biological systems such as the human body. The use of power harvesting devices to capture the energy lost during everyday human life is a captivating idea and has been one of the main topics facilitating the rapid growth of the power harvesting field. The following research presented here has investigated numerous ideas of obtaining energy from both human and animal activity.

Possibly the first investigation of power scavenging systems incorporated into a biological environment was performed in 1984 by Hausler and Stein, who published a paper proposing the use of an implantable physiological power supply using PVDF films (Hausler and Stein, 1984). Based on the concept that the energy expended for respiration could be converted into electric power, Hausler and Stein used the relative motion of the ribs to periodically stretch a converter. A miniaturized prototype was designed and used to conduct an animal experiment. The converter was fixed to the ribs of a mongrel dog and spontaneous breathing led to a peak voltage of 18 V, which corresponded to a power of about 17 μW. However, the power generated was insufficient to power the desired electronics, making it ineffective for use as an implanted power supply. It is speculated that optimization of the PVDF film properties, as well as a more suitable converter attachment at the ribs would make it possible to develop power converters with an output of 1 mW, yielding a mechanical power load of 20 mW. In addition, this study was performed at an early stage in low-power electronic and computer technology, suggesting that the use of more efficient electronics, now available, would have resulted in significantly more promising results.

Throughout our daily activity, a significant amount of energy is expended in various forms, some of which make for attractive power harvesting locations. Starner (1996) has performed an investigation into the amount of power expended for a vast range of human activities. His paper explores the possibility of eliminating bulky and inconvenient power systems by harnessing the energy expended in everyday activity and using it to generate power for a computer. The paper contains a survey of various power generation methods ranging from body heat and breath to finger and upper limb motion. An analysis of the power available from each of the different locations is presented. He calculates that approximately 67 W of power is lost during walking and that a piezoelectric device mounted inside a shoe with a conversion efficiency of 12.5% could achieve 8.4 W of power. Two methods of power generation during walking are identified, piezoelectric and rotary generator, with the advantages and weaknesses of each outlined. One idea he explains is to place piezofilm patches in the joints of clothing to harvest the energy lost during bending and he states that about 0.33 W could be obtained. In addition to investigating the possible location and power converters to be used, he realizes that the energy generated will never be constant and, at times, energy may not be produced at all, making the use of a power storage medium a must. Power would be accumulated when the energy is plentiful and would be used when insufficient energy is produced. The paper investigates two methods of power storage: the capacitor and rechargeable batteries. He states that energy storage in a capacitor would be sufficient for low-power areas such as blood pressure and body heat, but rechargeable batteries are a necessity for higher power areas, such as limb motion and walking.

The work of Starner (1996) brought the possibility of power harvesting locations around the human body to the attention of many researchers and the work in wearable power supplies began to grow. Post and Orth (1997) investigated the concept of "smart fabric" for wearable clothing. Their research described techniques used in building circuits from commercially available fabrics, fasteners, etc. Multiple different conductive fabrics were explored, including silk organza, constructed of silk thread wrapped in thin copper foil running in one direction and plain silk in the other. This material was highly conductive, had a high tensile strength, and could withstand high temperatures, allowing it to be sewn using industrial machines. A second type of conductive yarn is manufactured with both conductive and cloth fiber interspersed throughout the material. Post and Orth (1997) state that by varying the amount of conductive material the resistance of the fiber can be adjusted and other components, such as capacitors and coils, can be sewn directly into the fabric.

The use of this type of material has led to the development of several devices constructed of fabric, including a type of fabric keyboard that can be crumpled up, thrown in the wash and even used as a potholder without losing its ability to function. These materials would be very effective for transmitting the energy generated around the body to the storage medium in a convenient and unnoticeable way.

Kymissis et al. (1998) studied the use of piezoelectric actuators located inside the sole of a shoe for power harvesting. Their research examined three different devices that could be built into a shoe to harvest excess energy and generate electrical power parasitically while walking. The devices that were considered included a "Thunder" actuator constructed of piezoceramic composite material located in the heel, a rotary magnetic generator also located under the heel, and a multilayer PVDF foil laminate patch located in the sole of the shoe. The Thunder actuator was developed by the National Aeronautics and Space Administration (NASA) and has a rainbow (arch) configuration that allows the high impact vertical energy of the heel to be translated into bending strain for electrical power generation. The electromagnetic generator used the pressure of the heel to spin a flywheel and rotary generator, to extract the power from the pressure of the heel during walking. The last device used was the laminate of piezofilm, or "stave", which was used to harness the energy lost during the bending of the sole. In order to compare the performance of the three methods, a working prototype was constructed for each and its performance was measured. The peak powers were observed to approach 20 mW for the PVDF stave and 80 mW for the PZT unimorph. However, because of slow excitation, the average power generated from both the PVDF stave and the Thunder actuator was significantly lower, approximately 1 and 2 mW, respectively. The shoe mounted rotary generator resulted in a peak power of about 1 W and averaged to about 0.25 W over a 5 s sample period. However, the rotary generator was not easily integrated into the shoe and significantly interfered with the user's gait, unlike the PVDF stave and PZT Thunder actuator. Because of these two limitations of the rotary generator, it was determined that it was an unrealistic method of generating energy during walking. After examining the performance of the piezoelectric generators, their ability to power a battery-less active radio-frequency (RF) tag was tested. The authors developed a circuit that used a capacitor to accumulate the electrical energy along with various other components to regulate the charging and discharging cycle of the capacitor. The discharge of the capacitor was limited at 5 V to accommodate an encoder and transmitter used to transmit the RF tag. The circuit was found to be compatible with both the shoe mounted piezoelectric generator systems and was able to transmit five to six 12-bit signals every few steps. The circuitry developed in this study has also found use in the work of several other researchers. The research presented in this paper demonstrated the potential of piezoelectric power harvesting devices for use as a power supply of self-powered electronics. Further, the ability to use energy from power harvesting for transmitting data was shown and gained the attention of many researchers in the area of self-powered wireless sensors.

Similar to the work of Kymissis et al. (1998), Shenck (1999) demonstrated electrical energy generation from piezoelectric patches located in a shoe. He evaluated different regulation systems for conditioning the electrical energy harnessed by the piezoceramic source imbedded in the sole of a shoe. A rigid bimorph piezoceramic transducer was developed and integrated into a mass produced shoe insert. The use of a bimorph piezoelectric device posed several advantages over the previously used actuator. Since the vertical displacement of the transducer was required to be very small, so the use of a second piezoelectric patch allowed more energy to be generated. Additionally, with two piezoelectric patches present the electrical leads could be configured as parallel energy sources, improving the lumped impedance characteristics of the sources. Furthermore, it was determined that a bimorph transducer was stronger and less intrusive to the user, because it was capable of better adapting to various distributions of body weight and footfall velocity. The piezoelectric patch was configured similarly to the Thunder actuator previously mentioned, allowing it to absorb the energy of a heel strike and lift during walking, thus inducing a charge across the capacitive PZT. The energy stored was removed at its peak and converted into a useful form using a high-frequency switching technique.

A design study was conducted by Ramsey and Clark (2001), which investigated the feasibility of using a piezoelectric transducer as a power supply for an *in vivo* MEMS application. The 33- and 31- modes of operation for a piezoelectric generator were analyzed and compared, and it was determined that when using the 31- mode, or thin plate configuration, there existed a strong mechanical advantage in converting applied pressure to working stress. For very low-pressure sources, the 31- mode had a greater advantage in energy conversion, which became important when attempting to implement this technology in a biological microsystem application. A design study was used to investigate whether or not the 31- mode was well suited for the *in vivo* environment, and it was carried out using a square thin plate driven by blood pressure. It was shown that ample power existed from various sources in the body to meet the requirements of their investigation, and additional calculations illustrated the feasibility of providing intermittent power instead of continuous power.

7. Damping Effect of Power Harvesting

When a power harvesting system is integrated into a structure, energy is removed in the form of electricity. Because energy is removed from the structure, it must see some effect on its dynamics. The subsequent papers have looked to quantify this damping effect.

Lesieutre et al. (2002) investigated the damping added to a structure due to the removal of electrical energy from the system during power harvesting. The damping was first estimated using analytical methods and later verified through experimental results. It is stated that optimal power transfer is achieved when the operating rectifier output voltage is half the open circuit voltage; this assumption allows the effective loss factor of the system to be dependent only on the coupling coefficient. Using this simplification the study analytically predicted the damping loss factor from power harvesting to be 2.3% in the fundamental mode of vibration of a cantilever beam. The prediction was then verified to be 2.2% through experimental results, showing excellent agreement between theory and their experimental work. This result was found

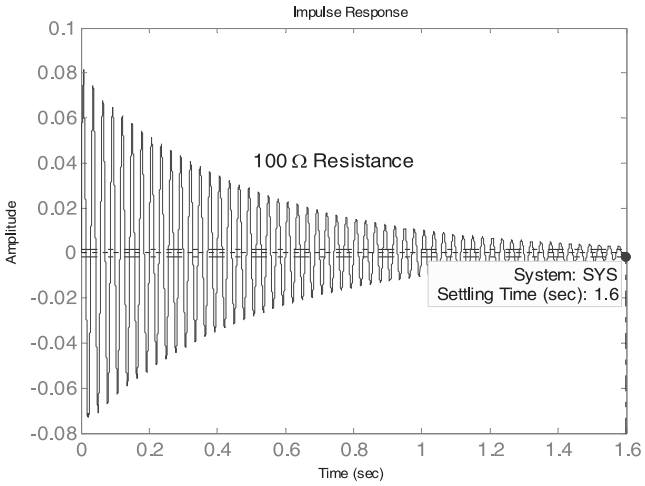

Figure 2. Impulse response with a 100Ω resistive load (Sodano et al., 2004a)

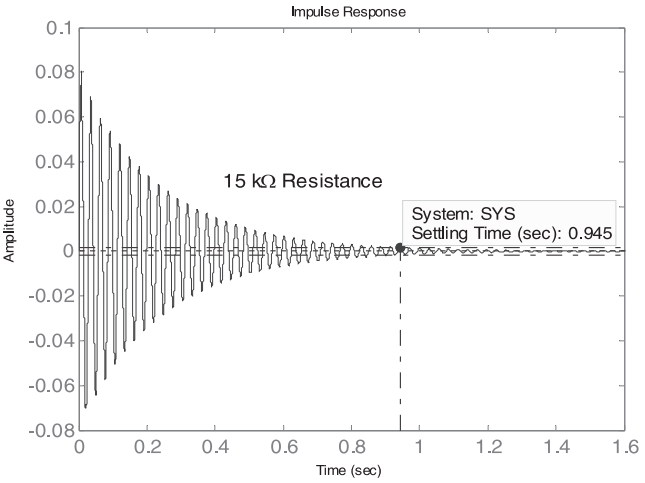

Figure 3. Impulse response with a 15 kΩ resistive load (Sodano et al., 2004a)

to be comparable to that of resistive shunting while not having the frequency dependency that shunting does.

Sodano et al. (2004b) presented a paper that developed a model of a power harvesting system. The model was derived from variational principles and was used to predict the amount of electrical energy that could be generated through the vibration of piezoelectric patches on a beam structure. To validate the accuracy of the model, a composite beam with a complex layout of four piezoelectric patches was experimentally tested and compared to the results of the simulation. It was shown that the model provided a very accurate estimate of the power generated independent of the excitation frequency and load resistance. Following the validation of the model, it was used to show the effects of power harvesting on the damping of a structure that has energy being generated from it. The impulse response of a cantilever beam was shown for a power harvesting system that had three different load resistances; the effect of power harvesting on each of these

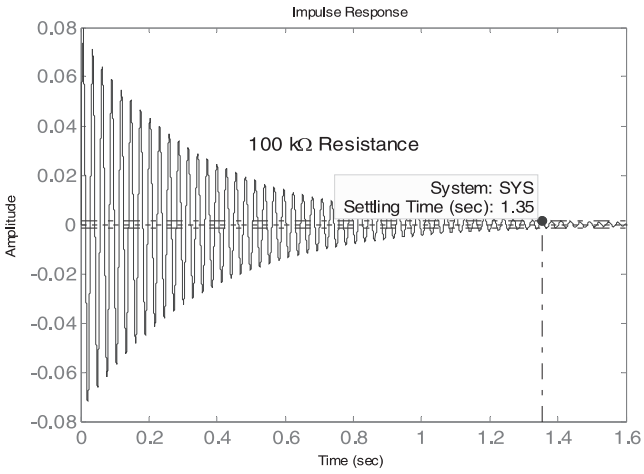

Figure 4. Impulse response with a 100 kΩ resistive load (Sodano et al., 2004a)

three cases is shown in Figures 2, 3 and 4. It was shown that for a small load resistance, the damping did not become much larger than the mechanical damping of the structure, because only a slight amount of energy was being removed from the system. As the resistance increases, more energy is removed from the system and the damping increases, as shown in Figure 3. At the optimal load resistance the maximum energy is removed from the system and the damping becomes far larger than that of the structure. As the load resistance moves past the optimal value the damping begins to decrease again, as shown in Figure 4. The damping begins to decrease at higher load resistances because as the load increases in impedance the circuit begins to look like an open circuit, thus interfering with the ability of the generated electricity to efficiently flow out of the piezoelectric material. This simulation showed that power harvesting works very much like a shunt damping system with the major difference being that the energy is stored rather than dissipated.

8. Future of Power Harvesting

The idea of carrying electronic devices such as a portable radio and never worrying about when the batteries will need to be replaced could be far closer than one would think. This thought has caused the desire for self-powered electronics to grow quickly, leaving only one limitation before these devices can become a reality. The one issue that still needs to be resolved is a method to generate sufficient energy to power the necessary electronics. However, with the advances in power harvesting that have been outlined in this paper the ability to obtain and accumulate the necessary amount of energy to power such devices is clearly possible.

The major limitations facing researchers in the field of power harvesting revolve around the fact that the power generated by piezoelectric materials is far too small to power most electronics. Therefore, methods of increasing the amount of energy generated by the power harvesting device or developing new and innovative methods of accumulating the energy are the key technologies that will allow power harvest-

ing to become a source of power for portable electronics and wireless sensors. One recent advance that shows great promise for power harvesting is the use of rechargeable batteries as a means of accumulating the energy generated during power harvesting. Much of the early research into power harvesting looked to the capacitor as a method of storing energy and powering electronics. However, the capacitor has poor power storage characteristics because of its quick discharge time, causing the electrical output of such circuitry to switch on and off as the capacitor charges and discharges. This aspect of the capacitor is not suitable for powering computational electronics. However, the rechargeable battery can be charged and then used to run any number of electronic devices for an extended period of time while being continuously charged by ambient motion. Innovations in power storage such as the use of rechargeable batteries with piezoelectric materials must be discovered before power harvesting technology will see widespread use.

Furthermore, the efficiency of the power harvesting circuitry must be maximized to allow the full amount of energy generated to be transferred to the storage medium. The continuous advances that are being made in low-power electronics must be studied and utilized both to optimize power flow from the piezoelectric and to minimize circuit losses. Gains in this area are a necessity for the successful use of piezoelectric materials as power harvesting devices. Additionally, the intended location of the power harvesting system must be identified so that its placement can be optimized and the excitation range realized to allow for tuning of the power harvesting device. By tuning the power harvesting medium with the structure, the excitation can be made to maximize the strain of the piezoelectric material using the concept of resonance.

Finally, practical applications for power harvesting systems such as wireless sensors and self-powered damage detection units must be clearly identified to encourage growth in this area of research, thus allowing the contributions and in flow of ideas to increase. With the advances in wireless technology and low-power electronics, power harvesting is the missing link for completely self-powered systems.

References

Amirtharajah, R., and Chandrakasan, A. P, 1998, "Self-Powered Signal Processing Using Vibration Based Power Generation," *IEEE Journal of Solid-State Circuits*, Vol. 33, No. 5, 687–695.

Banks, H. T., Smith, R. C., and Wang, Y., 1996, *Smart Materials and Structures: Modelling, Estimation and Control*, Wiley, New York.

Clark, R. L., Saunders, W. R., and Gibbs, G. P., 1998, *Adaptive Structures: Dynamics and Control*, Wiley, New York.

Crawley, E., and Anderson, E., 1990, "Detailed Models of Piezoceramic Actuation of Beams," *Journal of Intelligent Materials and Structures*, Vol. 1, No. 1, 4–25.

Crawley, E. F., and de Luis, J., 1987, "Use of Piezoelectric Actuators as Elements of Intelligent Structures", *AIAA Journal*, Vol. 25, No. 10, 1373–1385.

Culshaw, B., 1996, *Smart Structures and Materials*, Artech House, Boston, MA.

Elvin, N. G., Elvin, A. A., and Spector, M., 2001, "A Self-Powered Mechanical Strain Energy Sensor," *Smart Materials and Structures*, Vol. 10, 293–299.

Gandhi, M. V., and Thompson, B. S., 1992, *Smart Materials and Structures*, Kluwer Academic, Dordrecht.

Goldfarb, M., and Jones, L. D., 1999, "On the Efficiency of Electric Power Generation with Piezoelectric Ceramic," *ASME Journal of Dynamic Systems, Measurement, and Control*, Vol. 121, 566–571.

Hagood, N. W., Chung, W. H., and von Flotow, A., 1990, "Modeling of Piezoelectric Actuator Dynamics for Active Structural Control," *Journal of Intelligent Materials Systems and Structures*, Vol. 1, 327–354.

Hausler, E., and Stein, E., 1984, "Implantable Physiological Power Supply with PVDF Film," *Ferroelectrics*, Vol. 60, 277–282.

Hofmann, H., Ottman, G. K., and Lesieutre, G. A., 2002, "Optimized Piezoelectric Energy Circuit Using Step-Down Converter in Discontinuous Conduction Mode," *IEEE Transactions on Power Electronics*, Vol. 18, No. 2, 696–703.

Ikeda, T., 1996, *Fundamentals of Piezoelectricity*, Oxford University Press, New York.

Inman, D. J., and Cudney, H. H., 2000, "Structural and Machine Design Using Piezoceramic Materials: a Guide for Structural Design Engineers," Final Report NASA Langley Grant NAG-1-1998.

Kasyap, A., Lim, J., Johnson, D., Horowitz, S., Nishida, T., Ngo, K., Sheplak, M., and Cattafesta, L., 2002, "Energy Reclamation from a Vibrating Piezoceramic Composite Beam," in Proceedings of 9th International Congress on Sound and Vibration, Orlando, FL, Paper No. 271.

Kymissis, J., Kendall, C., Paradiso, J., and Gershenfeld, N., 1998, "Parasitic Power Harvesting in Shoes," in Proceedings of the 2nd IEEE International Symposium on Wearable Computers, October 19–20, Pittsburg, PA, 132–139.

Lesieutre, G. A., Hofmann, H. F., and Ottman, G. K., 2002, "Electric Power Generation from Piezoelectric Materials," in Proceedings of the 13th International Conference on Adaptive Structures and Technologies, October 7–9, Potsdam/Berlin, Germany.

Near, C. D., 1996, "Piezoelectric Actuator Technology," in Smart Structures and Materials 1996: Smart Structures and Integrated Systems, San Diego, CA, *Proceedings of SPIE*, Vol. 2717, 246–258.

Niezrecki, C., Brei, D., Balakrishnam, S., and Moskalik, A., 2001, "Piezoelectric Actuation: The State of the Art," *Shock and Vibration Digest*, Vol. 33, No. 4, 269–280.

Ottman, G. K., Hofmann, H., Bhatt A. C., and Lesieutre, G. A., 2002, "Adaptive Piezoelectric Energy Harvesting Circuit for Wireless, Remote Power Supply," *IEEE Transactions on Power Electronics*, Vol. 17, No.5, 669–676.

Post, E. R., and Orth, M., 1997, "Smart Fabric, or Wearable Clothing," in Proceedings of the 1st International Symposium on Wearable Computers, October 13–14, Cambridge, MA, 167–168.

Ramsey, M. J., and Clark, W. W., 2001, "Piezoelectric Energy Harvesting for Bio MEMS Applications," in Proceedings of the SPIE 8th Annual Smart Materials and Structures Conference, Newport Beach, CA, Vol. 4332-2001, 429–438.

Shenck, N. S., 1999, "A Demonstration of Useful Electric Energy Generation from Piezoceramics in a Shoe," Masters of Science Thesis Proposal, Department of Electrical Engineering and Computer Science, Massachusetts Institute of Technology.

Smits, J., Dalke, S., and Cooney, T. K., 1991, "The Constituent Equations of Piezoelectric Bimorphs," *Sensors and Actuators*, Vol. 28, 41–61.

Smits, J., and Choi, W., 1991, "The Constituent Equations of Heterogeneous Bimorphs," *IEEE Transactions on Ultrasonic, Ferroelectrics and Frequency Control*, Vol. 38, No. 3, 256–270.

Sodano, H. A., Magliula, E. A., Park, G., and Inman, D. J., 2002, "Electric Power Generation from Piezoelectric Materials," in Proceedings of the 13th International Conference on Adaptive Structures and Technologies, October 7–9, Potsdam/Berlin, Germany.

Sodano, H. A., Park, G., Leo, D. J., and Inman, D. J., 2003, "Use of Piezoelectric Energy Harvesting Devices for Charging Batteries," in SPIE 10th Annual International Symposium on Smart Structures and Materials, March 2–6, San Diego, CA, Vol. 5050, pp. 101–108.

Sodano, H. A., Park, G., and Inman, D. J., 2004a, "An Investigation into the Performance of Macro-Fiber composites for Sensing and Structural Vibration Applications," *Mechanical Systems and Signal Processing*, Vol. 18, pp. 683–697.

Sodano, H. A., Park, G., Leo, D. J., and Inman, D. J., 2004b, "Model of Piezoelectric Power Harvesting Beam," in ASME International Mechanical Engineering Congress and Expo, November 15–21, Washington, DC, Vol. 40, No. 2.

Srinivasan, A. V., and McFarland, D. M., 2001, *Smart Structures: Analysis and Design*, Cambridge University Press, Cambridge.

Starner, T., 1996, "Human-Powered Wearable Computing," *IBM Systems Journal*, Vol. 35 No. 3–4, 618–628.

Umeda, M., Nakamura, K., and Ueha, S., 1996, "Analysis of Transformation of Mechanical Impact Energy to Electrical Energy Using a Piezoelectric Vibrator," *Japanese Journal of Applied Physics*, Vol. 35, Part 1, No. 5B, 3267–3273.

Umeda, M., Nakamura, K., and Ueha, S., 1997, "Energy Storage Characteristics of a Piezo-Generator using Impact Induced Vibration," *Japanese Journal of Applied Physics*, Vol. 36, Part 1, No. 5B, 3146–3151.

Williams, C. B., and Yates, R. B., 1996, "Analysis of a Micro-Electric Generator for Microsystems," *Sensors and Actuators*, Vol. 52, No. 1–3, 8–11.

Worden, K., Bullouh, W. A., and Haywood, J., 2003, *Smart Technologies*, World Scientific, River Edge, NJ.

Harvesting of Electrical Energy from a Backpack Using Piezoelectric Shoulder Straps

Henry A. Sodano, Jonathan Granstrom, Joel Feenstra
Department of Mechanical Engineering – Engineering Mechanics
Michigan Technological University
Houghton, MI 49931

Kevin Farinholt
NanoSonic, Inc.
Blacksburg, VA 24060

ABSTRACT

Over the past few decades the use of portable and wearable electronics has grown steadily. These devices are becoming increasingly more powerful, however, the gains that have been made in the device performance has resulted in the need for significantly higher power to operate the electronics. This issue has been further complicated due to the stagnate growth of battery technology over the past decade. In order to increase the life of these electronics, researchers have begun investigating methods of generating energy from ambient sources such that the life of the electronics can be prolonged. Recent developments in the field have led to the design of a number of mechanisms that can be used to generate electrical energy, from a variety of sources including thermal, solar, strain, inertia, etc. Many of these energy sources are available for use with humans, but their use must be carefully considered such that parasitic effects that could disrupt the user's gait or endurance are avoided. These issues have arisen from previous attempts to integrate power harvesting mechanisms into a shoe such that the energy released during a heal strike could be harvested. This study develops a novel energy harvesting backpack that can generate electrical energy from the differential forces between the wearer and the pack. The goal of this system is to make the energy harvesting device transparent to the wearer such that his or her endurance and dexterity is not compromised. This will be accomplished by replacing the traditional strap of the backpack with one made of the piezoelectric polymer polyvinylidene fluoride (PVDF). Piezoelectric materials have a structure such that an applied electrical potential results in a mechanical strain. Conversely, an applied stress results in the generation of an electrical charge, which makes the material useful for power harvesting applications. PVDF is highly flexible and has a high strength allowing it to effectively act as the load bearing member. In order to preserve the performance of the backpack and user, the design of the pack will be held as close to existing systems as possible. This paper develops a theoretical model of the piezoelectric strap and uses experimental testing to identify its performance in this application.

Keywords: Energy harvesting, piezoelectric, self-powered, PVDF.

INTRODUCTION

The advances in low power electronics, wireless technology, and wearable computing devices have led to an ever increasing amount of electronics carried by a person. While these devices increase our ability to communicate they can also be cumbersome and require the use of electrochemical batteries to supply power to each device. In the case of emergency personnel, field-based environmental researchers, or backcountry sport enthusiasts, these devices also result in substantial loads. These loads are further increased due to the need to carry heavy electrochemical batteries as the energy source for each device, greatly increasing the carried load. Additional complications occur due to stagnant battery technology which has not progressed along with the increasing power demands of current electronics, as shown in Figure 1. Furthermore, since each battery only contains a finite lifespan the individual must be regularly resupplied.

Power harvesting is the act of converting ambient energy into electrical energy that can then be used to power other devices. Recent developments in the field have led to the design of a number of mechanisms that can be used to generate electrical energy from a variety of sources including thermal, solar, strain, inertia, etc. Many of these energy sources are available from humans, but their integration must be carefully considered such that parasitic effects that could disrupt the

user's gait or endurance are avoided. Using the power harvested, it is desirable to construct the system such that it can be used to provide a direct energy source to the electronics, as a means of supplementing the electrochemical battery to increase its life, or to recharge the battery.

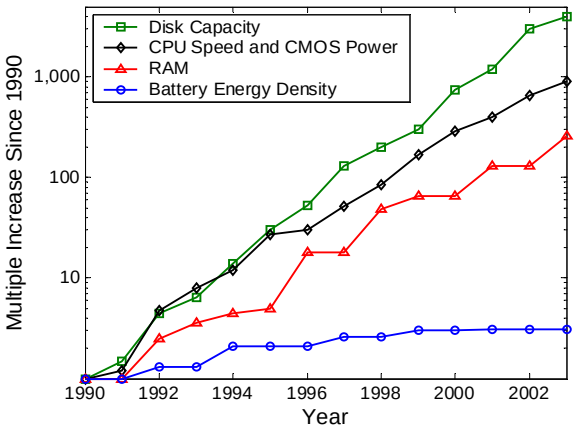

Figure 1: Advances in computer and battery technology since 1990. (Data from Paradiso and Starner, 2005).

Several studies have been performed to investigate the energy available from various sources of human power. Perhaps the earliest of these was published by Starner (1996) who examined the energy available from the leg motion of a human and surveyed other human sources of mechanical energy including blood pressure, breathing, and typing. The author claimed that 8.4 watts of useable power could be achieved from a PZT device mounted in a shoe to harvest the force generated during walking. While the extraction of energy from walking motion can generate high levels of power, the device typically interferes with the user's gait resulting in a reduction of the wearer's endurance. Several studies have been performed to investigate the power available from the force generated between the heel and shoe. Kymissis *et al*. (1998) examined three different devices that could be built into a shoe to harvest excess energy and generate electrical power parasitically while walking. The devices that were considered included a "Thunder" actuator constructed of piezoceramic composite material located in the heel, a rotary magnetic generator also located under the heel, and a multilayer PVDF foil laminate patch located in the sole of the shoe. The Thunder actuator was developed by NASA and has a rainbow (arch) configuration that allows the high impact vertical energy of the heel to be translated into bending strain for electrical power generation. The electromagnetic generator used the pressure of the heel to spin a flywheel and rotary generator to extract the power from the pressure of the heel during walking. The last device used was the laminate of piezofilm, or "stave", which was used to harness the energy lost during the bending of the sole. In order to compare the performance of the three methods, a working prototype was constructed for each and its performance was measured. The peak powers were observed to approach 20mW for the PVDF stave, 80mW for the PZT unimorph, and the shoe mounted rotary generator averaged to about 250mW. For a full review of power harvesting using piezoelectric materials see Sodano *et al*. (2004a).

More recently, SRI International built a dielectric elastomer generator that was designed to replace the sole of a soldier's boot (Kornbluh *et al.*, 2002). The study configured the dielectric elastomer materials such that when the heel pressed down it ballooned between a set of holes built into the frame, thus increasing the strain applied to the material. The device was capable of generating 800mW of power per shoe when walking at a pace of 2 steps per second. While the system was demonstrated to effectively generate large power levels, the system requires a substantial bias voltage and a switching circuit to pull energy from the material and maximize charge. This can make the system difficult to implement.

Several studies have also investigated the storage of electrical energy generated by a power harvesting device. Umeda *et al*. (1997) investigated the characteristics of energy storage by a piezo-generator with a bridge rectifier and capacitor. Their study used a small piezoelectric bender as the energy source and varied several parameters to determine the effect on energy storage. Kymissis *et al*. (1998) also investigated the storage of energy in a capacitor and developed a circuit that used a capacitor to accumulate the electrical energy along with various other components to regulate the charging and discharging cycle of the capacitor. The circuit was found to function well in their application, but the capacitor charged and discharged very quickly resulting in only intermitted power output, as shown in Figure 2 (Sodano *et al*., 2005a). Later Sodano *et al*. (2005a, 2005b) performed a series of studies investigating the use of an electrochemical battery as the energy storage device. The authors

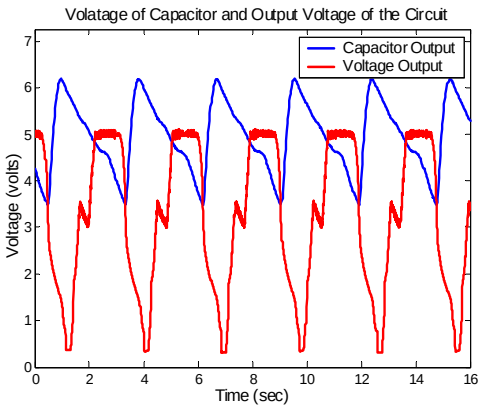

Figure 2: Plot of the capacitor's voltage and the corresponding voltage output for a commonly used power harvesting circuit (Sodano *et al*., 2003).

showed that a piezoelectric patch could recharge a small nickel metal hydride battery in a few hours when excited with the level of energy available on an automobile engine.

Previous studies have demonstrated that it is difficult to obtain electrical energy from a shoe without disrupting the wearer's gait or endurance. To avoid these issues researchers have begun to look into obtaining electrical energy from the differential forces between a human and backpack that occur during walking. Rome *et al*. (2005) investigated the design of a backpack that could convert mechanical energy from the vertical movement of carried loads to electricity. The study designed the backpack such that a linear bearing and a set of springs suspended the load relative to a frame and shoulder harness. This configuration allows the load to move vertically relative to the frame. This relative motion was then converted to electrical energy using a rotary electric generator with a rack and pinion, as shown in Figure 3. This system was demonstrated to generate a maximum power of approximately 7.37W. However, the authors indicate through analysis of the O_2 intake and CO_2 produced by the wearer that the motion of the pack increased the energy expended by 19.1W or about a 3.2% increase over the energy expelled without the harvesting device, (Kuo, 2005). While the backpack does generate significant power levels, the additional degree of freedom provided to the load could impair the user's dexterity and lead to increased fatigue.

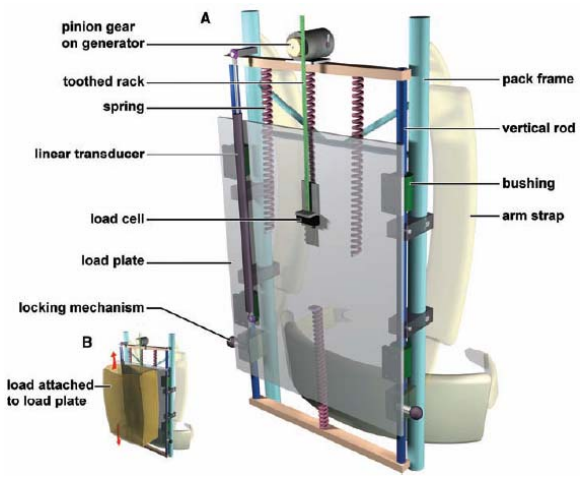

Figure 3: Schematic showing the energy harvesting backpack developed by Rome et al. (2005).

While many of these systems are compatible with the energy present around an emergency worker or soldier, they typically do not generate sufficient energy, are cumbersome, or interfere with the gait of the wearer. Thus the focus of this research is to design the system such that the power harvesting backpack provides no additional stress or load to the soldier over that of a conventional backpack. The research effort presented here will utilize the piezoelectric polymer polyvinylidene fluoride (PVDF). The PVDF bulk material is widely available, and is low cost; however, it requires processing to obtain its piezoelectric properties. Piezoelectric materials function in such a way that an applied electric potential forms a mechanical strain and an applied strain results in the formation of an electrical charge. In order to make the backpack as close to a typical design as possible, the fabric straps are to be replaced with a PVDF polymer strap. As the soldier walks with the backpack, the differential forces between wearer and backpack would be transferred to the polymer straps which then convert the applied force to electrical energy. PVDF polymer is a high density polymer and has an elastic modulus approximately equal to that of nylon or PVC, which makes it well suited for this application because a 100N load on a 100μm thick strap will only result in a 0.6% strain of the strap. This indicates that the strap would perform very similarly to the traditional strap in this application. This level of strain does not pose an issue for the PVDF material, however, typical electrodes consist of a solid metallic film that is applied to the surface of the polymer using sputter coating and cannot withstand high levels of cyclic strain or the high shear stress associated with the proposed design. Therefore, the use of a PVDF polymer strap necessitates the application of an advanced electrode that can withstand the intended environment. To overcome this issue, a nanostructured electrode has been fabricated using NanoSonic's proprietary self-assembly process. This electrode design provides the required robustness and durability such that the functionality of the pack can be guaranteed in the harsh conditions experienced during outdoor activities. A model of this power harvesting system will be developed and experimentally verified to identify the level of power available from this energy harvesting mechanism. Results of this work will show that this system could be used as a power supply for low power electronics or sensors.

MODEL OF POWER HARVESTING SYSTEM

In order to predict the energy generated by a strap of piezoelectric material subjected to a dynamic tension, the piezoelectric constitutive equations are used in coordination with a single degree of freedom model. When defining the constitutive equations it is typical that the poling direction of the strap be defined as the -3 direction and loading be in the -1 direction for this application, as shown in Figure 4. The linear constitutive equations for piezoelectric materials are defined as

$$S_1(t) = s_{11}^E T_1(t) + d_{31} E_3(t)$$
$$D_3(t) = d_{31} T_1(t) + \varepsilon_{33}^T E_3(t) \quad (1)$$

where $S_1(t)$ is the strain, s_{11} is the compliance, $T_1(t)$ is stress, d_{13} is the piezoelectric coupling coefficient, $E_3(t)$ is the electric field, $D_3(t)$ is the electric displacement, ε_{33} is the dielectric permittivity, and the subscripts represent the direction of each property. The first equation defines the mechanical response of the material while the second equation defines the electrical response. Because our system is not operating over a wide range of frequencies and assuming the strap is subjected to a known tension (neglecting bending, see Sodano *et al.* 2004b for general power harvesting models) from the experimental characterization, the constitutive equations can be simplified using the following relationships

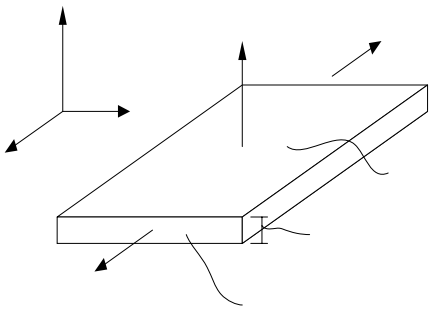

Figure 4: Schematic of the sign convention used in the piezoelectric constitutive equations.

$$S_1(t) = \frac{x(t)}{L} \qquad T_1(t) = \frac{F(t)}{A_{cs}} \qquad E_1(t) = \frac{v(t)}{t} \qquad D_3(t) = \frac{Q_3(t)}{A} \quad (2)$$

where $x(t)$ is the displacement, $Q(t)$ is the charge, L is the length of the strap, t is the material thickness, A_{cs} is the cross-sectional area, A is the surface area, $F(t)$ is the applied force, and $V(t)$ is the voltage. Because the system will include a number of straps mechanically in parallel to strengthen the strap while maintaining a desired capacitance, the number of straps, n, is introduced into the equations. This term affects the capacitance as well but has been omitted from the equations because the variation is dependent on the electrical connection between each strap, which can be modified. Substitution of these terms allows the constitutive equations to be written as

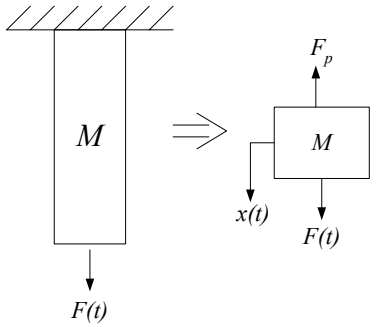

Figure 5: Single degree of freedom representation of the piezoelectric strap.

$$x(t) = \frac{L}{nA_{cs}E} F_p(t) + \frac{d_{31}L}{t} v(t) \quad (3)$$

$$Q(t) = \frac{d_{31}L}{t} F(t) + \frac{\varepsilon_{33}^T A}{t} v(t). \quad (4)$$

With the constitutive equations in a convenient form they can be used with the single degree of freedom model shown in Figure 5 to define the dynamics of the strap. Solving the force balance in Figure 5, substituting the piezoelectric force in equation (3), and realizing $v(t)=Q(t)/C$ allows the mechanical response of the system to be written as

$$M\ddot{x} = -F_p(t) + F(t) \quad \Rightarrow \quad M\ddot{x} + \frac{EnA_{cs}}{L} x(t) - \frac{d_{31}EnA_{cs}}{t} C^{-1} Q(t) = F(t) \quad (5)$$

where C is the capacitance defined as $C=\varepsilon_{33}A/t$. The electrical response can then be defined by solving for $v(t)$ in equation (4) and substituting the longitudinal stiffness $k=EA/L$ to give

$$-v(t) - C^{-1} \frac{d_{31}AE}{t} x(t) + C^{-1} Q(t) = 0. \quad (6)$$

Once the dynamics of the system have been coupled to the electrical response of the piezoelectric material, the electrical boundary conditions can be included by defining the load resistance R as

$$v(t) = -R\dot{Q}(t) \quad (7)$$

Substituting equation (7) into equations (5) and (6) gives the coupled electro-mechanical response of the power harvesting system as

$$M\ddot{x} + \frac{EnA_{cs}}{L}x(t) - \frac{d_{31}EnA_{cs}}{t}C^{-1}Q(t) = F(t)$$
$$R\dot{Q}(t) - C^{-1}\frac{d_{31}AE}{t}x(t) + C^{-1}Q(t) = 0 \tag{8}$$

where $i(t) = \dot{Q}(t)$, and the voltage output of the system across the load resistance is defined by the $v(t) = R\dot{Q}(t)$ term. The power output can then be calculated assuming that the load impedance will be the same as the source defined as

$$Z = \frac{1}{j\omega C} = \frac{t}{j\omega\varepsilon_{33}^{T}A} \tag{9}$$

where ω is the walking frequency and j defines the complex impedance of the capacitive piezoelectric material. Using the defined impedance of equation (9) the power can then be defined as

$$P = \frac{v^2}{R}. \tag{10}$$

With the equation defined above, the electric response of the strap material when subjected to a known dynamic tension can be determined.

EXPERIMENTAL SETUP

In order to identify the level of energy available for a backpack instrumented with a PVDF polymer strap, the dynamic tension resulting from walking with a 50lb (220 N) load was identified. The varying tension was measured using a load cell integrated into the top and bottom of the backpack strap to allow direct measurement of the tension, as shown in Figure 6. A 50lb (220 N) steel plate was placed inside the pack to act as the load and the pack was worn during walking on a treadmill at speeds ranging from 2-3mph (0.9 – 1.3 m/s). The results of these tests showed that the load from the pack was not evenly distributed through the strap. The resulting force measured in the top and bottom sections of the strap are shown in Figure 7. These results indicate that the load is very close to evenly dispersed over the top and bottom straps of the pack. The mean load in the top strap was determined to be 18.81 lbs (84 N) and 18.67 lbs (83 N) measured in the bottom strap. The data obtained from these tests can be directly used along with a theoretical model to predict the power output from the alternating force in the PVDF strap.

Figure 6: Instrumented backpack used to experimentally determine the loading in the straps.

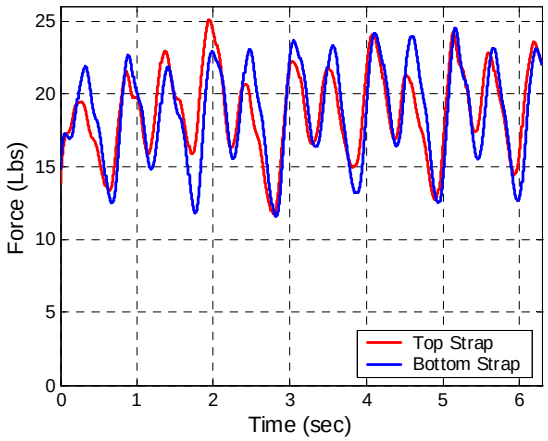

Figure 7: Resulting load applied to the top and bottom strap of the pack.

After characterizing the loading in the backpack straps, a set of PVDF straps were fabricated for experimental characterization and validation of the model. The flexibility of the harness design requires a series of equally flexible electrodes which can withstand the rigors of everyday use. To be successful in this application the electrodes must possess four distinct properties. The first is the flexibility and conformability of the electrode to avoid failure and prevent interference with the mobility of the wearer. The second is the resistance properties of the electrode as a function of strain and high cycle loading. The third feature corresponds to the adhesion and durability properties of the electrode while the fourth is the patterning capabilities of the electroding method.

Typically PVDF sensors use a thin metallized film for electrodes of either aluminum which cannot withstand high strain and cyclic loading or a silver ink which has poor adhesion properties. Therefore, the sensor developed here uses a self-assembly method which offers the ability to produce highly uniform coatings and electrodes which range from nano to macro-scale. The electrostatic self-assembly (ESA) process is shown in Figure 8, and consists of the simple soaking of a chosen substrate into alternate aqueous solutions containing anionic and cationic materials resulting in covalently bonded layers with a nearly perfect molecular order of the individual monolayers. Design of the individual precursor molecules, and control of the order of the multiple molecular layers through the thickness of the film, allows control over the macroscopic properties. For this specific application, NanoSonic's proprietary nanocomposite Metal Rubber™ offers performance capabilities that can be tailored to meet the necessary requirements for this power harvesting system. Metal Rubber™ has the ability to undergo strains of 1000% while maintaining conductivity, and return to its original shape and conductivity when released. The modulus properties can be tailored from less than 0.1MPa to greater than 500MPa and the resistive properties can be tuned to provide near constant conductivity for strains less than 5%. NanoSonic has also demonstrated the ability to fabricate complex electrode patterns using their self-assembly process.

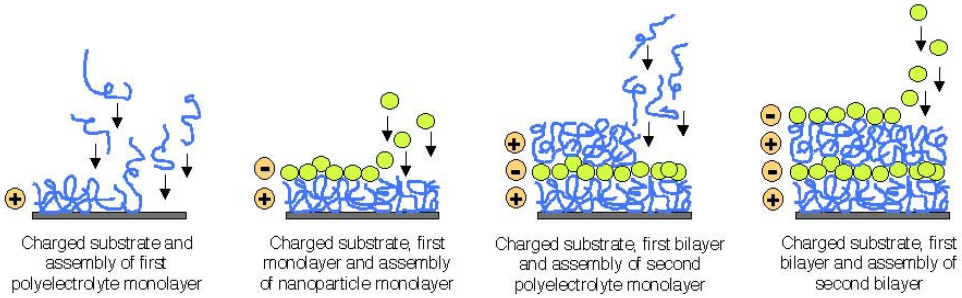

Figure 8: Summary of the electrostatic self assembly process.

Several 20.32 x 24.4 cm samples of the unmetallized 28µm and 52µm films were self-assembled with Metal Rubber™ using systematic variations in the initial chemical treatment of the samples to prepare them for the ESA process; a sample coating is shown in Figure 9. This initial treatment corresponds to the first step in the ESA summary shown in Figure 8. Electrode thickness is estimated to be ~100nm based upon the number of cycles used in the ESA process. The electrode resistance was measured along each edge of the samples, and along the diagonal. The surface resistance slowly increases over 4sec when probes are applied to the electrode, rising from 0 Ω to 5.8 Ω where it stabilizes. This behavior was also seen in the metallized samples purchased from MSI and occurs due to the samples capacitance. The samples were then poled using a 71MV/m field on the 28µm films and a field of 36MV/m on the 52µm films. Two separate field values were used due to limitations in the power supply used for poling. However, both samples exhibited equally high coupling.

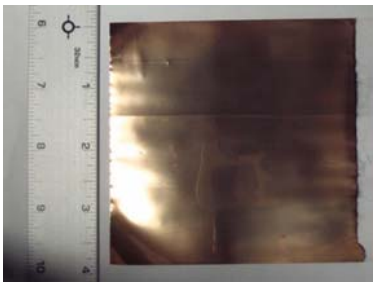

Figure 9: Piezo film transducer fabricated with self-assembled Metal Rubber surface electrodes.

Once the PVDF samples had been fabricated, experimental testing was performed to characterize their use for energy harvesting in a backpack strap and to validate the accuracy of the model such that predictions on the available power output from the entire backpack harness could be made. Testing was performed using a material testing system (MTS) with 1-4 straps, such that the energy output could be identified for various strength straps and the effect of the electrical connection between the samples could be identified. This configuration was used such that a controlled tension equivalent to the measurements made during testing of the backpack could be applied to the sample while the energy output was measured. The MTS machine with the PVDF samples is shown in Figure 10. Since the straps did not have any protective coating applied, multiple straps were electrically separated using spacer blocks. These spacers had electrical contacts to complete the circuit with the piezoelectric and allowed for wiring in series and parallel configurations. A preload of approximately 40 N was applied to the straps to simulate the static weight in the backpack while a 20 N sine wave with frequency of 5 Hz was applied to simulate the alternating load in the backpack. This load was chosen because it is representative of the force found during testing of the loaded backpack. The MTS load cell was fixed to the stationary clamp to avoid its inertia affecting the dynamics of the system. Tests of two or more straps were

run using load control; however single strap tests required position control because the PVDF is too compliant for the MTS to auto-tune its controller. Figure 11 shows a comparison of the load during each of the tests and it can be seen that the loading remained fairly consistent between each run, with the exception of the tests with three, 28μm thick straps having slightly less amplitude than the others.

Figure 10: Experimental setup used to apply a controlled tension to the strap while the power output is measured.

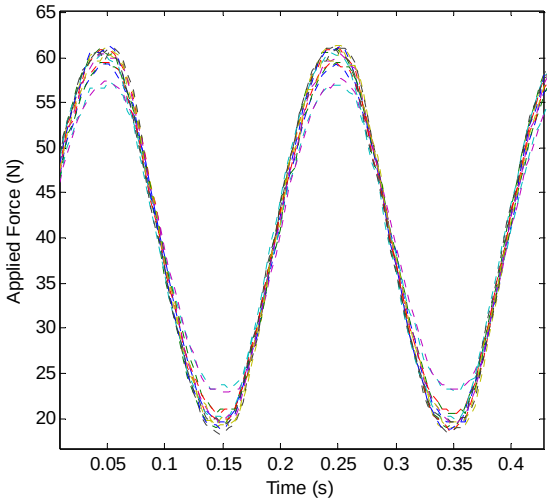

Figure 11: Load applied to each strap, demonstrating the consistency between samples.

For each test, the capacitance of the piezoelectric straps was measured and a resistive load with matched impedance was applied across the piezoelectric strap. The resistance was matched for each configuration taking into account the input impedance of the oscilloscope and attached probe. The voltage output was measured using a Tektronix **(**model TDS 2002) digital oscilloscope with a 10X probe to increase the voltage range of the oscilloscope. The oscilloscope was set to record a time history of the voltage output of the piezoelectric and the tensile force on the strap during the test. These two datasets were used in modeling the system to validate its accuracy. Tables 1 and 2 summarize the strap properties and test configurations performed.

Table 1: Mechanical and electrical properties of the PVDF materials.

Material Property	Symbol	PVDF Thickness	
		28 μm	52 μm
Elastic Modulus	E	4 GPa	5 GPa
Piezoelectric Coupling	d_{31}	25 pC/N	27 pC/N
Permittivity	ε_{33}	110 pF/m	110 pF/m
Strap Width	w	21.7 mm	21.7 mm
Strap Active Length	L	180 mm	180 mm
Strap Mass	m	0.33 g	0.60 g

Table 2: Capacitance and impedance of the PVDF strips.

Thickness	No. of Straps	Series		Parallel	
		Capacitance (nF)	Resistance (MΩ)	Capacitance (nF)	Resistance (MΩ)
28μm	1	19.5	1.65	19.5	1.65
	2	9.6	3.20	39.0	0.83
	3	7.0	4.70	60.0	0.57
	4	5.2	6.60	75.0	0.43
52μm	1	10.5	0.78	10.5	0.78
	2	5.0	6.10	21.0	1.46
	3	3.4	8.90	32.0	1.00
	4	2.6	10.00	41.0	0.77

RESULTS AND MODEL VALIDATION

Experimental tests were performed with one, two, three, and four straps with both parallel and series configurations. The data collected from each of the test scenarios was used to validate the accuracy of the theoretical model such that a prediction of the total power output from a complete backpack could be identified. The first set of tests performed was for the straps wired in series. Connecting the piezoelectric straps in this way increases voltage output, decreases capacitance, and increases impedance. However, since the testing was performed using load control, the voltage output remained fairly consistent even when the number of straps was altered. This is due to a decrease in strain per strap as the number of straps was increased for the same load. Figure 12 shows the comparison between the voltage and corresponding power for the experimental and simulated data for one and four strips, respectively, in parallel and series configurations. The plots show that the model accurately predicts the voltage output and the system dynamics. The predicted power amplitude for a single strap is slightly lower than the experimental data because the model under-predicts power for single strap tests. This may result from overstraining the piezoelectric strip in the test stand leading to a nonlinear stiffness and higher strain than the model would predict under the same load. Figure 12c depicts the voltage and power output of 4 straps wired in parallel. In this configuration, the voltage output is decreased while the current output is increased, resulting in approximately the same amount of power as the four strip test wired in series. Again, the model accurately predicts the voltage and power output.

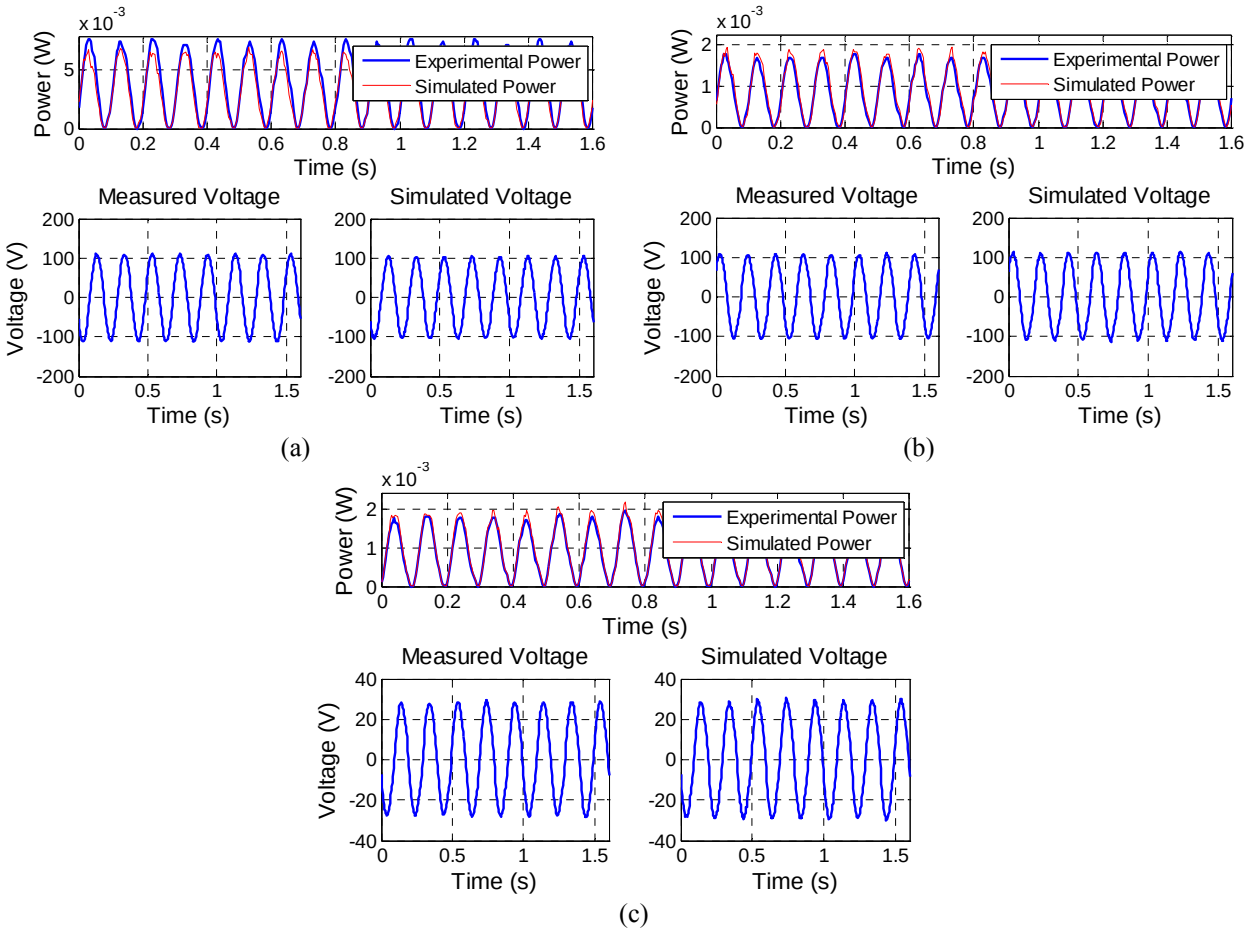

Figure 12: Measured and simulated voltage and power output, (a) one strap, (b) four straps in series, and (c) four straps in parallel.

Figure 13a-d shows plots of the mean power against the number of straps for the 28 μm (figures a and b) and 52 μm (figures c and d) thicknesses in series (figures a and c) and parallel (figures b and d) wiring configurations. From these figures, it can be seen that the model accurately predicts the power output over each of the 14 configurations tested. The plots display the decreasing power output as the number of straps is increased, which results due to less strain applied to each strap. The apparent dip in the mean power output for the 28 μm, 3 strap configuration results because the load

impedance was not tuned to the piezo impedance as well as in the other runs. This was because of the difficulty in creating an appropriate resistance while using the 10X probe and oscilloscope. However, the model captures the impedance mismatch, thus demonstrating that it can be accurately used to predict the cases in which the load electronics may not be tuned to the piezoelectric's impedance. The test of a single, 52µm strap also did not have impedance matched exactly, resulting in a lower than expected power output. Table 3 lists the mean power output and the percent difference between the experimental and simulated results. The model is capable of predicting power output within 13 percent of the actual value for all cases.

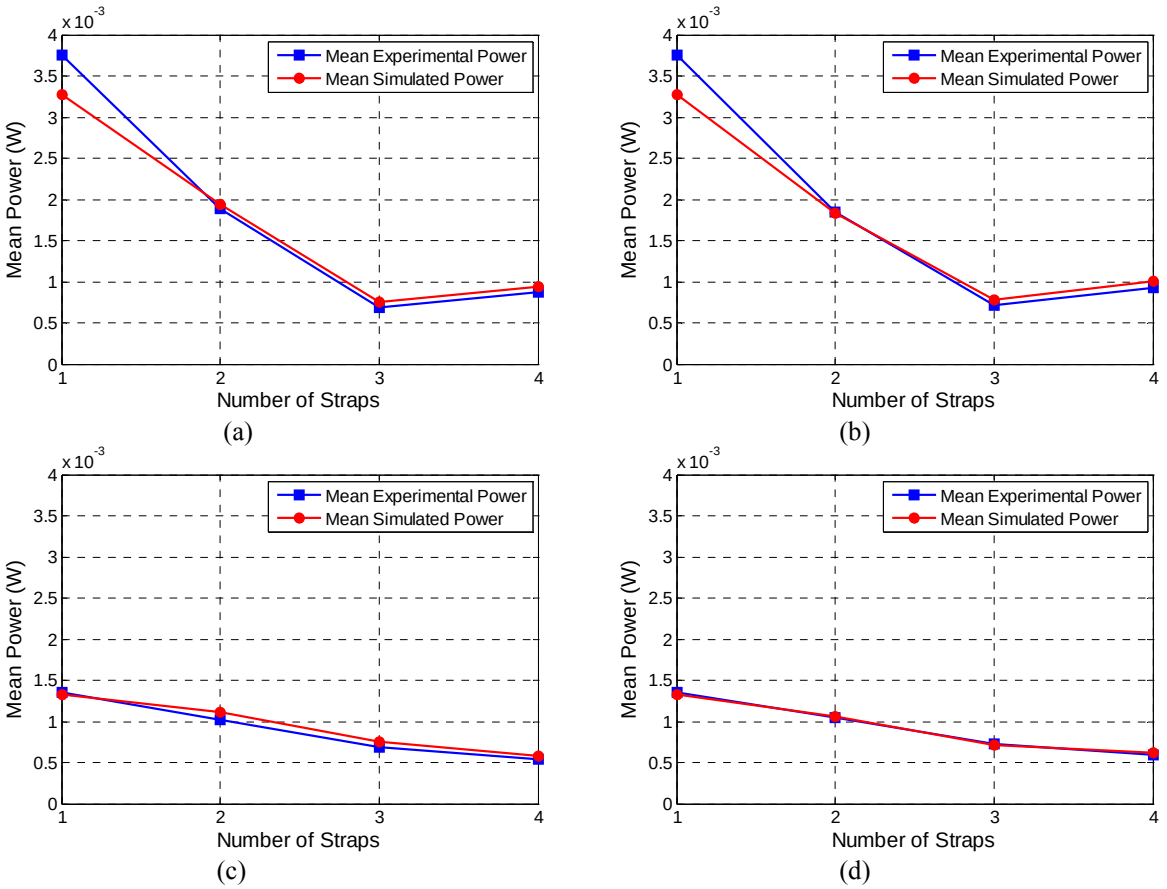

Figure 13: Mean power output for each case tested, (a) 28µm series, (b) 28µm parallel, (c) 52µm series, and (d) 52µm parallel.

Table 3: Mean power output for each case experimentally tested and the error in the predicted output.

Thickness	Number of Straps	Mean Power in Series (mW)			Mean Power in Parallel (mW)		
		Exp.	Sim.	Percent Difference	Exp.	Sim.	Percent Difference
28 µm	1	3.75	3.28	12.6			
	2	1.89	1.94	2.8	1.85	1.83	0.8
	3	0.68	0.76	10.4	0.71	0.78	10.2
	4	0.87	0.94	7.6	0.93	1.01	9.3
52 µm	1	1.36	1.33	2.3			
	2	1.02	1.12	9.1	1.05	1.06	1.1
	3	0.68	0.75	9.9	0.73	0.71	2.5
	4	0.53	0.57	7.5	0.60	0.62	4.9

BACKPACK POWER PREDICTION

Once the model had been validated using the results of the experimental tests, it was used to predict the power that could be generated by a backpack containing piezoelectric straps. The power output was theoretically predicted rather than experimentally identified because the MTS machine could not support the length of PVDF strap required. Table 4 lists the backpack strap parameters used to estimate the power output from a loaded pack. In order to generate the highest level of power possible, the strap length must be maximized. This is achieved by using a continuous strap running through the pack's frame and making a complete loop as shown in Figure 23. From this table it can be seen that the total strap length is 1.2m. The loading applied in this simulation was identical to that identified through testing of an instrumented backpack carrying a 444N load as previously discussed. The strap tension walking data was then used to run the simulation. Figure 24 illustrates the estimated power output for a backpack with two, 52µm thick piezoelectric straps per backpack shoulder strap (four 52µm piezoelectric straps total) connected electrically in parallel. From this simulation, the maximum instantaneous power can be seen to be 0.345W and an average power of 45.6mW over the duration of the simulation. This configuration of strap thickness and number does not generate the highest power, but was found to provide enough strength to carry the simulated load.

Figure 23: Schematic of the backpack with piezoelectric straps.

Table 4: Mechanical and electrical properties and dimensions used to simulate a PVDF backpack harness.

Material Property	Symbol	PVDF Thickness	
		28 µm	52 µm
Elastic Modulus	E	4.0 GPa	5.0 GPa
Piezoelectric Coupling	d_{31}	25 pC/N	27 pC/N
Permittivity	ε_{33}	110 pF/m	110 pF/m
Strap Width	W	51 mm	51 mm
Strap Active Length (top)	L	1.016 m	1.016 m
Strap Active Length (bottom)		203 mm	203 mm
Mass per Strap	m	3.5 g	6.3 g

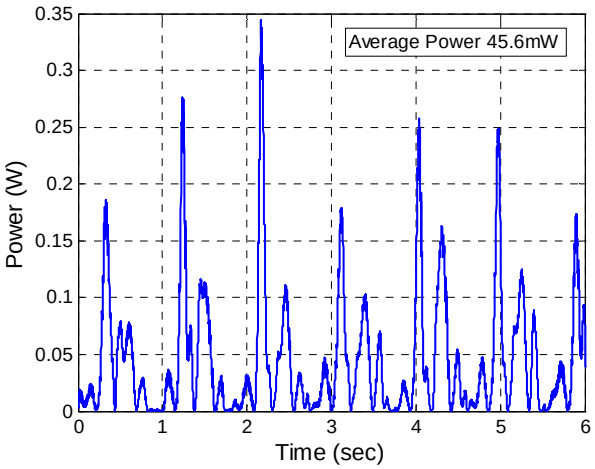

Figure 24: Predicted power output for a PVDF backpack harness with a single piece of 52µm film on each strap.

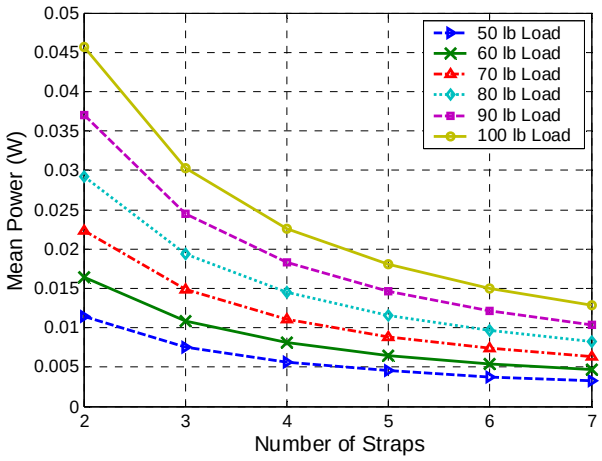

Figure 25: Mean power output for the each of the simulated conditions.

The plot shown in Figure 25 shows the power output for the two shoulder straps based on the load in the backpack and the number of piezoelectric straps per shoulder strap for a 52µm strap thickness. Due to the high impedance of the

PVDF material, the energy output is at a very large voltage, but low current. For this reason, a parallel wiring configuration is typically chosen to generate lower voltages with higher current levels. The increase in current compared to a series configuration would be more beneficial when used for charging small batteries or super-capacitors. As is seen in the figure, the load plays a very important role in the level of power generated by the energy harvesting system. Also, fewer straps create more power because they have higher associated strains. Figure 26 provides a surface plot demonstrating the mean power output (continuous power) for a variety of loads and number of straps. This figure can be compared with those of Figures 9 and 10 to understand the energy output on the factor of safety. The resulting power output could certainly be used to power some small, low power electronics or could be accumulated over the duration of the excursion leading to supplemental energy and lower number of batteries carried without increasing the mass of the pack or inducing parasitic effects on the wearer. This backpack design will lead to minimal parasitic effects therefore making it a feasible method of gathering energy from human motion.

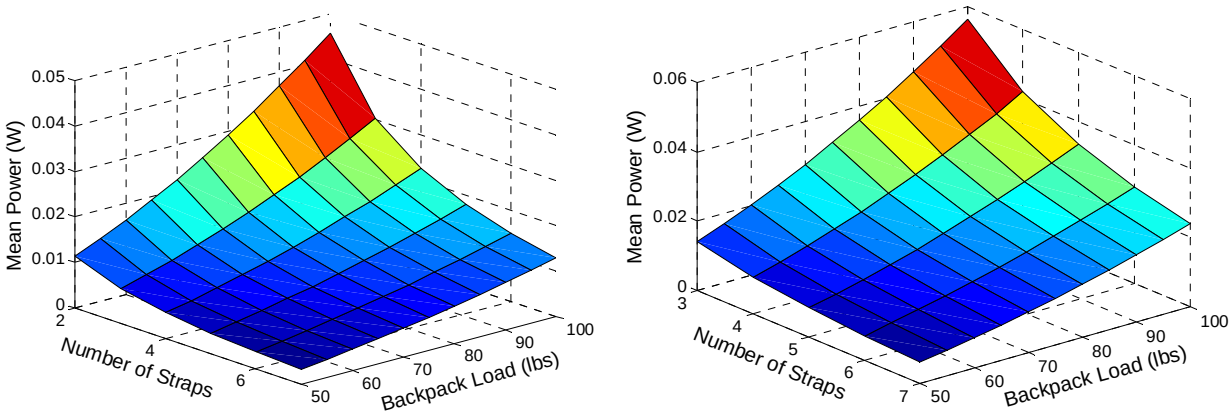

Figure 26: Mean power output for several loads and number of straps; left) 52μm, right) 28μm.

CONCLUSIONS

The past decade has seen a rapid increase in the number of wireless sensors deployed and portable electronics carried by the modern individual. Each of these devices is typically powered using a traditional electrochemical battery which can lead to issues due to their finite lifetime. To overcome this issue, the field of power harvesting has grown which looks to convert ambient energy surrounding the system to usable electrical energy. This effort has investigated the development of a novel energy harvesting system which generates electrical energy from the differential forces generated in the straps of a backpack due to walking. This system uses the piezoelectric polymer, PVDF, which has mechanical properties very similar to nylon; it however generates electrical energy when strained. To ensure the strap can withstand the rigors of use in an outdoor environment and high cyclic loading, a compliant electrode was built on the surface using electrostatic self-assembly (ESA) processes. A theoretical model of the energy harvesting system has been developed and experiments were performed to measure the loading in the backpack. The model's accuracy was validated through testing of the straps on a material testing system (MTS). The results demonstrated that the model predicted the power output better than 13% for every case tested. Once the model had been verified, simulations were performed to predict the energy available from a complete backpack with two piezoelectric straps. The results showed that 1.42mW of power could be obtained from this system.

The development of energy harvesting systems that can generate electrical energy could lead to improved life of portable electronics or in the ideal case to power the electronics for their useful life. However, many systems that are currently being designed result in significant parasitic effects to the wearer. The backpack proposed and investigated here is designed to preserve both the wearer and pack performance by holding the system as close to existing harnesses as possible. Because the mechanical properties of the PVDF strap are almost identical to the nylon straps commonly used, this system results in energy generation from sources that are truly lost.

ACKNOLEDGEMENTS

This work has been sponsored by NanoSonic Inc., under Contract No. #060803. The authors gratefully acknowledge this support.

REFERENCES

Kornbluh, R.D., Pelrine, R., Pei, Q., Heydt, R., Stanford, S. Oh, S. and Eckerle, J., 2002, "Electroelastomers: Applications of Dielectric Elastomer Transducers for Actuation, Generation, and Smart Structures, *Smart Structures and Materials 2002: Industrial and Commercial applications of Smart Structures Technologies,* SPIE Vol. 4698, pp. 254-270.

Kuo, A.D., "Harvesting Energy by Improving the Economy of Human Walking," *Science*, Vol. 309, pp. 1686-1687.

Kymissis, J., Kendall, C., Paradiso, J. and Gershenfeld, N., 1998, "Parasitic Power Harvesting in Shoes," Second IEEE International Symposium on wearable Computers, October 19-20th, Pittsburg, PA, pp. 132-139.

Paradiso, J.A. and Starner T., 2005, "Energy Scavenging for Mobile and Wireless Electronics," *Pervasive Computing*, January-March, pp. 18-27.

Rome, L.C., Flynn, L., Goldman, E.M. and Yoo, T.D., 2005, "Generating Electricity While Walking with Loads," *Science,* Vol. 309, pp. 1725-1728.

Sodano, H.A., Park, G. and Inman, D.J., 2004a, "A Review of Power Harvesting Using Piezoelectric Materials," *Shock and Vibration Digest*, Vol. 36, No. 3, pp. 197-206.

Sodano, H.A, Park, G. and Inman, D.J., 2004b, "Estimation of Electric Charge Output for Piezoelectric Energy Harvesting," *Journal of Strain*, Vol. 40, pp. 49-58.

Sodano, H.A., Park, G. and Inman, D.J., 2005a, "Generation and Storage of Electricity from Power Harvesting Devices," *Journal of Intelligent Material Systems and Structures*, Vol. 16, No. 1, pp. 67-75.

Sodano, H.A., Park, G., and Inman, D.J., 2005b, "Comparison of Piezoelectric Energy Harvesting Devices for Recharging Batteries," *Journal of Intelligent Material Systems and Structures*, Vol. 16, No. 10, pp. 799-807.

Starner, T., 1996, "Human-Powered Wearable Computing," *IBM Systems Journal*, Vol. 35 No.3-4, pp. 618-628.

Umeda, M., Nakamura, K. and Ueha, S., 1997, "Energy Storage Characteristics of a Piezo-Generator using Impact Induced Vibration," *Japanese Journal of Applied Physics*, Vol. 36, Part 1, No. 5B, May, pp. 3146-3151.

Linear Electromechanical Model of Ionic Polymer Transducers – Part I: Model Development

KENNETH M. NEWBURY AND DONALD J. LEO*

Mechanical Engineering Department, Center for Intelligent Material Systems and Structures, Virginia Tech, Blacksburg, VA 24061-0261, USA

ABSTRACT: A linear electromechanical model is developed for ionic polymer materials. The model is based on an equivalent circuit representation that is related to the mechanical, electrical, and electromechanical properties of the material. Expressions for the quasi-static and dynamic mechanical impedance are derived from beam theory. The Golla-Hughes-McTavish model of viscoelasticity is incorporated into the model to include effects due to a rate dependent modulus. Similar to previous research, the electrical impedance is modeled as a series combination of resistive and capacitive elements. The major contribution of this work is the derivation of an electromechanical coupling term that is related to an effective bending strain coefficient. This parameter is also frequency dependent to model the low-frequency relaxation that has been measured in certain ionic polymer materials. The resulting linear electromechanical model is based on the measurement of the effective permittivity, elastic modulus, and effective strain coefficient. All input-output relationships related to sensing and actuation can be derived using these three material parameters and the transducer geometry. This model also emphasizes a reciprocity between sensing and actuation that has not been discussed before in relation to these materials. The result of this work is a comprehensive model that enables the design of devices and material systems that incorporate ionic polymer materials as either sensors or actuators.

Key Words: ionic polymer, electroactive polymer

INTRODUCTION

IONIC polymers are a class of active material that exhibits electromechanical coupling. Ionic polymer materials generally consist of a perflourinated membrane that has been plated on both sides with a conductive metal. Application of an electric field across the thickness of the material produces mechanical deformation. Conversely, mechanical deformation of the material produces a measurable electrical signal. Thus, ionic polymers can be used as both sensors and actuators for applications in motion measurement and control. The advantage of these materials compared to other types of sensors is that they are compliant materials that operate in a hydrated environment. This has motivated the development of biomimetic sensors and actuators that exploit their unique properties. A discussion of the early history of these materials and their use as biomimetic transducers is contained in Shahinpoor et al. (1998).

Previous modeling efforts for ionic polymer materials can generally be separated into empirical models or models based on first principles. Models of electromechanical impedance were developed for the purpose of relating applied voltage to current (Kanno et al., 1995). Early work on these materials utilized a linear model of actuation to estimate the relationship between applied field and mechanical deformation (Kanno et al., 1996). Both of these models utilized curvefits of experimental data to model electromechanical coupling. Recently, Newbury and Leo (2002) developed a two-port electromechanical model that accounted for both sensing and actuation within the material. This model was also based on curve fits of experimental data.

Models based on first principles have also been developed by Nemat-Nasser and Li (2000), Tadokoro et al. (2000), de Gennes et al. (2000), Asaka and Oguro (2000), and, most recently, Nemat-Nasser (2002). These models are based on the interaction of electrostatic and hydraulic forces within the polymer membrane. Nemat-Nasser and Li (2000) and Nemat-Nasser (2002) place more emphasis on the electrostatic interaction while the models by de Gennes et al. (2000), Tadokoro et al. (2000), and Asaka and Oguro (2000) are based on the relationship between solvent flux and pressure gradients. Of the models, the ones by Nemat-Nasser, Tadokorao, and Asaki are able to match the dynamic behavior of an ionic polymer material when excited with DC and AC

*Author to whom correspondence should be addressed. E-mail: donleo@vt.edu

1045-389X/03/06 0333–10 $10.00/0 DOI: 10.1177/104538903034976

fields. Recently, a sensing model based on charge redistribution in the polymer was proposed by Farinholt and Leo (2002). This model was shown to accurately predict the charge sensitivity of ionic polymer sensors as a function of material geometry.

Our goal is to develop a dynamic model that is useful for the design of material systems that incorporate ionic polymer materials. The present model expands upon the two-port linear model developed by Newbury and Leo (2002) for the purpose of analyzing both sensing and actuation. In this work, we will focus on a semi-empirical approach which yields a set of fundamental material parameters that model the electromechanical coupling. The model of an ionic polymer sensor and actuator is developed as a function of these material parameters and the transducer geometry. Unlike the work by Kanno et al. (1996), this model is coupled in the sense that it accounts for both the sensing and actuation properties of the material. With the fundamental material parameters determined, our model can be used to scale the sensing and actuation properties for the purpose of designing devices that utilize ionic polymer transducers.

The model developed in this paper complements and extends previous research in several ways. Although the model is not based on first principles, the model does produce a set of material parameters that will be useful for guiding the development of new models based on charge and solvent transport within the polymer. Secondly, our model predicts the sensing and actuation behavior within a single framework. This contrasts with the more detailed developments by Nemat-Nasser (2002) and Asaka and Oguro (2000) which focus only on actuation of the material. Modelling both sensing and actuation within a single framework allows us to study the concept of reciprocity between strain and charge distribution. This work complements the recent paper by Asaka and Oguro (2000) in which the charge–deformation relationship was explored in depth for current excitation of polymer benders. Finally, the model presented in this paper is intended to extend the realm of engineering design using ionic polymer benders through the framework of an equivalent circuit model. Framing the analysis in this manner allows the model to be used in a manner similar to models of other types of electroactive materials.

A final objective of this work is to develop a model that allows us to compare the properties of ionic polymers directly with other types of transducers. For this reason we focus on the development of a linear model that contains terms that are functionally equivalent to models of other linear transducers. This will allow a one-to-one comparison of the mechanical, electrical, and electromechanical coupling properties of the ionic polymers to other types of transducers.

The paper is organized as follows. First we will derive the linear circuit model and identify the mechanical, electrical, and electromechanical coupling terms of the model. Then, expressions for actuation and sensing will be obtained from the model for a general equivalent circuit and one in which we have made a simplifying assumption regarding the reflected impedance. The result is a set of expressions which can be used to design sensors, actuators, or material systems that contain ionic polymer materials. The paper closes with a discussion of our results and a statement of the major conclusions. Experimental validation of the model is examined in an accompanying paper.

EQUIVALENT CIRCUIT MODEL

Our model will be based on an equivalent circuit representation of an ionic polymer transducer. Equivalent circuits are convenient means of representing electromechanical transduction. Defined properly, the individual circuit elements have clear physical interpretations, and the user can examine the relationships between the various elements without being forced to study the underlying equations. Only linear circuits are considered in this work, and Laplace domain circuit analysis provides a straightforward means for obtaining the relationships between any set of system variables. The energy conversion between the electrical and mechanical domains can be represented using an ideal, linear transformer, as shown in Figure 1. This type of modeling has been used to represent electromagnetic speakers (Beranek, 1954), piezoelectric transducers (Germano, 1972; Ikeda, 1996), as well as electrostatic devices.

In Figure 1, the electrical quantities are shown on the left side of the transformer, and the mechanical quantities are on the right. Transducer voltage and current are denoted by v and i, respectively. The external force applied to the transducer is represented by f, and the velocity of the force application point is $\dot{u}$.

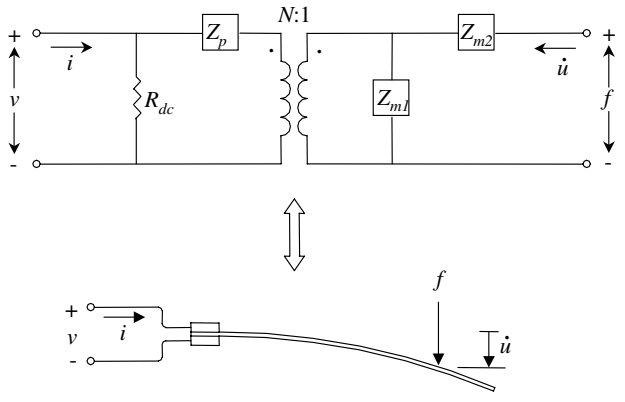

Figure 1. *Equivalent circuit for ionic polymer transducer.*

Laplace domain expressions for each of the circuit elements, in terms of material parameters, transducer geometry, and transducer dimensions, are developed in the following sections of this paper.

Mechanical Terms

The portion of the mechanical impedance due to the stiffness of the polymer transducer is represented in Figure 1 by Z_{m1}. For a cantilevered bender, an expression for the mechanical stiffness can be derived by considering the quasi-static relationship between applied force and deflection for an Euler–Bernoulli beam. The application of a load f at a distance L_d from the supported end, as shown in Figure 2, results in a bending moment

$$M = f\,(L_d - x), \tag{1}$$

where x is the distance from the supported end along the length of the bender. For small deflections, the bending moment and the deflection are related through (Shigley and Mischke, 1989)

$$\frac{M}{YI} = \frac{d^2u}{dx^2}, \tag{2}$$

where Y is the Young's (elastic) modulus and I is the area moment of inertia of the bender's cross section. Substituting Equation (1) into Equation (2) and integrating twice with respect to x gives

$$u(x) = \frac{f}{YI}\left(\frac{L_d x^2}{2} - \frac{x^3}{6} + C_1 x + C_2\right), \tag{3}$$

where C_1 and C_2 are constants of integration. Incorporating the boundary conditions for a cantilevered beam ($u(x)=0$ and $du/dx=0$), writing the area moment of inertia in terms of the transducer's width w and thickness t, and evaluating at $x = L_d$ yields the expression

$$u = f\,\frac{4L_d^3}{Ywt^3}. \tag{4}$$

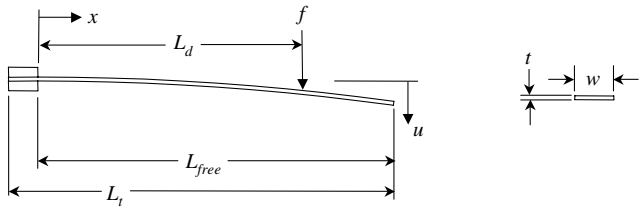

Figure 2. *Tranducer dimensions used for mechanical terms of equivalent circuit.*

To obtain a Laplace domain expression for Z_{m1}, which represents force over velocity (well below resonance), Equation (4) is multiplied by the Laplace variable s and solved for f/su. The result is

$$Z_{m1} = \frac{1}{s}\,\frac{Ywt^3}{4L_d^3} \tag{5}$$

Unlike linear elastic materials (e.g. steel, aluminum), polymers typically exhibit viscoelastic behavior, in which the stress–strain relationship has both liquid-like and solid-like features (Ward and Hadley, 1993). If linear viscoelastic behavior is assumed, the stress in the polymer is linearly related to both the strain and the strain rate, a combination of linear elastic and viscous behavior. This type of response is often described mathematically using a stress relaxation function $G(\tau)$, which represents the stress response to a unit strain input. The expression for a one-dimensional stress–strain relationship in a linear viscoelastic material can be written as

$$\sigma(\tau) = G(\tau)e(0) + \int_0^T G(\tau - \xi)\,\frac{d}{d\xi}e(\xi)\,d\xi, \tag{6}$$

where e is the strain and σ is the stress. The integral's lower limit of zero (as opposed to $-\infty$) is based on the assumption that, prior to $\tau = 0$, the strain has been at zero several times longer than the slowest time constants in $G(\tau)$. Applying Laplace transform analysis to Equation (6), the stress–strain relationship can also be represented using a complex modulus

$$Y(j\omega) = Y_1(\omega) + jY_2(\omega). \tag{7}$$

Y_1 represents the storage modulus, the linear elastic component of the viscoelastic material's behavior, and Y_2 represents the loss modulus, the viscous (dissipative) component of the behavior. One of the simplest models that accurately represents a linear viscoelastic material is the 'standard linear solid' model (Ward and Hadley, 1993) shown in Figure 3(a). The equilbrium, or quasi-static modulus is represented by the spring on the left, and the spring and damper connected in series account

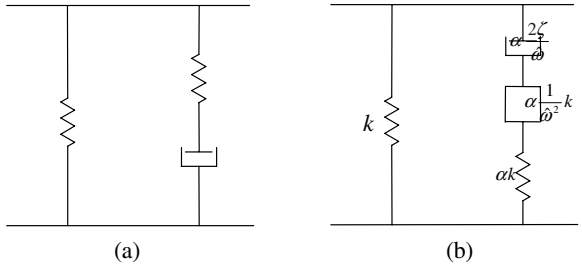

Figure 3. *Models for linear viscoelasticity: (a) Standard linear solid model; (b) GHM method.*

for the additional (beyond the quasi-static stress) stress levels that will occur at higher frequencies. McTavish and Hughes (1993) presented a similar approach, referred to as the GHM Method. They added a mass in series with the spring and damper, as shown in Figure 3(b), to create what they termed a 'mini-oscillator.' Like the standard linear solid model, the physical interpretation of the forces generated by the mini-oscillator is that they account for the stress levels beyond the quasi-static values. The GHM Method is well suited to structural analysis because it preserves the desired symmetry and definiteness of the mass, damping, and stiffness matrices that define a typical second order structural model. Because of its generality, the GHM method, it will be employed to represent the viscoelastic behavior of the ionic polymer transducers.

The combined stiffness of the two branches in Figure 3(b) is

$$k\left[1+\alpha\frac{s^2+2\zeta\hat{\omega}s}{s^2+2\zeta\hat{\omega}s+\hat{\omega}^2}\right], \tag{8}$$

where α, ζ, and $\hat{\omega}$ are the 'GHM parameters' that determine the frequency dependence of the modulus. The static stiffness is represented by k. To apply the GHM method to ionic polymers, k is replaced by Y_∞, the static modulus, resulting in the expression

$$Y = Y_\infty\left[1+\alpha\frac{s^2+2\zeta\hat{\omega}s}{s^2+2\zeta\hat{\omega}s+\hat{\omega}^2}\right]. \tag{9}$$

This equation for Y will be used in the mechanical stiffness term Z_{m1} (Equation (5)).

The useful frequency range of the transducer model can be extended by adding an inertial term, represented by Z_{m2} in Figure 1. This term will improve the model accuracy at frequencies approaching the first natural frequency of the bender. In general, the mass term is derived using the quasi-static bender stiffness (derived earlier in this section) along with the closed form solution for the bender's natural frequency to determine an equivalent mass.

The natural frequency of the first mode of transverse vibration of a slender cantilevered beam is (Inman, 1994)

$$\omega_n = \frac{\Gamma^2}{L_{\text{free}}^2}\sqrt{\frac{YI}{\rho_m A}}, \tag{10}$$

where Γ is the first solution to the characteristic equation that corresponds to the clamped free boundary conditions, ρ_m is the transducer's density, A is the cross sectional area, and L_{free} is the unsupported length of the transducer, as shown in Figure 2. The value of Γ is 1.875.

The well known relationship

$$\omega_n^2 = \frac{k}{m} \tag{11}$$

between stiffness k, mass m, and natural frequency of a single degree of freedom system can be used in conjunction with Equations (10) and (4) to determine an equivalent mass for the polymer transducer. First, Equation (4) is solved for the transducer stiffness (force over displacement at the driving point). The result, along with Equation (10) is substituted into Equation (11). Solving for the mass gives

$$m = \frac{3L_{\text{free}}^4\rho_m wt}{L_d^3\Gamma^4} \tag{12}$$

To convert Equation (12) to an expression for Z_{m2}, consider Newton's Second Law, written in the Laplace domain

$$f = s^2 m. \tag{13}$$

Substituting Equation (12) for the mass and solving for force over velocity (f/su) gives

$$Z_{m2} = s\frac{3L_{\text{free}}^4\rho_m wt}{L_d^3\Gamma^4}. \tag{14}$$

It should be noted that the approximations for Z_{m1} and Z_{m2} will result in an accurate natural frequency prediction. However, as the operating frequency approaches the first natural frequency, the accuracy of the polymer transducer mechanical impedance will drop slightly. This inaccuracy is a result of the shape of the bender vibration 'shifting' towards the first mode shape from the quasi-static shape.

Electrical Terms

The model of the transducer electrical properties is based upon the approach discussed in Kanno et al. (1995). For completeness, we will reiterate the discussion here and place the results in the context of the equivalent circuit model. The electrical impedance of the polymer transducer is represented by two terms in the equivalent circuit of Figure 1. R_{dc} represents the DC resistance, and Z_p models the ability of the transducer to store electrical charge. In order to produce simple expressions for R_{dc} and the circuit elements that will be used to describe Z_p, the polymer transducer will be viewed as a homogeneous material with perfectly conductive electrodes on both surfaces.

The DC resistance of the transducer, expressed in terms of a resistivity ρ_{dc} and the polymer dimensions is (Halliday and Resnick, 1978)

$$R_{dc} = \frac{\rho_{dc} t}{L_t w}, \tag{15}$$

where L_t is the total length of the transducer, including the length clamped between the electrodes.

The electrical impedance of the polymer is resistive with high magnitude at DC, resistive with small magnitude at high frequencies, and it has a strong capacitive component at intermediate frequencies. This behavior suggests that Z_p should consist of parallel branches of R-C elements that are connected in series, as shown in Figure 4. The number of branches n will determine the number of degrees of freedom available for describing the electrical impedance.

As with R_{dc}, each resistor R_i in Figure 4 can be represented by a resistivity ρ_i and the polymer dimensions using

$$R_i = \frac{\rho_i t}{L_t w} \tag{16}$$

Viewing the polymer transducer as a parallel plate capacitor, the C_i are (Halliday and Resnick, 1978)

$$C_i = \frac{\epsilon_i L_t w}{t} \tag{17}$$

where the ϵ_i are permittivities.

Using Laplace domain circuit analysis, the impedance Z_p of the circuit in Figure 4 is

$$Z_p = \frac{1}{\sum_{i=1}^{n} (sC_i/1 + sC_i R_i)} \tag{18}$$

Substituting Equations (16) and (17) into this result yields

$$Z_p = \frac{t}{sL_t w} \frac{1}{\sum_{i=1}^{n} (\epsilon_i/1 + s\epsilon_i R_i)} \tag{19}$$

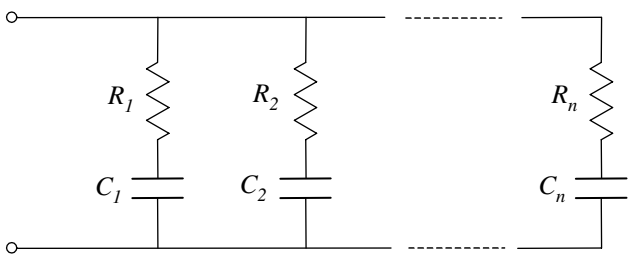

Figure 4. *Circuit model for Z_p.*

Electromechanical Coupling

The electromechanical coupling in the linear transformer (Figure 1) is represented by the turns ratio N. Typically, the tranformer turns ratio in electromechanical equivalent circuit models is a constant. Because of the complex nature of ionic polymer transducer behavior, the turns ratio in this work will be permitted to be frequency dependent, with varying magnitude and phase. Consider the frequency range below resonance and above DC, where the mass term Z_{m2} is negligible and the DC resistance R_{dc} can be considered very large relative to the magnitude of Z_p. In this frequency range, the turns ratio N represents the relationship between open-circuit voltage and the external force acting on the polymer, specifically

$$\frac{v}{N} = \frac{f}{1} \quad \text{with} \quad i = 0. \tag{20}$$

For modeling materials with linear electromechanical coupling, such as piezoelectric materials (Ikeda, 1996), the coupled equations are used,

$$\begin{aligned} S &= s^E T + dE \\ D &= dT + \epsilon^T E, \end{aligned} \tag{21}$$

where S and D are the mechanical and electrical displacements (strain and charge density), and T and E are the applied stress and the electric field. The variable s^E is the shortcircuit (zero electric field) elastic compliance, and ϵ^{T} is the permittivity with no external loading (zero applied stress). The piezoelectric coupling is represented by d, which relates induced strain to applied electric field (first row of Equation (21)) and generated charge per unit surface area to applied stress (second row of Equation (21)). If we assume that the coupling in ionic polymer transducers can be modeled in a similar fashion, the second row in Equation (21) can be used to find an expression for the tranformer turns ratio N. Towards this end, the permittivity ϵ^{T} is replaced by a frequency dependent term $\eta^T(s)$. This change is necessary because the electrical impedance of polymer transducers cannot be accurately represented with capacitance alone. The expression for $\eta^T(s)$ can be found by comparing Equation (19) for Z_p to Equation (17) for a parallel plate capacitor. The resulting relation is

$$\eta^T(s) = \sum_{i=1}^{n} \frac{\epsilon_i^T}{1 + s\epsilon_i^T \rho_i^T}, \tag{22}$$

where the superscript T has been added to the ϵ_i and ρ_i to represent the zero applied stress condition. Also, researchers that have attempted to understand the

mechanisms responsible for the electromechanical coupling have suggested that the electromechanical coupling in ionic polymer transducers occurs at the interface between the electrode and the polymer itself (Nemat-Nasser and Li, 2000). For this reason, T will be interpreted as the applied stress *at the polymer surface*.

To convert the electric displacement (charge density) term in Equation (21) to charge, both sides of the equation are integrated over the polymer width w and length L_t. Prior to integrating, the stress at the polymer surface T must be related to the applied force f. These two quantities can be related using the well known equation for a beam in bending (Shigley and Mischke, 1989)

$$T = \frac{My}{I}, \tag{23}$$

where M is the applied moment, y is the distance from the neutral axis, and I is the area moment of inertia. Substituting $t/2$ for y and Equation (1) for the moment yields

$$T(x) = \frac{f\,(L_d - x)t}{2I}. \tag{24}$$

The second row of Equation (21) can now be written as

$$Q = \int_0^{L_t} \int_{-w/2}^{w/2} \left(d\frac{f\,(L_d - x)t}{2I} + \frac{\eta^T v}{t} \right) dz\,dx, \tag{25}$$

where z is the coordinate in the direction of the polymer width. Integrating (remember that $f = 0$ for $x \geq L_d$) and substituting $\mathrm{I} = wt^3/12$ results in the relation

$$Q = \frac{3dL_d^2}{t^2} f + \frac{\eta^T L_t w}{t} v. \tag{26}$$

To obtain an expression for N, set $Q = 0$ (open-circuit condition) and solve for v/f. The resulting expression for the turns ratio N is

$$N = \frac{3dL_d^2}{\eta^T L_t w t}. \tag{27}$$

The derivation of the equivalent circuit parameters is now complete. It is important to note that the above derivation only considers single axis bending and is therefore limited to slender beams. If the transducer becomes wide relative to its length (starts to becomes more like a plate than a beam), then bending about two axes must be considered.

EQUIVALENT CIRCUIT ANALYSIS

The equivalent circuit in Figure 1 can be solved to yield various input–output relationships, such as free deflection or blocked force. A useful intermediate step is to solve the circuit for a pair of linearly coupled equations that can represent the general behavior of the equivalent circuit. These coupled equations can be found by using the voltage and current relationships for ideal linear transformers and the mesh-current method of circuit analysis (Nilsson, 1983). Figure 5 shows the variables used in the mesh current analysis. The resulting mesh equations, along with the relationships between voltage and current for an ideal transformer are

$$\begin{aligned} v_0 &= R_{\mathrm{dc}}(i - i_2) \\ Z_p i_2 + v_2 + R_{\mathrm{dc}}(i_2 - i) &= 0 \\ f_2 + Z_{m1}(\dot{u}_2 - \dot{u}) &= 0 \\ f &= Z_{m2}\dot{u} + Z_{m1}(\dot{u} - \dot{u}_2) \\ v_2/N &= f_2/1 \\ -i_2 N &= \dot{u}_2 \end{aligned} \tag{28}$$

To obtain a pair of linearly coupled equations, the variables v_2, i_2, f_2, and $\dot{u}_2$ are eliminated from Equation (28), resulting in the matrix equation

$$\begin{Bmatrix} v \\ f \end{Bmatrix} = \begin{bmatrix} \dfrac{R_{\mathrm{dc}}(N^2 Z_{m1} + Z_p)}{R_{\mathrm{dc}} + N^2 Z_{m1} + Z_p} & \dfrac{N R_{\mathrm{dc}} Z_{m1}}{R_{\mathrm{dc}} + N^2 Z_{m1} + Z_p} \\ \dfrac{N R_{\mathrm{dc}} Z_{m1}}{R_{\mathrm{dc}} + N^2 Z_{m1} + Z_p} & \dfrac{(Z_{m1} + Z_{m2})(R_{\mathrm{dc}} + Z_p) + N^2 Z_{m1} Z_{m2}}{R_{\mathrm{dc}} + N^2 Z_{m1} + Z_p} \end{bmatrix} \times \begin{Bmatrix} i \\ \dot{u} \end{Bmatrix}. \tag{29}$$

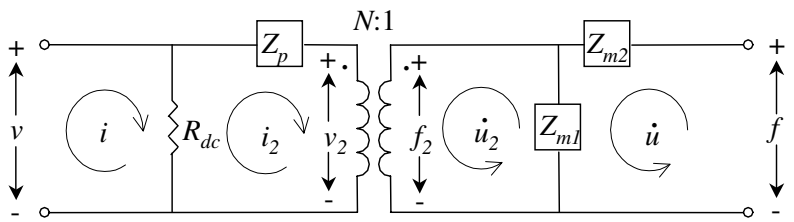

Figure 5. *Equivalent circuit model with variables used for mesh current circuit analysis.*

This set of equations can also be viewed as a two-port model that describes the behavior of an ionic polymer bender, similar to the model presented by Newbury and Leo (2002). The advantage of the model in this work is that each of the matrix coefficients has been explicitly defined in terms of transducer dimensions and geometry and a set of basic material parameters, which are independent of geometry. In short, unlike the previous two-port model, the model presented in this work is scalable.

The coefficients in Equation (29) can be simplified by introducing the assumption that the reflected mechanical impedance is negligible relative to the electrical impedance term Z_p. This assumption takes two forms, depending on whether the blocked or free boundary condition is considered. For the blocked boundary condition, the assumption can be expressed as

$$N^2 Z_{m1} \ll Z_p. \tag{30}$$

For the free boundary condition, the assumption is

$$N^2 \frac{Z_{m1} Z_{m2}}{Z_{m1} Z_{m2}} \ll Z_p. \tag{31}$$

Equations (30) and (31) will be used to simplify the input-output relationships that are derived from Equation (29).

The general model can be simplified under the assumptions that the reflected impedance is negligible. This assumption was verified for the data obtained in this experiment. Under this assumption, Equation (29) reduces to

$$\begin{Bmatrix} v \\ f \end{Bmatrix} = \begin{bmatrix} \dfrac{Z_p}{1 + Z_p/R_{\mathrm{dc}}} & N\dfrac{Z_{m1}}{1 + Z_p/R_{\mathrm{dc}}} \\ N\dfrac{Z_{m1}}{1 + Z_p/R_{\mathrm{dc}}} & Z_{m1} + Z_{m2} \end{bmatrix} \begin{Bmatrix} i \\ \dot{u} \end{Bmatrix} \tag{32}$$

where the equations for the electrical and mechanical impedances can be found in the second section of this paper. The expressions for the electromechanical impedance can be simplified even further at frequencies in which $|Z_p/R_{\mathrm{dc}}| \ll 1$, which is true above approximately 0.5 Hz for the polymer samples tested in this paper. The result can be written as

$$\begin{Bmatrix} v \\ f \end{Bmatrix} = \frac{1}{s} \begin{bmatrix} \dfrac{t}{L_t w}\dfrac{1}{\eta^T} & \dfrac{3}{4}\dfrac{t^2}{L_d L_t}\dfrac{dY}{\eta^T} \\ \dfrac{3}{4}\dfrac{t^2}{L_d L_t}\dfrac{dY}{\eta^T} & \dfrac{Ywt^3}{4L_d^3} + s^2\dfrac{3L_{\mathrm{free}}^4 \rho_m wt}{L_d^3 \Gamma^4} \end{bmatrix} \begin{Bmatrix} i \\ \dot{u} \end{Bmatrix} \tag{33}$$

INPUT–OUTPUT RELATIONSHIPS FOR SENSING AND ACTUATION

It is useful to solve Equation (29) for common input–output relationships, such as blocked force and free deflection, apply the assumptions in Equations (30) and (31), then replace each circuit element with its definition in terms of the transducer dimensions and material parameters derived in section. The resulting expressions can be used to determine the suitability of a transducer for specific applications. Also, they facilitate comparison to competing transducer technologies. Yet another important use of these input–output relations is to provide insight into the effects of the various dimensions on transducer performance – they are practical design tools. In solving for the relationships presented in the following sections, one of the variables in Equation (29) is set to zero. Following the convention used by Ikeda (1996), the variable that is set to zero will be denoted using a superscript. For example,

$$\left(\frac{f}{v}\right)^{\dot{u}} \tag{34}$$

will represent blocked force (velocity is zero) with a voltage input.

Actuator Equations

If $\dot{u}$ in Equation (29) is set to zero, corresponding to the blocked boundary condition, the remaining equations can be solved for force over voltage, resulting in the expression

$$\left(\frac{f}{v}\right)^{\dot{u}} = \frac{NZ_{m1}}{Z_p} = \frac{3dtwY^E}{4L_d}. \tag{35}$$

Note that the circuit element definitions (in terms of transducer material parameters and geometry) were substituted into the middle expression to yield the expression on the right hand side.

To obtain an equation for blocked force with a current input $\ddot{u}$ is set to zero, and the second row of Equation (29) is solved for $(f/i)^{\ddot{u}}$, resulting in

$$\left(\frac{f}{i}\right)^{\ddot{u}} = \frac{NR_{\mathrm{dc}}Z_{m1}}{R_{\mathrm{dc}} + Z_p} = \frac{3dt^2 Y^E \rho_{\mathrm{dc}}}{4L_d L_t (1 + s\eta^T \rho_{\mathrm{dc}})}. \tag{36}$$

If the force f in Equation (29) is set to zero and an s-domain integration performed, the expression

$$\left(\frac{u}{v}\right)^{f} = \frac{-NZ_{m1}}{sZ_p(Z_{m1} + Z_{m2})} = \frac{-3dL_d^2}{(12\rho_m L_f^4/\Gamma^4 Y^E)s^2 + t^2} \tag{37}$$

for the free deflection with a voltage input is obtained. The left hand term in the denominator accounts for the

actuator inertia and can be ignored at frequencies well below the first resonance, effectively setting the mass term Z_{m2} equal to zero. Below resonance, the expression for free deflection with a voltage input becomes

$$\left(\frac{u}{v}\right)^f = \frac{-N}{sZ_p} = \frac{-3dL_d^2}{t^2}. \tag{38}$$

To model the actuator working against a load, a circuit element can be added to the mechanical terminals of the Figure 1 circuit and the circuit analysis adjusted accordingly.

Sensor Equations

Equation (29) can also be solved for relationships that describe the use of a polymer transducer as a sensor. In this case, either short-circuit charge (or current) or open-circuit voltage would be measured. Setting v in Equation (29) to zero and solving for current over velocity yields the sensor equation

$$\left(\frac{i}{\dot{u}}\right)^v = \frac{-NZ_{m1}}{Z_p} = \frac{-3dtwY^E}{4L_d}. \tag{39}$$

Integrating (dividing by the Laplace variable s) both the numerator and denominator shows that the same expression also applies to the short-circuit charge with a displacement input.

Another potentially useful sensor equation is found by setting i in Equation (29) to zero and solving for the open-circuit voltage with a force input. The result is

$$\left(\frac{v}{f}\right)^i = \frac{NR_{dc}Z_{m1}}{(Z_{m1}+Z_{m2})(R_{dc}+Z_p)}, \tag{40}$$

which yields a cumbersome expression once expressed in terms of geometry and the transducer parameters. If we assume operation at a frequency well below the first resonance, the inertial term Z_{m2} can be neglected. Furthermore, if we assume operation at a frequency above which the electrical impedance term Z_p becomes small relative to R_{dc}, the relation simplifies to

$$\left(\frac{v}{f}\right)^i = N = \frac{3dL_d^2}{\eta^T L_t wt} \tag{41}$$

A third sensor relation involves measuring the open-circuit voltage resulting from a displacement input. Setting i in Equation (29) to zero and solving for s times voltage over velocity yields

$$\left(\frac{v}{u}\right)^i = \frac{sNR_{dc}Z_{m1}}{R_{dc}+Z_p} \tag{42}$$

To model a sensor driving an electrical load, such as a signal conditioning circuit, elements representing the load can be connected to the electrical terminals of the Figure 1 circuit before performing the circuit analysis.

Impedances

Two additional relations that will be used later in this work are the electrical and mechanical impedances of the ionic polymer transducer. The electrical impedance with blocked boundary condition is calculated by setting $\dot{u}$ in Equation (29) to zero and solving the first row of the equation for v/i, resulting in the expression

$$\left(\frac{v}{i}\right)^{\dot{u}} = \frac{N^2R_{dc}Z_{m1}+R_{dc}Z_p}{N^2Z_{m1}+Z_p+R_{dc}}. \tag{43}$$

The electrical impedance with free boundary conditions is calculated by setting f in Equation (29) to zero and solving the second row for $\dot{u}$. The result is substituted into the first row, and the equation is solved for v/i. The result is

$$\left(\frac{v}{i}\right)^f = \frac{R_{dc}(N^2Z_{m1}Z_{m2}+Z_p(Z_{m1}+Z_{m2}))}{N^2Z_{m1}Z_{m2}+(Z_{m1}+Z_{m2})(R_{dc}+Z_p)} \tag{44}$$

When the assumptions in Equations (30) and (31) are applied, Equations (43) and (44) both reduce to

$$\frac{v}{i} = \frac{R_{dc}Z_p}{R_{dc}+Z_p}, \tag{45}$$

the parallel combination of R_{dc} and Z_p. In the accompanying paper, experimental data that demonstrates that the electrical impedance is independent of the mechanical boundary conditions will be presented, validating the assumptions in Equations (30) and (31).

The mechanical impedance, applied force over velocity, can be calculated with both short-circuit and open-circuit boundary conditions. Setting $i=0$ in Equation (29) and solving for $f/\dot{u}$ gives

$$\left(\frac{f}{\dot{u}}\right)^i = \frac{(Z_{m1}+Z_{m2})(R_{dc}+Z_p)+N^2Z_{m1}Z_{m2}}{N^2Z_{m1}+R_{dc}+Z_p}, \tag{46}$$

the open-circuit mechanical impedance. Setting $v=0$ in Equation (29) and solving for $f/\dot{u}$ results in

$$\left(\frac{f}{\dot{u}}\right)^v = \frac{N^2Z_{m1}Z_{m2}+Z_p(Z_{m1}+Z_{m2})}{N^2Z_{m1}+Z_p}, \tag{47}$$

the short-circuit mechanical impedance. Applying the assumptions in Equations (30) and (31) to Equations (46) and (47) gives

$$\frac{f}{\dot{u}} = Z_{m1} + Z_{m2}, \tag{48}$$

which shows that, providing Equations (30) and (31) are valid, the mechanical impedance is independent of the electrical boundary conditions.

DISCUSSION

The equations presented in this chapter are very similar to those commonly used to represent piezoelectric bimorphs. This similarity is expected, since both the equivalent circuit in Figure 1 and Equation (21) appear in piezo-oriented literature. Some notable differences are as follows. First, the basic piezotransducer parameters d_{ij} and ϵ^{T} are considered to be constant, real numbers (independent of frequency). Because of the complex nature of ionic polymer transducer response relative to piezoelectric devices, the equivalent ionic polymer transducer parameters d and η^{T} are permitted to be frequency dependent, with both magnitude and phase. Also, the piezoelectric parameters are typically given subscripts that correspond to the direction of stress, strain, electric field, etc. relative to the poling direction of the piezoelectric material. In this work, we consider only bender transducers, so the electric field is always perpendicular to the induced strain, eliminating the need for subscripts. Another difference is that we have applied the second row of Equation (21) at the surface of a bender transducer only as opposed to allowing it to apply to the entire transducer volume. As a result, T represents the surface stress, and d represents the electromechanical coupling at the bender surface, unlike the more general T and d_{31} applied to piezoelectric transducers. It is emphasized that the similarity between the equations presented in this work and those used to describe piezoelectric benders does not imply a correspondance in the underlying physics.

Because of the symmetry of the Equation (29) coefficient matrix, each of the actuator equations has a corresponding sensor equation with the same Laplace domain expression, except for the sign in certain cases. For example, the relationship between an applied voltage and the resulting free deflection is identical to the relationship between an applied force and the resulting short-circuit current. A sign change occurs when comparing the equivalent force–voltage and current–velocity equations. The existence of these relationships is analogous to the reciprocity exhibited by linear electric circuits and by linear elastic structures. In physical terms, they imply that the same mechanism is responsible for the energy conversion between mechanical and electrical domains, regardless of the direction of the conversion. The four related actuator and sensor expressions are

$$\begin{aligned} \left(\frac{i}{f}\right)^{v} &= \left(\frac{\dot{u}}{v}\right)^{f} \quad \left(\frac{v}{\dot{u}}\right)^{i} = \left(\frac{f}{i}\right)^{\dot{u}} \\ \left(\frac{i}{\dot{u}}\right)^{v} &= -\left(\frac{f}{v}\right)^{\dot{u}} \quad \left(\frac{v}{f}\right)^{i} = -\left(\frac{\dot{u}}{i}\right)^{f} \end{aligned} \tag{49}$$

CONCLUSIONS

The equivalent circuit model developed in this work presents a convenient means of analyzing the sensing and actuation properties of ionic polymer materials. The model is based upon the assumption of linear electromechanical coupling, and, as such, the model has functional similarity to equivalent circuit models used for piezoelectric elements. The primary difference is the fact that all of the terms are allowed to be frequency dependent and a viscoelastic model of the mechanical modulus is directly incorporated into the equations. The input–output model simplifies considerably if it is assumed that the reflected impedance is negligible in a mechanically blocked or mechanically free boundary condition. Under this assumption we can derive expressions for important input–output relationships for sensing and actuation. In addition, the model highlights a reciprocity between sensing and actuation that has not been discussed rigorously in the literature on ionic polymer materials. This reciprocity could have deeper implications with regards to physics-based modeling of these materials.

ACKNOWLEDGMENT

This work was supported by the National Science Foundation, grant number CMS0093889.

REFERENCES

Asaka, K. and Oguro, K. 2000. "Bending of Polyelectrolyte Membrane Platinum Composites by Electrical Stimui, Part II: Response Kinetics," *Journal of Electroanalytical Chemistry*, 480:186–198.

Beranek, L.L. 1954. *Acoustics*. McGraw-Hill Book Company, New York.

de Gennes, P., Okumura, K., Shahinpoor, M. and Kim, K.J. 2000. "Mechanoelectric Effects in Ionic Gels," *Europhysics Letters*, 50(4):513–518.

Farinholt, K. and Leo, D. 2003. "Modeling of Electromechanical Charge Sensing in Ionic Polymer Transducers," to appear in *Mechanics of Materials*.

Germano, C. 1972. *Technical Pulication TP-223 Ceramic Bender Bimorphs*. Morgan Matroc Electro Ceramics, Bedford, OH.

Halliday, D. and Resnick, R. 1978. *Physics, Parts 1 and 2*. John Wiley and Sons, New York.

Ikeda, T. 1996. *Fundamental of Piezoelectricity*. Oxford Press, New York.

Inman, D.J. 1994. *Engineering Vibration*. Prentice-Hall, Englewood Cliffs.

Kanno, R., Tadokoro, S., Takamori, T. and Hattori, M. 1996. "Linear Approximate Dynamic Model of ICPF Actuator," In: *Proceedings of the IEEE International Conference on Robotics and Automation*, pp. 219–225.

Kanno, R., Tadokoro, S., Takamori, T., Hattori, M. and Oguro, K. 1995. "Modeling of ICPF Actuator – Modeling of Electrical Characteristics," In: *Proceedings of the International Conference on Industrial Electronics, Control, and Instrumentation*, pp. 913–918.

McTavish, D. and Hughes, P. 1993. "Modeling of Linear Viscoelastic Space Structures," *Journal of Vibration and Acoustics*, 115:102–110.

Nemat-Nasser, S. 2002. "Micro-mechanics of Actuation of Ionic Polymer-metal Composites," *Journal of Applied Physics*, 92(5):2899–2915.

Nemat-Nasser, S. and Li, J. 2000. "Electromechanical Response of Ionic Polymer Metal Composites," *Journal of Applied Physics*, 87(7):3321–3331.

Newbury, K.M. and Leo, D.J. 2002. "Electromechanical Modeling and Characterization of Ionic Polymer Benders," *Journal of Intelligent Material Systems and Structures*, 13(1):51–60.

Nilsson, J. 1983. *Electric Circuits*. Addison-Wesley, Reading, MA, USA.

Shahinpoor, M., Bar-Cohen, Y., Simpson, J. and Smith, J. 1998. "Ionic Polymer-Metal Composites (IPMCs) as Biomimetic Sensors, Actuators and Artificial Muscles – a Review," *Smart Materials and Structures*, 7(6):R15–R30.

Shigley, J. and Mischke, C. 1989. *Mechanical Engineering Design*, McGraw-Hill, New York.

Tadokoro, S., Yamagami, S., Takamori, T. and Oguro, K. 2000. "Modeling of Nafion-Pt Composite Actuators (ICPF) by Ionic Motion," In: *Proceedings of the SPIE*, Vol. 3987, pp. 92–102.

Ward, I. and Hadley, D. 1993. *An Introduction to the Mechanical Properties of Solid Polymers*. John Wiley and Sons, Chichester, NY.

Linear Electromechanical Model of Ionic Polymer Transducers – Part II: Experimental Validation

KENNETH M. NEWBURY AND DONALD J. LEO*

Mechanical Engineering Department, Center for Intelligent Material Systems and Structures, Virginia Tech, Blacksburg, VA 24061-0261, USA

ABSTRACT: A series of experiments are performed to assess the validity of an equivalent circuit model of ionic polymer transducers. The fundamental parameters of the model are the dielectric permittivity of the material, the viscoelastic modulus, and the effective strain coefficient of the transducer. The results demonstrate the validity of a simplifying assumption regarding the reflected impedance of the polymer. This allows us to use a simpler set of expressions to predict the time and frequency response of the polymer. The expressions for sensing and actuation are verified in a series of step response and frequency response tests of cantilevered transducers. The curvefit algorithm used for parameter identification works well but there is always a tradeoff in accuracy between the time domain and frequency domain measurements. This could imply the existence of an input-level dependence on the parameters. In spite of this level dependence, the linear model is able to predict the response of an input–output pair that is independent of the parameter identification. This result supports the validity of the linear model. Experimental results also support the use of a reciprocal model in which each expression for actuation has a dual expression for sensing. Scaling experiments verify the predictions of the model with respect to changes in transducer length and width.

Key Words: ionic polymer, electroactive polymer

INTRODUCTION

A linear model of ionic polymer materials has been developed by Newbury and Leo (2002a) based on an equivalent circuit representation of the mechanical, electrical, and electromechanical properties. The fundamental material parameters of the model are the electric permittivity, the viscoelastic modulus, and an effective strain coefficient that models electromechanical coupling. Any input–output relationship for both sensing and actuation can be determined from these three material parameters and the geometry of the transducer.

The purpose of this work is to present a rigorous experimental validation of this model within the linear operating regime of the material. This is not a straightforward task due to several factors. First, the material requires hydration to maximize the electromechanical coupling. Our experiments are performed in air, therefore it is of utmost importance to maintain a consistent level of hydration to produce repeatable experimental results. Second, the material exhibits noticeable memory which leads to nonrepeatable measurements of force and deflection under (nominally) equivalent operating conditions. Finally, back relaxation occurs when subjected to step changes in applied field. At certain times this back relaxation produces steady-state force and deflection that is opposite to the initial motion, whereas at other times it produces a steady-state response that is consistent with the initial motion. This nonrepeatability limits the ability to accurately predict the static response of the polymer.

In spite of these difficulties, our goal is to perform a set of experiments that validate the key aspects of the model developed by Newbury and Leo (2002a). These key aspects include (1) the simplifying assumption regarding the reflected impedance under blocked and free mechanical boundary conditions, (2) empirical methods for determining the three fundamental material parameters, and (3), the scaling in length and width as predicted by the model.

MODEL VALIDATION

To obtain quantitative information from the equivalent circuit model presented in Newbury and Leo (2002a), one must first determine values for several material parameters. The fact that the underlying mechanisms responsible for ionic polymer transducer behavior have not yet been conclusively identified precludes an analytical approach to parameter estimation that is based only on well understood, fundamental

*Author to whom correspondence should be addressed. E-mail: donleo@vt.edu

1045-389X/03/06 0343–15 $10.00/0 DOI: 10.1177/104538903034977

physics and known (or easily measured) material properties. To avoid this issue, an experimental approach is taken in this work.

Because significant variations in the performance of different transducers with similar dimensions have been observed, all of the model parameter identification experiments were performed on the same ionic polymer transducer. Also, the validation experiments that are compared to simulated responses were performed using the same transducer used in the identification process.

This paper is organized in the following manner. First, the experiments used to identify material parameters and to validate the model are described. Next is a detailed description of the identification procedure for each parameter. Results that validate the model follow.

Experiment Description

A variety of experiments were performed to identify material parameters and to validate the model. This section describes the methods and hardware used to generate the inputs applied to the ionic polymer transducers and to measure electrical and mechanical quantities of interest. These inputs and measurements will be referenced in later sections in this paper. Unless otherwise specified, the ionic polymer transducers were clamped between a pair of gold electrodes. All experiments were performed in air, and deionized water was brushed on the transducers at approximately one minute intervals – frequently enough to keep the surface of the transducers wet. When not in use, the transducers were stored in deionized water.

Voltage inputs for the time domain experiments were generated using a dSPACE DS1102 DSP, and random voltage inputs were generated by a Tektronix FFT analyzer with signal generator. Before being applied to the transducer, the voltage inputs were amplified using a Hewlett Packard power amplifier. Current inputs were applied using a transconductance amplifier, whose input signal was produced by either the dSPACE or the Tektronix.

The electrical current applied to the transducer was measured by placing a 0.1 Ω resistor in series with the polymer, between the polymer and ground. The voltage across the resistor was amplified and measured using either the dSPACE or the Tektronix. The electrical current was calculated during post processing by dividing the voltage drop across the resistor by 0.1 Ω. The applied voltage was measured directly using either the dSPACE or the Tektronix.

In an experiment used to verify the model's symmetry, the short-circuit charge was measured while the polymer was excited mechanically. This measurement was accomplished using an op-amp based charge amplifier, which converted short-circuit charge to a voltage signal. During postprocessing, the charge amp output was divided by the complex gain of the amplifier circuit because the lower end of the frequency range of interest was near the corner frequency of the charge amp circuit.

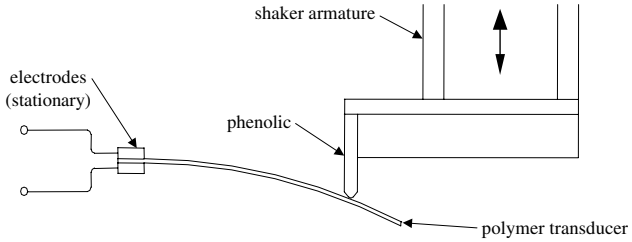

Figure 1. *Mechanically driven polymer.*

Some experiments involved mechanically driving the polymer transducer. Motion was imparted to the polymer using an APS Dynamics APS 113 long stroke shaker. A bracket with a wedge shaped piece of phenolic (see Figure 1) was mounted to the shaker armature to provide the interface between the transducer and the shaker. The position of the armature was measured using a Novotechnik T25 linear potentiometer and an appropriate signal conditioning circuit. Manufacturer's specifications indicate that the linear potentiometer repeatability is 0.002 mm, and the linearity is 0.06 mm. To assure that the armature displacement corresponded to the polymer displacement at the point of contact, the polymer was positioned relative to the shaker such that a preload was applied, and constant contact between the polymer transducer and the phenolic was maintained.

All force measurements in this work were made using a Transducer Techniques GSO-10 10 g load cell with a TMO-1 signal conditioning circuit. The load cell precision, repeatability, and linearity were 0.05 mN. The force measurement was also relatively noisy, with a typical noise level of 0.02 mN rms. The force between the polymer transducer and the load cell sensing element was transferred through a nylon screw that was screwed into the tapped hole provided in the load cell sensing element. In some experiments, the polymer was positioned relative to the load cell such that there was a slight preload on the polymer. For time domain analyses, this preload was subtracted out during postprocessing. The purpose of the preload was to allow 'negative' forces to be measured, which was especially important when an AC signal was applied to the transducer.

Two methods were used to obtain noncontact measurements of transducer displacement. For experiments that were analyzed in the frequency domain, a Polytec OFV-303 laser vibrometer head with OFV-3001 controller and OVD-20 demodulator was used, resulting in a position signal with a resolution of 5 μm. Because the angle of the bender transducer surface changes with displacement, this method was limited to small displacements. Also, the electroded polymer surface was a poor target, and reliable tracking was difficult to achieve.

Most observations of the polymer actuator's displacement were made using a RedLake PCI 2000 high speed digital video camera. The camera is capable of frame rates up to 2000 Hz; however, only 8 s of continuous data can be recorded at this rate. A frame rate of 125 Hz was used for the experiments reported in this work – a rate fast enough to capture the polymer motion, but slow enough to allow recording of up to 60 s of continuous data. A small 'dot' of correction fluid (white-out), placed on the polymer edge, acted as a target for the Image Express MotionTrace image analysis software. During postprocessing, the MotionTrace software was used to create a time history of the target's position. Under ideal conditions, MotionTrace is capable of determining the target position with resolution on the order of tenths of a pixel. In the experiments reported in this work, one pixel corresponded to approximately 0.1–0.2 mm. The resolution achieved in a particular experiment depends on many factors, such as lighting, target size and shape, and lens quality. Though its resolution was limited compared to the laser vibrometer, the video camera and motion analysis software provided a reliable means by which to measure large transducer displacements.

VALIDATION OF IMPEDANCE ASSUMPTIONS

This section presents data that validates the assumptions in Equations (30) and (31) from Newbury and Leo (2002a). Figure 2 shows a plot of the measured frequency domain electrical impedance and time domain electrical response of a ionic polymer transducer ($w = 5\,\text{mm}$, $L_t = 20\,\text{mm}$, $L_{\text{free}} = 15\,\text{mm}$, $L_d = 13\,\text{mm}$) with both free and blocked boundary conditions. The plots corresponding to the two boundary conditions are identical, which matches the analytical result derived in Newbury and Leo (2002a).

To see that the experimental results in Figure 2 show that the Equations (30) and (31) assumptions are true, consider the following argument. Analysis of the Figure 1 circuit for both blocked ($\dot{u} = 0$) and free ($f = 0$) mechanical boundary conditions yields the following expressions for the impedance seen at the electrical terminals

$$\begin{aligned} \left(\frac{v}{i}\right)\dot{u} &= R_{\text{dc}} \| (Z_p + N^2 Z_{m1}) \text{ and} \\ \left(\frac{v}{i}\right) f &= R_{\text{dc}} \| (Z_p + N^2 (Z_{m1} \| Z_{m2})), \end{aligned} \tag{1}$$

where the symbol $\|$ indicates parallel circuit elements, whose equivalent impedance is the inverse of the sum of the inverses of the individual impedances. Providing that the following three conditions are met, the only way the expressions in Equation (1) can become equivalent to one another is if the assumptions in Equations (30) and (31) are true, resulting in

$$\frac{v}{i} = R_{\text{dc}} \| Z_p. \tag{2}$$

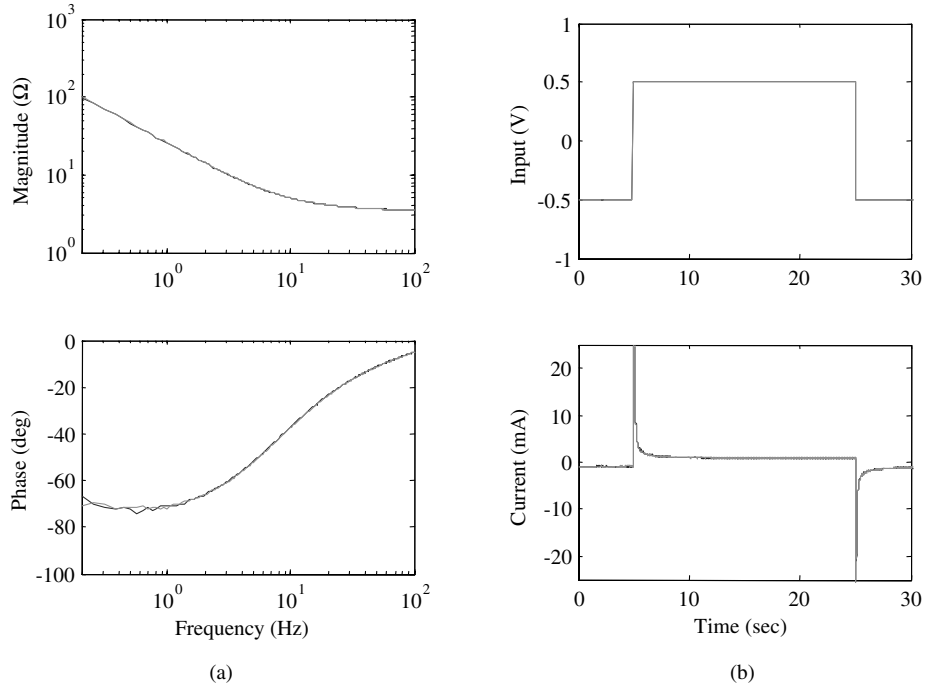

Figure 2. *Electrical response with free and blocked boundary conditions: (a) frequency domain impedance; (b) time domain current response with a voltage input.*

The first condition is that the polymer stiffness term Z_{m1} is nonzero. Second, R_{dc} must be as the same order as or greater than Z_p. If R_{dc} was very small relative to Z_p, both expressions in Equation (1) would reduce to $(v/i) = R_{dc}$. The fact that the frequency domain impedance plot in Figure 2 has a phase other than 0 or 180° shows that the impedance is not purely real, as it would be if $(v/i) = R_{dc}$. Therefore, the second condition is met. The third condition is that the inertial term Z_{m2} must be small relative to the stiffness term over at least part of the frequency range examined. If this condition is not met, then $Z_{m1} \| Z_{m2} \simeq Z_{m1}$. This condition was satisfied for all frequencies well below the first resonance of the transducer, which was approximately 150 Hz for the transducer used to generate the data for Figure 2.

Now that the Equations (30) and (31) assumptions are justified, the simplified expressions developed in Newbury and Leo (2002a) can be used with confidence. Also, since the electrical impedance does not depend on the mechanical boundary conditions, and the mechanical impedance is independent of the electrical boundary conditions, the superscripts on the parameters Y^E and η^T will be omitted.

IDENTIFICATION OF MODEL PARAMETERS

In general, the approach to parameter identification taken in this work was to consider the analytical expressions corresponding to several measurable input–output relationships and identify the expressions that are strongly affected by the term of interest but contain as few additional material parameters as possible. This approach allowed the material parameters to be isolated and then identified.

All the parameter identification experiments were performed on the same ionic polymer transducer. The transducer dimensions were: $t = 0.2$ mm, $w = 5$ mm, $L_t = 33$ mm, $L_{free} = 25$ mm, and the distance L_d between the electrode (the clamped end) and driving point was 20 mm.

One issue that hampered the parameter identification process as well as the model validation process was the relatively inconsistent behavior exhibited by the polymer transducers. Figure 3 shows results of identical blocked force with voltage input experiments that were performed only minutes apart, without disturbing any of the hardware used in the experiment. While the current responses overlay very well, there are significant differences in portions of the blocked force. In one experiment, the transducer exerted a steady-state blocked force in the same direction as the initial force. In the other experiment, the opposite was true. With the polymer used in the identification process, the response with steady-state force in the opposite direction from the initial force was seen more frequently. Inconsistent behavior was less of an issue for the experiments that were analyzed in the frequency domain. The greater consistency seen in frequency domain data may be due to the fact that data from a much greater period of time were averaged. Also, it is possible that the transducers behave more consistently above approximately 1 Hz.

Mechanical Terms

The mechanical parameters of the ionic polymer transducer are the static modulus Y_∞, the GHM parameters α, ζ, ω, and the density ρ_m. The density was determined by measuring the mass of the polymer transducer using a Mettler Toledo model AB204

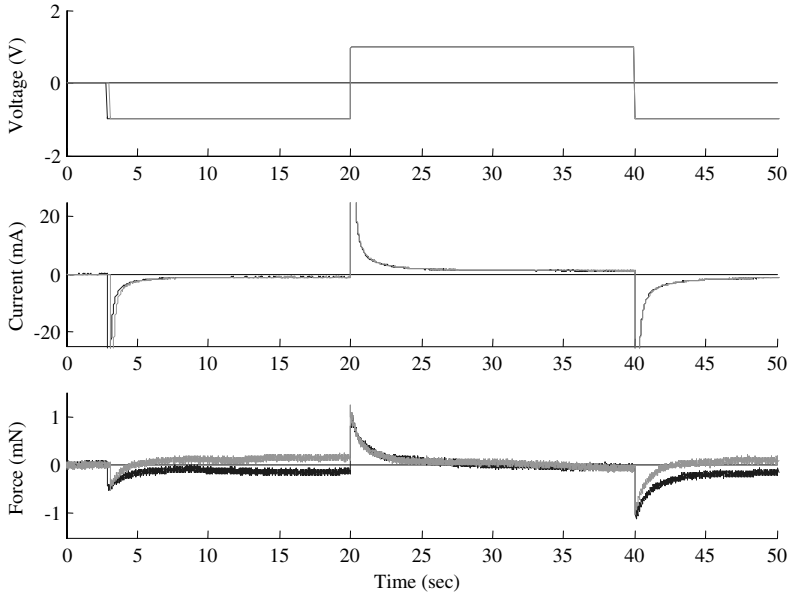

Figure 3. *Blocked force with voltage input experiments that illustrate inconsistent polymer transducer behavior.*

precision balance, then dividing by the volume. Just before placing the transducer on the balance, any excess water present on the electrode surfaces was removed by gently patting the surface with a paper towel. The mass of the transducer was 85 mg, resulting in a density of 2.6E3 kg/m^3. Because the transducer was brushed with water to keep it hydrated during experiments, some water was present on the transducer surface during the experiments. The mass of the transducer, with as much water as it could hold on its surface was 121 mg, a 42% increase over the mass with no water on the surface. The effective mass of the polymer during experiments was most likely between these two extreme values; however, unless one is considering an input–output relationship that is strongly affected by the density, any error that is introduced will be small.

The static modulus and the GHM parameters were determined using an experiment in which the load cell was mounted to the shaker armature. The transducer was given a displacement input using the shaker, and the required force was measured. To determine the static value of the elastic modulus Y_∞, a step displacement was imparted to the polymer by moving the shaker armature manually. The stiffness (force divided by deflection) versus time was measured and plotted. For a sample response, see Figure 4(a). Little variation in the stiffness was seen after the displacement input, so the measured stiffness was assumed to correspond to the static modulus. Equation (4) from Newbury and Leo (2002a), the static relationship between force and deflection of a cantilevered beam, was used to convert the stiffness to a modulus, resulting in $Y_\infty = 0.40$ GPa (corresponding to a stiffness of 0.5 N/m).

To determine the GHM parameters, a random signal was applied to the shaker and the frequency response between the force measured by the load cell and the position was measured and recorded. A small preload was first applied to the transducer, so that it would not lose contact with the load cell during the motion.

It is common practice to mount a load cell between a shaker and the structure being excited in order to measure the force acting on the structure. Typically, the forces exerted on the structure are much higher than the inertial forces acting on the load cell sensing element, and the force measurement accurately represents the force exerted on the structure. This convenient relationship between exerted force and inertial forces acting on the load cell sensing element does not hold true in the experiment used to estimate the modulus and GHM parameters. This fact is illustrated in Figure 4(b), where plots of the load cell response with no polymer in the fixture and with a polymer in the fixture are shown. Above approximately 2 Hz, the 'accelerometer response' from the load cell becomes significant. To compensate for the fact that the load cell used also acts as an accelerometer, postprocessing of the data was performed to remove the component of the measured force that did not correspond to the force exerted on the polymer bender.

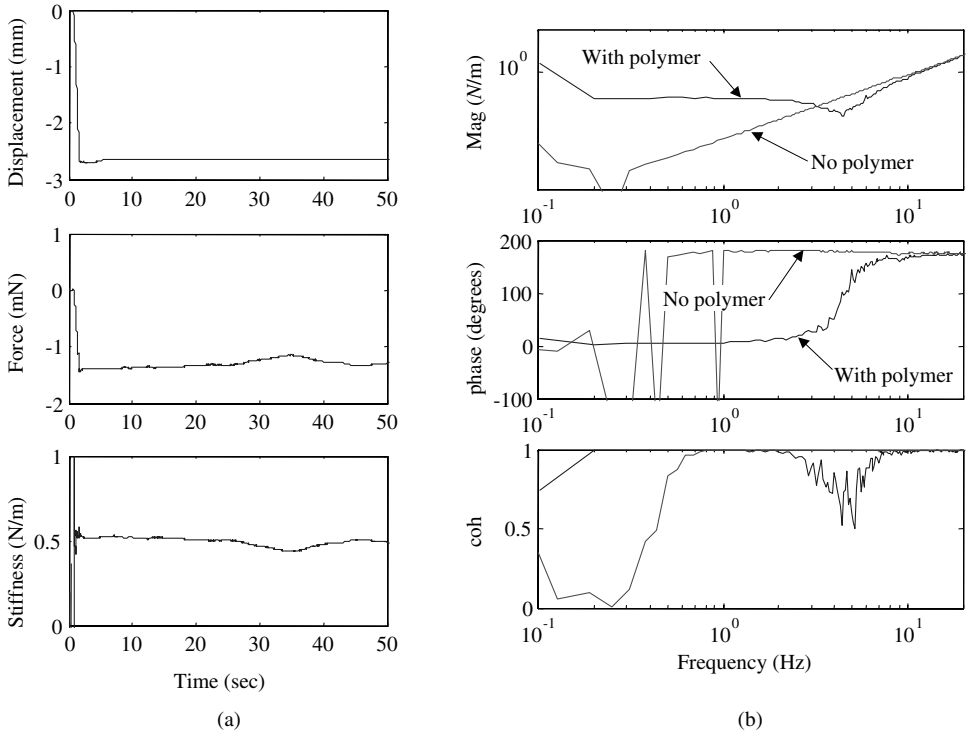

Figure 4. *Responses from polymer transducer mechanical experiments: (a) Time domain measurement with step displacement input; (b) Frequency domain load cell response.*

The MATLAB constrained minimization routine *fmincon* was used to determine the GHM parameters α, ζ, and $\hat{\omega}$ by minimizing the error between the measured frequency dependent stiffness (experimental data) and the stiffness corresponding to the frequency response of the modulus described by Equation (9) in Newbury and Leo (2002a). Specifically, the error function that was minimized, denoted by Υ is

$$\Upsilon = \frac{1}{M}\sum_{i=1}^{M} \left\| k_{\text{pred}}(f_i) - k_{\text{meas}}(f_i) \right\|^2, \tag{3}$$

where the f_i represents the M discrete frequencies at which the stiffness was measured, and the subscripts 'pred' and 'meas' denote the predicted and measured values of the frequency response.

The resulting parameters are $\alpha = 5.2$, $\zeta = 0.68$, and $\hat{\omega} = 2100$. Note that the value of $\hat{\omega}$ is well beyond the frequency range of the experimental data. The measured polymer stiffness showed little frequency dependence, indicating that viscoelasticity is not significant in the 0–20 Hz range – the ionic polymer acts predominantly like a linear elastic material. With so little frequency dependence in the measured stiffness, accurate determination of the GHM parameters from the experiment described above cannot be expected. Once all of the model parameters were identified, a simulated free deflection over voltage frequency response was compared to a measured response. The displacement measurement was performed using the laser vibrometer, and the frequency range of the test included the first resonant frequency of the transducer. The GHM parameters were 'adjusted' to provide a good match between the simulated and measured damping of the first resonance. The resulting values, which are used in the remainder of this work, are $\alpha = 2.2$, $\zeta = 0.6$, and $\hat{\omega} = 2100$. Because viscoelasticity is not significant in the frequency range considered in this work, the frequency dependent modulus, modeled using the GHM method, amounts to little more than a convenient means through which to model the small amount of damping present in the transducer response. However, if the frequency range of the model is extended, the viscoelastic terms will become more important.

Electrical Terms

The electrical terms to be identified are the resistivity from Equation (15) in Newbury and Leo (2002a) and the n resistivities and permittivities in Equation (19) in Newbury and Leo (2002a). A combination of time and frequency domain data were used to estimate values for these terms.

First, consider the DC response of the electrical side of the circuit shown in Figure 1 in Newbury and Leo (2002a). Because there is a capacitor in series with the resistor in each of the branches of the Z_p circuit, Z_p will not conduct current at DC. This fact can be shown by applying the Final Value Theorem (Franklin et al., 1994) to the inverse of the Laplace domain expression for Z_p in Equation (18) in Newbury and Leo (2002a). The result, zero, represents the DC current conducted by Z_p with a constant voltage input. Because Z_p will not conduct DC current, the only circuit element that is related to the DC response of the left hand side of the equivalent circuit is R_{dc}, whose value is determined by the material parameter ρ_{dc} and the transducer dimensions. To estimate ρ_{dc}, the current was measured while applying a step voltage to the transducer. A sample step response is shown in Figure 5. The step magnitude was divided by the steady state current resulting in a value of 400 Ω for R_{dc}. Using this value for the left hand side of Equation (15) and solving for ρ_{dc} gives $\rho_{\text{dc}} = 330\,\Omega\,\text{m}$.

The values for the material parameters ρ_i and ϵ_i, which are needed to calculate Z_p were determined using the MATLAB constrained minimization routine *fmincon*. The constraints placed on the minimization were $\rho_i > 0$ and $\epsilon_{\text{i}} > 0$. The errors in the simulated voltage step response, the simulated current step response, and the simulated frequency response of the parallel combination of R_{dc} and Z_p were used in the function Υ that was minimized. The step responses were included in the identification process in order to capture the low frequency dynamics of the transducer response, which are at frequencies below those that are practical to

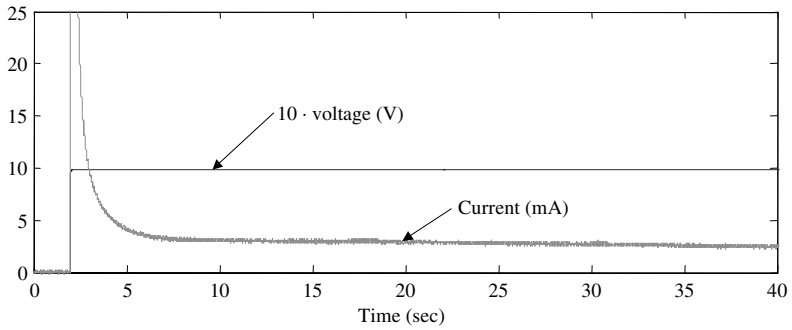

Figure 5. *Current response with a voltage step input – used to determine polymer transducer DC resistance.*

observe with frequency domain methods. The error in the frequency response was multiplied by a frequency dependent weighting function, so that the higher frequencies, where the impedance is relatively small, would not be ignored during the minimization. The relative weights of the step response errors and the frequency response error were also adjusted.

Figure 6 contains a plot of the measured electrical impedance, the frequency dependent weighting function used in the minimization, and the product of the weighting function and the impedance. The weighting function is

$$\Psi(f_i) = \begin{cases} f_i^{0.8} \text{ for } f_i < 12.5 \\ 12.5^{0.8} \text{ for } f_i > 12.5 \end{cases} \quad (4)$$

The prediction error to a voltage step input was quantified using

$$e_1 = \sqrt{\frac{1}{M}\sum_{i=1}^{M}(x_{i,\text{pred}} - x_{i,\text{meas}})^2}, \quad (5)$$

where the x_i are the values of the current at the M discrete points in the experimental time history, and the subscripts 'pred' and 'meas' denote predicted and measured values. The prediction error to a current step, represented by e_2, was determined in the same manner. The function that was minimized is

$$\Upsilon = w_1 e_1 + w_2 e_2 + w_3 \frac{1}{P}\sum_{i=1}^{P}\Psi(f_i)\left|Z_{\text{pred}}(f_i) - Z_{\text{meas}}(f_i)\right|, \quad (6)$$

where $Z(f_i)$ denotes the electrical impedance at frequency f_i, and w_1, w_2, and w_3 are scalars that can be adjusted to bias the fit towards either the step responses or the frequency domain impedance measurement. Four resistivities and permittivities (to describe η) were required to obtain a reasonable fit to the experimental responses. Figure 7 contains plots of the experimental and predicted responses with $w_1 = 100$, $w_2 = 0.5$, and $w_3 = 2$ – the corresponding transducer parameters are given in Table 1. The inputs were a 1 V voltage step, a 5 mA current step, and a 0.18 Vrms 0–50 Hz random input. The experimental frequency response is based on

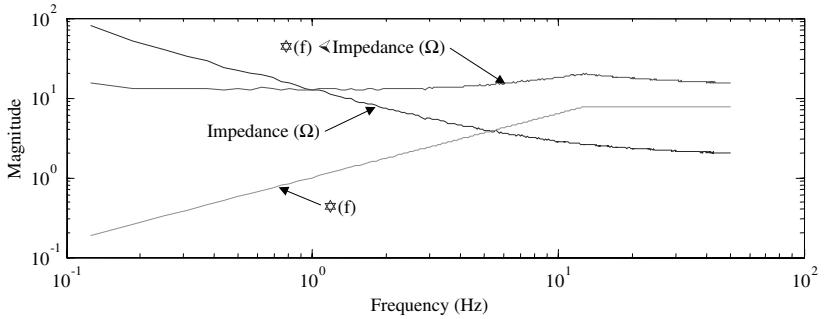

Figure 6. *Weighting function used in minimization of frequency response prediction error.*

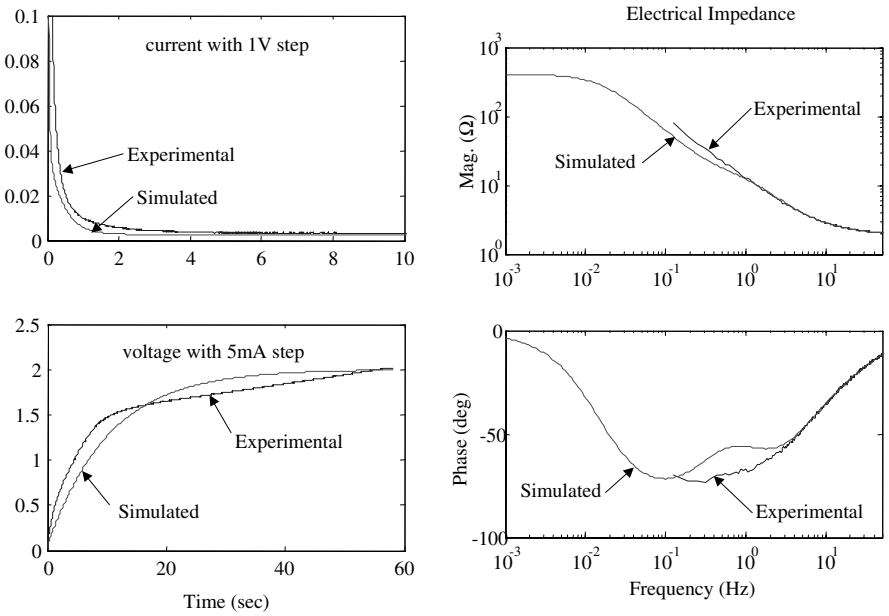

Figure 7. *Simulated vs. experimental electrical response with $w_1 = 100$, $w_2 = 0.5$, and $w_3 = 2$.*

15 averages of a 2048 point FFT with a sampling rate of 128 Hz.

Several combinations of w_1, w_2, and w_3 were tried in attempts to obtain a better fit to the experimental data than that shown in Figure 7. It was found that an improvement in the step response fits and a better fit to the frequency domain data were mutually exclusive, indicating that the dynamics in the transducer response may be input level dependent. It is unlikely that the difficulty in fitting both the time and frequency domain data is a result of experimental error, since the same signal conditioning circuits and test fixtures were used for all the experiments.

Electromechanical Coupling Term

In Newbury and Leo (2002a), the transformer turns ratio N, which represents the electromechanical coupling, was interpreted as the relationship between open-circuit voltage and applied force. For this interpretation to apply, the transducer's DC resistance R_{dc} (400) must be large relative to the impedance Z_p, so that the charge generated by the electromechanical coupling is not 'bled off' through R_{dc}. Inspection of the electrical impedance plot in Figure 7 reveals that the parallel combination of Z_p and R_{dc} is at least an order of magnitude less than the value of R_{dc} for approximately 0.1 Hz and above. This order of magnitude ratio will not occur unless R_{dc} is very large relative to Z_p. Therefore, the physical interpretation for N, along with the ensuing derivation in terms of dimensions and material parameters, is valid for 0.1 Hz and above.

Table 1. Resistivities and permittivities for $w_1 = 100$, $w_2 = 0.5$, and $w_3 = 2$.

Permittivity (F/m)	ϵ_1	ϵ_2	ϵ_3	ϵ_4
	0.018	0.0084	0.0035	0.00040
Resistivity (Ω m)	ρ_1	ρ_2	ρ_3	ρ_4
	32.8	4.24	3.0	11.2

The identification of the strain coefficient d is based on the expression for the blocked force exerted by the polymer transducer when excited by a voltage input. This experiment was chosen because it depends on only two material parameters, the modulus Y and the strain coefficient d. Because the blocked force is independent of the other material parameters, the identification of the d parameter can only be affected by inaccuracies in the identification of the modulus – it will be not be affected by errors in any of the other material parameters.

The blocked force expression, derived in Newbury and Leo (2002a) is

$$\left(\frac{f}{v}\right)^{\dot{u}} = \frac{3dtwY}{4L_d}. \tag{7}$$

As with the terms responsible for the dynamics of the electrical impedance, a combination of time and frequency domain data was used in the identification process. Both the force produced by a 1 V step input and the force produced by a 0–20 Hz 0.61 Vrms random input were considered. The frequency domain data is based on 10 averages of a 2048 point FFT with a sampling rate of 51.2 Hz.

To help determine the nature of the function used to represent d, the blocked force step response, an example of which is shown in Figure 8(a), was analyzed. One

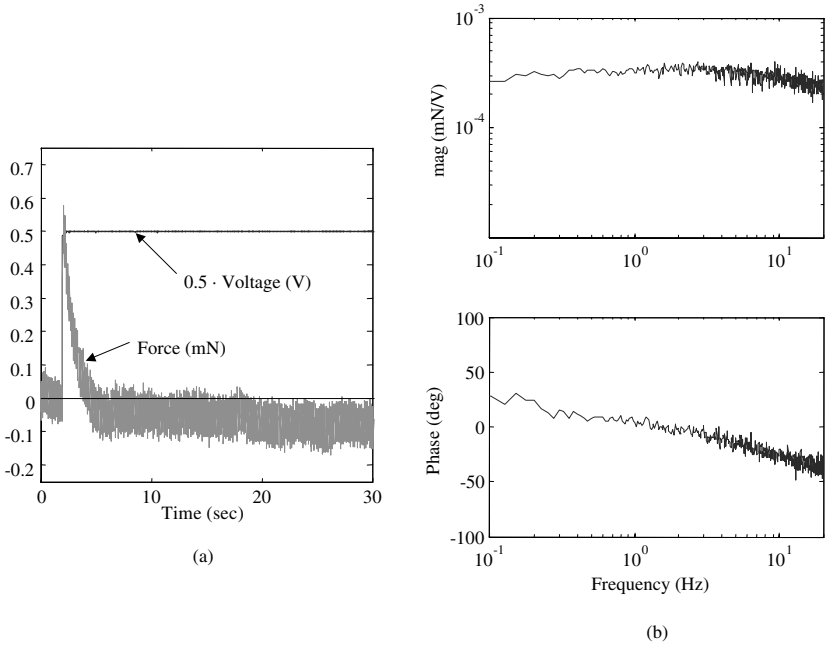

Figure 8. *Blocked force with voltage input: (a) Step response; (b) Frequency response.*

important response feature is that the initial force and the DC gain have opposite signs. By the following argument, this feature leads to the conclusion that d is nonminimum phase. Consider modeling the response to a step with magnitude V_s using an expression with a single time constant, such as

$$f = V_s(-A + Be^{-br})1(\tau) \text{ with } B > A, \tag{8}$$

where A, B, and b are positive scalars, τ represents time, and $1(\tau)$ is the unit step function. This expression will have a positive initial response of B − A and a DC value of −A. Transforming Equation (8) to the Laplace domain and solving for the transfer function f/v gives

$$\frac{f}{v} = \frac{s(B-A) - Ab}{s+b}, \tag{9}$$

which has a pole at $-b$ and a zero at $Ab/B-A$. Since $B > A$, the zero is in the right half plane, and the expression in Equation (9) is nonminimum phase.

Further insight can be gained by also considering the frequency domain data for the blocked force, shown in Figure 8(b). Above 2 Hz, the phase starts to drop below 0°. The phase of the single pole–zero combination in Equation (9) will start at 180° and end up at 0°, but it cannot produce a net phase change greater than 180°. Therefore, additional terms will be necessary. Note that the additional phase lag cannot be accounted for by the frequency dependence of the modulus because the modulus adds phase lead to the blocked force transfer function.

The DC gain of the transfer function was first determined by examining the blocked force step response shown in Figure 8(a) and solving for the DC gain of d using Equation (7). The MATLAB constrained minimization routine *fmincon* was used to estimate the poles and zeros of a transfer function for d. The constraints imposed were that one of the zeros be positive and that the remaining poles and zeros be negative. Equation (7) was used to predict the blocked force corresponding to d. The prediction error for the step response was quantified using

$$e_1 = \sqrt{\frac{1}{M}\sum_{i=1}^{M}(x_{i,\text{pred}} - x_{i,\text{meas}})^2}, \tag{10}$$

where the x_i are the force values at the M discrete points in time, and the subscripts 'pred' and 'meas' denote predicted and measured values. The function that was minimized is

$$\Upsilon = w_1 e_1 + w_2 \sqrt{\frac{1}{P}\sum_{i=1}^{P}\left|F_{\text{pred}}(f_i) - F_{\text{meas}}(f_i)\right|^2}, \tag{11}$$

where $F(f_i)$ denotes the blocked force per volt at frequency f_i, and w_1 and w_2 are scalars that can be adjusted to bias the fit towards either the step response or the frequency domain measurement. A transfer function with three zeros and four poles gave a reasonable fit to both the step response and the frequency domain data. A comparison of the experimental and simulated responses is shown in Figure 9 with $w_1 = 5$ and $w_2 = 1$.

As with the identification process for the electrical parameters, it was not possible to obtain a 'good' fit to both the step response and the frequency domain data. If the fit was biased towards the frequency response, the

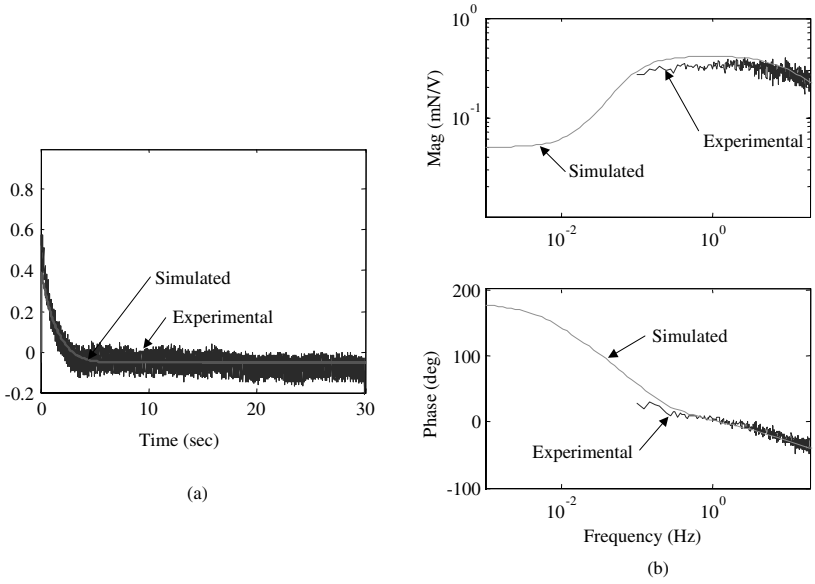

Figure 9. *Simulated and experimental blocked force with voltage input: (a) Step response; (b) Frequency response.*

peak value of the predicted step response was only 50–60% of the measured value. In the plot shown in Figure 9, the predicted peak of the step response is 72% of the measured value. This discrepancy is another indication that the material parameters may be dependent on excitation level.

Bode plots of the three key frequency dependent material parameters, η, d, and Y over the frequency range 0.01–20 Hz are shown in Figure 10. A brief summary of the more noteworthy features of each follows. The electrical term η, which replaces the permittivity in Equation (21), represents the relationship between charge density and the applied electric field. The highest charge densities will be achieved at very low frequencies, 0.1 Hz and below. Above this range, the value of η starts to decrease (at less than one decade per decade), and the phase approaches -90°, indicating that the resistive elements in Figure 4 start to dominate the relationship between the charge density and the applied electric field. The strain coefficient d, plotted in Figure 10(b), represents the electromechanical coupling in terms of the strain induced at the transducer surface when an electric field is applied perpendicular to the transducer. At very low frequencies, below 0.1 Hz, the magnitude of the coupling term decreases with decreasing frequency, indicating that the ionic polymer transducers considered in this work will make poor sensors and actuators for quasi-static applications. The coupling term magnitude also decreases with increasing frequency above approximately 5 Hz, though the slope is more gentle than the sub 0.1 Hz slope. This decrease in the strain coefficient will eventually limit the useful frequency range of ionic polymer transducers. Also, the term exhibits significant phase lag. The complex modulus shown in Figure 10(c) is relatively flat across the 0.01–20 Hz frequency range. The slight increase in magnitude along with a little phase lead represents the small amount of damping that was observed in the free deflection over voltage frequency response. The fact that the modulus plot is relatively flat indicates that viscoelasticity is not important in the frequency range considered.

MODEL VALIDATION

To validate the form of the model introduced in Newbury and Leo (2002a), as well as the material parameters identified in the previous section, simulated responses will be compared to experimental responses from the same transducer that was used in the parameter identification process. The comparison will be made for input–output relationships that are different than those used for parameter identification. As a result, the comparison will validate the form of the model, as opposed to just confirming the quality of the identification process for a particular parameter. The symmetry in the model, which results from the presence of the transformer, will also be demonstrated experimentally. To confirm that the circuit parameters scale correctly with changes in transducer dimensions, the results of several experiments conducted with different size transducers will be presented. The results are scaled using the relationships in the analytical expressions for

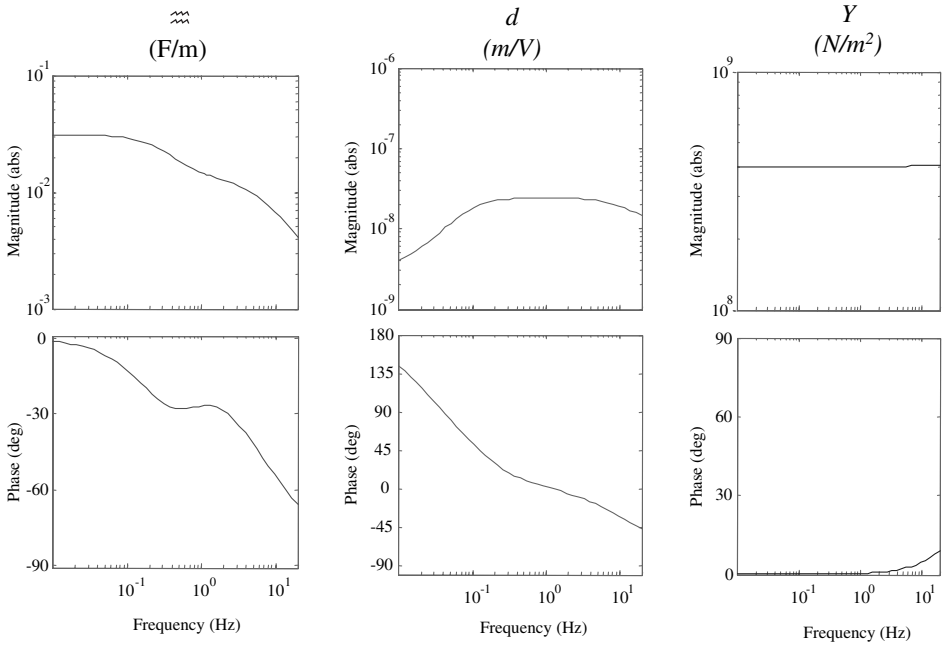

Figure 10. *Frequency domain plot of the key frequency dependent material parameters η, d, and Y.*

the various input–output relationships. Note that these comparisons will also confirm that the material parameters used in this paper are, in fact, independent of transducer dimensions.

Model Form Verification

Figure 11 shows a frequency domain comparison of experimental and simulated blocked force with a current input. The corresponding expression, in terms of transducer dimensions and material parameters (derived in Newbury and Leo (2002a)), is

$$\left(\frac{f}{i}\right)\dot{u} = \frac{NR_{\mathrm{dc}}Z_{m1}}{R_{\mathrm{dc}} + Z_p} = \frac{3dt^2 Y\rho_{\mathrm{dc}}}{4L_{\mathrm{d}}L_{\mathrm{t}}(1 + s\eta\rho_{\mathrm{dc}})}. \qquad (12)$$

In this expression, unlike the relation for blocked force over voltage, which was used to identify d, the electrical terms ρ_{dc} and η appear. The plot in Figure 11 verifies the magnitudes of the electrical parameters ρ_{dc} and η relative to d. A comparison of experimental and simulated step response was not made for blocked force over current for the following reason. To avoid the changes in the nature of the response that appear to occur with higher input levels (above approximately 1.25 V), input voltages were kept to 1 V or less. Because of the high DC resistance of the polymer transducer (400 Ω), this input level restriction would require a 2.5 mA or smaller step. The peak forces generated by such a small current step (0.04 mN predicted using the model) would be too small to measure with the 10 g load cell.

To further validate the form of the model, experimental and simulated free deflection are plotted in Figure 12. The analytical expression (derived in Newbury and Leo (2002a)) is

$$\left(\frac{u}{v}\right)^f = \frac{-NZ_{m1}}{sZ_p(Z_{m1} + Z_{m2})} = \frac{-3dL_{\mathrm{d}}^2}{\left(12\rho_m L_f^4/\Gamma^4 Y\right)s^2 + t^2}. \qquad (13)$$

Note that this expression also includes the mass term Z_{m2} and will, therefore, have a resonance. The natural frequency of the transducer is predicted accurately, but the simulated response is more heavily damped than the experimental response. This is another indication that the model would benefit from a better experiment for determining the mechanical material parameters. Besides the damping, the predicted results compare well to experimental data in the frequency domain. A time domain comparison is made using a 0.025 Hz 0.5 V square wave input. A square wave was used instead of a step input to avoid the permanent deformation that sometimes accompanies a DC input (Newbury and Leo, 2002b). As long as the frequency of the square wave is low relative to the dynamics in the system response, the shape of the response will be identical to that of repeated step inputs of opposite sign. Therefore, the time domain response comparison with a low frequency square wave input provides a means by which to examine the dynamics that are at frequencies below those included in the frequency domain data. The model slightly underpredicts the response peak, which corresponds to the overpredicted damping seen in the frequency response. The dominant time constants of the relaxation phase of the response also match. The biggest discrepancy between the simulated and experimental responses is in the DC gain. In this experiment, the steady-state displacement of the transducer was in the

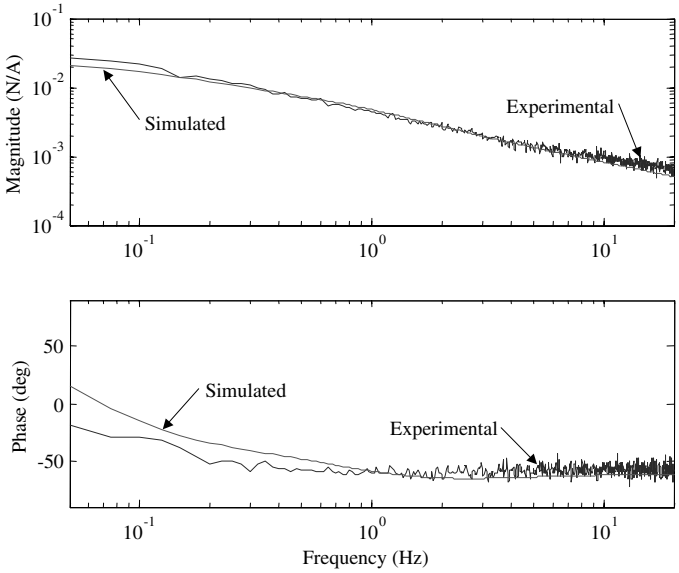

Figure 11. *Comparison of simulated and experimental blocked force with a current input.*

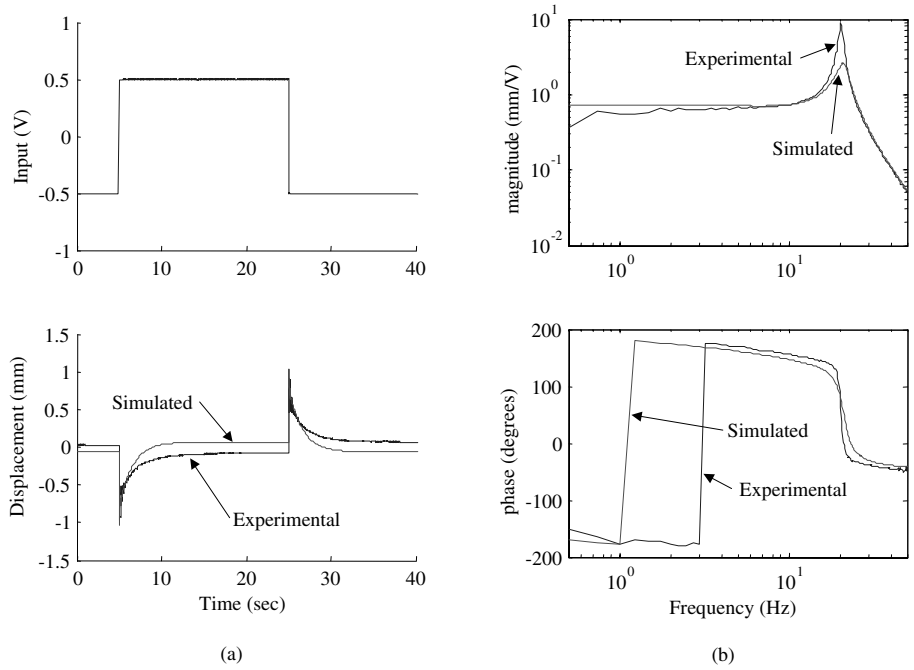

Figure 12. *Comparison of simulated and experimental free deflection with a voltage input: (a) Frequency response; (b) Square wave response.*

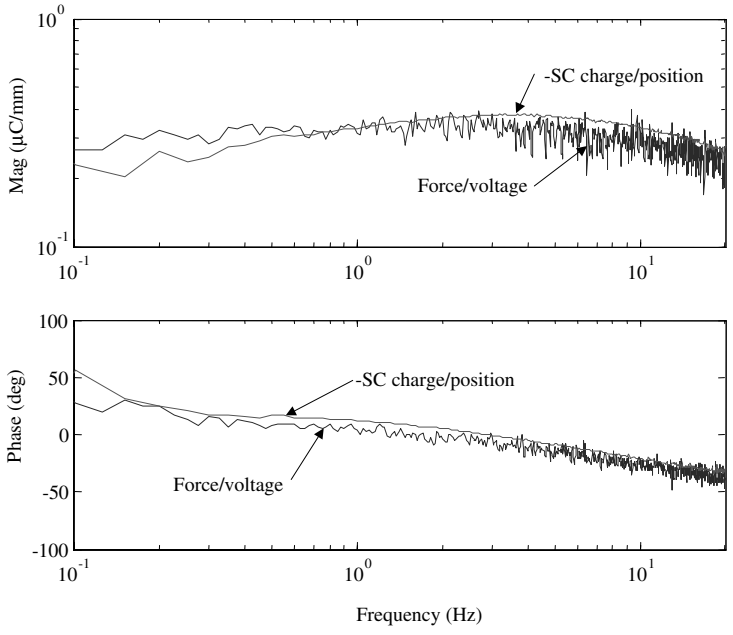

Figure 13. *Comparison of blocked force with voltage input and open circuit charge with displacement input.*

same direction as the initial motion, unlike the blocked force with voltage input experiments used in the identification of the d parameter. This discrepancy, however, is not surprising given the inconsistencies sometimes observed in identical experiments (illustrated in Figure 3).

Because the electromechanical coupling is modeled using a transformer (in the equivalent circuit in Figure 1), some of the actuator and sensor equations are identical, with the exception of the sign in some cases. One pair of these 'reciprocal relations' is blocked force with a current input $(f/i)^{\dot{u}}$ and open circuit voltage with a velocity input $(v/\dot{u})^{i}$. Another pair is blocked force with a voltage input $(f/v)^{\dot{u}}$ and short circuit charge with a displacement input $(q/u)^{v}$. Figure 13 contains a comparison of experimental data corresponding to $(f/v)^{\dot{u}}$ and $(q/u)^{v}$ for the same polymer on which the identification experiments were performed ($t = 0.2$ mm, $w = 5$ mm, $L_t = 33$ mm, $L_{free} = 25$ mm, $L_d = 20$ mm). The match is good, indicating that the bidirectional

electromechanical coupling represented by the transformer is exhibited by ionic polymer bender transducers. The slight discrepancy in magnitude may be due to small errors in measuring the distance L_d. Neither the nylon screw through the load cell sensing element nor the phenolic wedge have sharp edges where they contact the transducer. For this reason, it is difficult to determine L_d with greater precision than approximately 1 mm.

Scaling Verification

To further verify the form of the model as well as the expressions derived for the circuit elements, several different experiments were repeated as transducer dimensions and/or L_d, the distance between the electrodes (the clamped end of the cantilever) and the point at which force or deflection is measured, were varied. The results for each set of dimensions were then scaled to correspond to a single set of dimensions by multiplying by a constant. This constant was determined by the dimension(s) varied and the scaling law suggested by the appropriate input–output relation from Newbury and Leo (2002a). Sample transducers with different thicknesses were not available to the authors, so no experiments verifying the scaling with respect to thickness are presented in this work.

In the interest of obtaining consistent experimental results, each experiment in a set was performed on the same transducer with minimal changes to the experimental setup. It was necessary to use different polymers for different experiment sets because varying width w and total length L_t required cutting the transducer. For this reason, similar experiments performed on different transducers may not compare well when scaled to the same set of dimensions because of transducer to transducer variation. In other words, the material parameters sometimes vary from one transducer to another, an observation also made by other researchers.

In Figure 14(a), plots of the blocked force with a voltage input for $L_d = 11$, 13, 17, and 20 mm are shown. The other transducer dimensions were $w = 4.5$ mm, $L_t = 33$ mm, and $L_{free} = 25$mm, and they were not varied. The input was a 0–20 Hz 1 Vrms random signal, and each frequency response plot is based on five averages and 2048 point FFTs performed on data sampled at 51.2 Hz. Note that all the phase plots in Figure 14(a) match one another. Also, the vertical separation of the magnitude plots is essentially constant across the range of frequencies. This constant separation (with logarithmic horizontal and vertical axes) and the identical phase plots are signs that the plots are related through scalars. The expression for blocked force with a voltage input, derived in Newbury and Leo (2002a) is

$$\left(\frac{f}{v}\right)\dot{u} = \frac{3dtwY}{4L_d}, \tag{14}$$

which indicates that blocked force with a voltage input is inversely proportional to L_d. Figure 14(b) contains plots of the same data shown in Figure 14(a), except that each plot has been multiplied by (11 mm/L_d), so it can be directly compared to the data for $L_d = 11$. The magnitude plots overlay quite well, confirming that the blocked force with a voltage input is inversely proportional to L_d, as suggested by Equation (14) from Newbury and Leo (2002a).

In Figure 15(a), the blocked force over voltage input frequency response is plotted for three values of

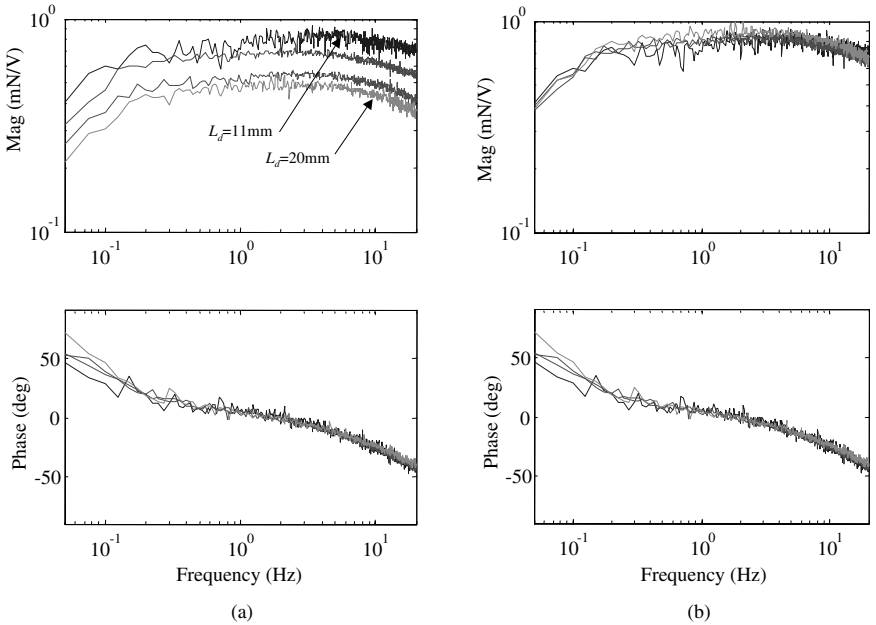

Figure 14. *Scaling of blocked force with voltage input as L_d is varied from 20 to 11 mm: (a) Raw data; (b) Scaled to $L_d = 11$ mm.*

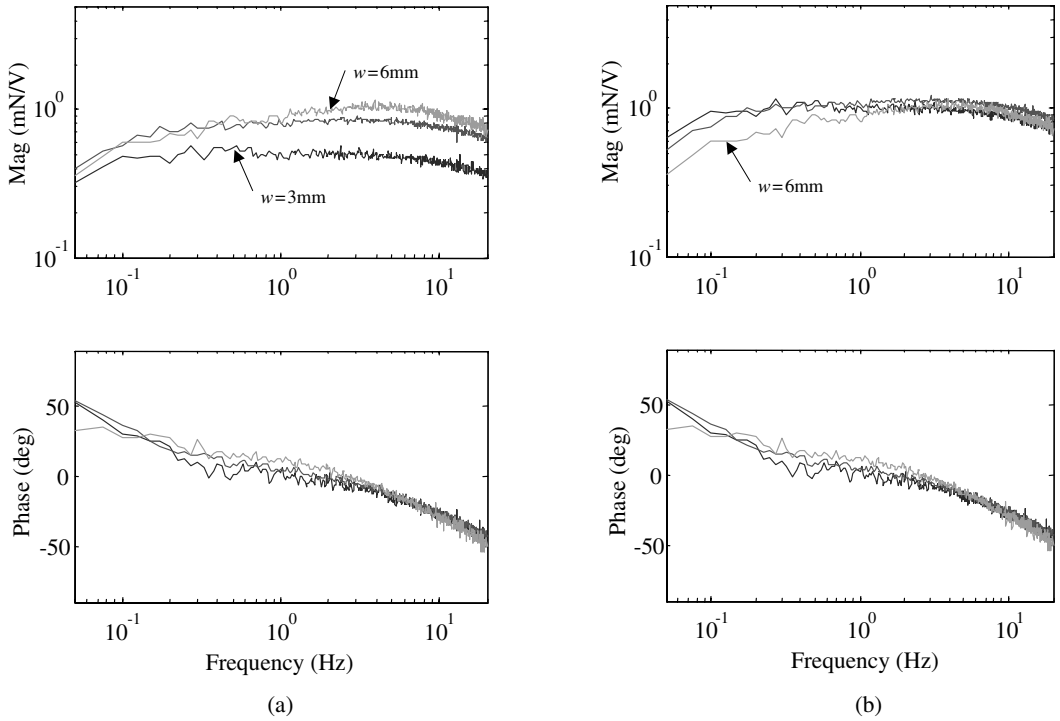

Figure 15. *Scaling of blocked force with voltage input as w is varied from 6 to 3 mm: (a) Raw data; (b) Scaled to w = 6 mm.*

transducer width, $w = 3$ mm, $w = 4.5$ mm, and $w = 6$ mm. The other transducer dimensions were $L_t = 33$ mm, $L_d = 17$ mm, and $L_{free} = 25$ mm, and they were held constant throughout the experiments. A 1 Vrms 0–20 Hz random input was applied to the transducer, and the frequency responses are based on five averages and 2048 point FFTs performed on data sampled at 51.2 Hz.

Examination of Equation (14) from Newbury and Leo (2002a) indicates that the blocked force with voltage input will be proportions to w, so the Figure 15(a) data was scaled by $6\,\text{mm}/w$ to allow direct comparison to the data for $w = 6$ mm. The scaled data are plotted in Figure 15(b). The phase plots match, and the magnitudes scale well, except that the $w = 6$ mm plot is low relative to the other plots for frequencies below 1 Hz.

Results for other input–output relationships are presented in Newbury (2002). The scaling laws predicted by the equivalent circuit model are shown to be valid. The degree of experimental error is approximately the same as the error shown for the blocked force to voltage frequency response. The experiments' results demonstrate that the basic form of the model is valid and that the assumption of negligible reflected impedance is appropriate for the transducers studied in this work.

CONCLUSIONS

The experiments verified the key elements of the model developed in Newbury and Leo (2002a). The results validated the assumption of the negligible reflected impedance, which allowed us to use the simpler form of the equivalent circuit model to estimate the expressions for actuation and sensing. A curvefitting technique was derived that utilized step response and frequency response data to determine the model parameters. Problems with obtaining good curvefits for both sets of data were attributed to an input-level dependence on the model parameters. In spite of this dependence on input level, the linear model was able to accurately predict both the time response and frequency response of an independent input–output relationship. Also, experiments demonstrated the reciprocity that exists between actuation and sensing with an ionic polymer transducer.

Our results also provide insight into the underlying physics of transduction in ionic polymers. For example, the relaxation attributed to Nafion-based transducers under the application of a step potential appears as a low-frequency rolloff in the effective strain coefficient of the polymer. This implies that the relaxation is due to a reduction in the applied force when excited with a step voltage, not due to relaxation in the polymer due to viscoelastic effects. Also, our results demonstrate that the electric permittivity exhibits a relaxation in the frequency range of 0.1–10 Hz. Finally, the results presented in this paper highlight the nonrepeatability of the static polymer response. As discussed in the paper, the response above approximately 1 Hz exhibited excellent

repeatability, whereas it was difficult to predict if the static response of the polymer would be minimum phase or nonminimum phase. This could be attributed to memory effects associated with charge redistribution within the polymer.

ACKNOWLEDGMENT

This work was supported by the National Science Foundation, grant number CMS0093889.

REFERENCES

Franklin, G., Powell, J. and Emami-Naeini, A. 1994. *Feedback Control Systems*. Addison-Wesley, Reading, MA.

Newbury, K.M. 2002. *Modeling, Characterization, and Control of Ionic Polymer Transducers*. Ph.D. Thesis, Virginia Polytechnic Institute and State University.

Newbury, K.M. and Leo, D.J. 2002a. "Linear Electromechanical Model of Ionic Polymer Transducers, Part I: Model Development," *Journal of Intelligent Material Systems and Structures*, 14(6):333–342.

Newbury, K.M. and Leo, D.J. 2002b. "Electrically-Induced Permanent Strain in Ionic Polymer Metal Composite Actuators," In: *Proceedings of the SPIE*, SPIE Paper Number 4695–11.